Finite Element Modelling of Reinforced Concrete Exterior Beam-Column Joint Retrofitted with Externally Bonded Fiber Reinforced Polymer (FRP)

A THESIS SUBMITTED IN THE PARTIAL FULFILLMENT OF THE REQUIREMENTS FOR THE AWARD OF DEGREE OF

MASTER OF ENGINEERING
IN
CIVIL ENGINEERING (STRUCTURES)

BY
AMIT JINDAL
Roll No. 801022002

UNDER THE SUPERVISION OF
Dr. Prem Pal Bansal,
Assistant Professor.

DEPARTMENT OF CIVIL ENGINEERING
THAPAR UNIVERSITY, PATIALA – 147004 (PUNJAB)

JUNE 2012

CERTIFICATE

This is to certify that the thesis entitled **"Finite Element Modelling of Reinforced Concrete Exterior Beam-Column Joint Retrofitted with Externally Bonded Fiber Reinforced Polymer (FRP)"**, being submitted by **Mr. Amit Jindal** (Roll No. 801022002), in the partial fulfillment of the requirements for the award of degree of **Master of Engineering in Civil Engineering (Structures)** at Thapar University, Patiala, is a bonafide work carried out by him under my guidance and supervision and that no part of this thesis has been submitted for the award of any other degree.

20/6/12

Dr. Prem Pal Bansal
Assistant Professor,
Department of Civil Engineering,
Thapar University, Patiala.

Date:

Countersigned By:

Maneek 25/6/12

Dr. Maneek Kumar
Professor & Head,
Department of Civil Engineering,
Thapar University, Patiala.

Dr. S.K. Mohapatra
Dean Academic Affairs,
Thapar University, Patiala.

ACKNOWLEDGEMENT

A dissertation cannot be completed without the help of many people who contribute directly or indirectly through their constructive criticism in the evolution and preparation of this work. It would not be fair on my part, if I don't say a word of thanks to all those whose sincere advice made this period a real educative, enlightening, pleasurable and memorable one.

First of all, I would like to express my sincere gratitude to my thesis supervisor **Dr. Prem Pal Bansal, Assistant Professor,** Department of Civil Engineering, Thapar University, Patiala for his gracious efforts and keen pursuit, which has remained a valuable asset for the successful completion of this work. His dynamism and diligent enthusiasm has been highly instrumental in keeping my spirit high. I am fortunate to have an opportunity to work under him.

I also thank **Dr. Maneek Kumar, Professor and Head,** Department of Civil Engineering, for providing excellent computational facilities and aid in preparation of this thesis. My special thanks to **Dr. Abhijit Mukherjee, Director,** Thapar University, Patiala for his guidance and motivation throughout the course of this work. I am greatly indebted for his keen interest and valuable time given to me.

I gratefully acknowledge the support given by the entire faculty and staff of the department.

Finally, I thank my parents and colleagues for their support and encouragement in the completion of this work.

Amit Jindal

Roll No. 801022002

ABSTRACT

The issue of upgrading the existing civil engineering infrastructure has been one of great importance for over a decade. Deterioration of bridge decks, beams, girders and columns, buildings, and others may be attributed to ageing, environmentally induced degradation, poor initial design and/or construction, lack of maintenance, and to accidental events such as earthquakes. The infrastructure's increasing decay is frequently combined with the need for upgrading so that structures can meet more stringent design requirements. Hence the aspect of retrofitting of civil engineering infrastructure has received considerable attention over the past few years throughout the world.

External wrapping with fiber-reinforced polymer (FRP) is a promising solution for retrofit of beam-column joints due advantages such as high strength-weight ratio, corrosion resistance, ease of application, low labour costs, and no significant increase in member size over other strengthening techniques. Also, recent research has attempted to simulate the behaviour of reinforced concrete structures strengthened with FRP composites using the finite element method (FEM). But limited work is done on the use of FEM to analyse retrofitted beam-column joints.

In the present study, finite element modelling of a reinforced concrete exterior beam-column joint retrofitted with externally bonded FRP is carried out with the help of commercially available software ANSYS 12.1. First, the control specimen is analysed and the results obtained are compared with an experimental study from the literature. Then, the specimen is retrofitted with externally bonded carbon-fiber-reinforced polymer (CFRP) sheets and analysed. The results from the retrofitted specimen are then compared with the results of the control specimen.

It is found that for the control specimen, the values of yield load and ultimate load obtained in ANSYS are very close to the values obtained from the experimental study. Comparison between the load-deflection results obtained from ANSYS for control and retrofitted specimens shows that the yield load and ultimate load has significantly increased for the retrofitted specimen. This is accompanied by lower deflections for the retrofitted specimen as compared to the control specimen. The deflection ductility ratio and energy absorption has also decreased for the retrofitted specimen.

CONTENTS

LIST OF FIGURES

LIST OF TABLES

Beam-column joints are recognized as the critical and vulnerable zone of a Reinforced Concrete (RC) moment resisting structure subjected to seismic loads. During an earthquake, the global response of the structure is mainly governed by the behaviour of the joints. If the joints behave in a ductile manner, the global behaviour generally will be ductile, whereas if the joints behave in a brittle fashion then the structure will display a brittle behaviour. The joints of old and non-seismically detailed structures are more vulnerable and behave poorly under the earthquakes compared to the joints of new and seismically detailed structures. Therefore, more often than not, the joints of such old structures require retrofitting in order to deliver better performance during earthquakes.

1.1 GENERAL

Under the action of seismic forces, beam-column connections are subjected to large shear stresses in the joint region. These shear stresses are a result of moments and shear forces of opposite signs on the member ends on either side of the joint core. Typically, high bond stresses are also imposed on reinforcement bars entering into the joint. The axial compression in the column and joint shear stresses result in principal tension and compression stresses that lead to diagonal cracking and/or crushing of concrete in the joint core. These problems have been highlighted in recent past by the damage observed in devastating earthquakes in different countries.

The two major failure modes for the failure at joints are: (a) joint shear failure and (b) end anchorage failure (**Fig. 1.1**). A typical example of a beam-column joint failure during the 1999 Turkey earthquake is shown in **Fig. 1.2**. The stresses in the joint core are resisted by the so-called strut and tie mechanism (**Paulay and Priestley, 1992**). To assure an increase of the shear strength after the cracking of the joint core by diagonal tension and sufficient rotational capacity, joint shear reinforcement is needed, which is therefore prescribed by the newer design codes (**ACI 318-08**; **NZS 3101:1995**; **IS 13920-1993**). Moreover, these codes

prescribe a large anchorage length of the bears terminating in case of exterior joints, so that a bond failure may be avoided.

(a) **(b)**

Fig. 1.1: Major failure modes for a RC beam-column joint: (a) Joint shear failure; (b) Inadequate reinforcement anchorage.

Fig. 1.2: Typical beam-column joint failures (1999 Turkey earthquake).

However, a vast majority of RC buildings worldwide consist of structures designed prior to the advent of modern seismic design codes. It has been identified that the deficiencies of joints are mainly caused by inadequate transverse reinforcement and insufficient anchorage capacity in the joint (**Liu, 2006**). **Fig. 1.3(a)** shows a few typical deficiencies found in the beam-column joints of old structures and **Fig. 1.3(b)** shows the corresponding new ductile detailing recommended by new codes.

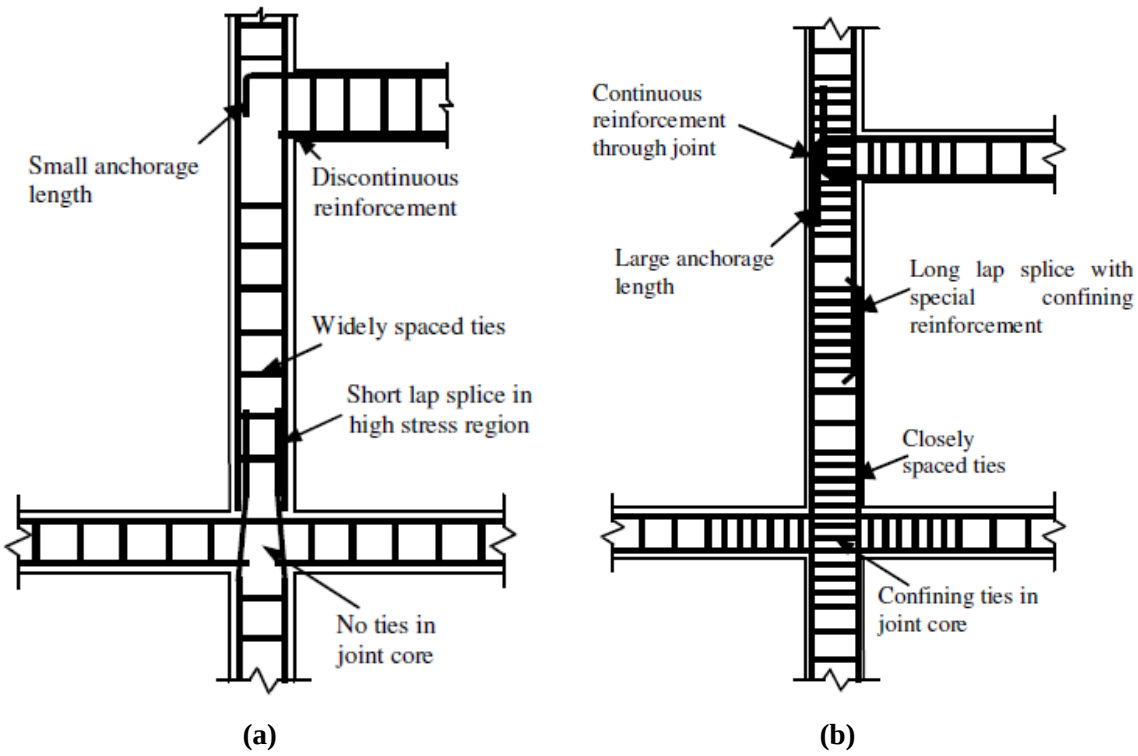

Fig. 1.3: (a) Typical non-ductile detailing prescribed by older codes; (b) Typical ductile detailing prescribed by newer codes.

1.2 MECHANICS AND SEISMIC EVALUATION OF BEAM-COLUMN JOINTS

Before a retrofitting can be suggested for a particular joint, it is necessary to evaluate the seismic performance of the joint in as-built condition. This needs a basic understanding of the mechanics of shear transfer within a joint. When RC moment frames are subjected to lateral seismic loading, high shear forces are generated in the joint core (**Paulay and Priestley, 1992**; **Hakuto et al., 2000**). **Fig. 1.4** shows the mechanics of an exterior joint when subjected to seismic forces. The lateral seismic loading on a frame leads to bending moments and shear forces that can be simulated in the joint as shown in **Fig. 1.4(a)**. Here the length of the beam L_b is half of the bay width and L_c is the story height. The horizontal shear, vertical shear and principal tensile stresses can be calculated by considering the equilibrium of the joint (**Paulay and Priestley, 1992**; **Tsonos, 2007**).

A system of diagonal compression strut and tension tie is developed in the concrete core to transmit the joint shear forces. Some of the internal forces, particularly those generated in the concrete will combine to develop a diagonal strut (**Paulay and Priestley, 1992**; **Hakuto et al., 2000**).

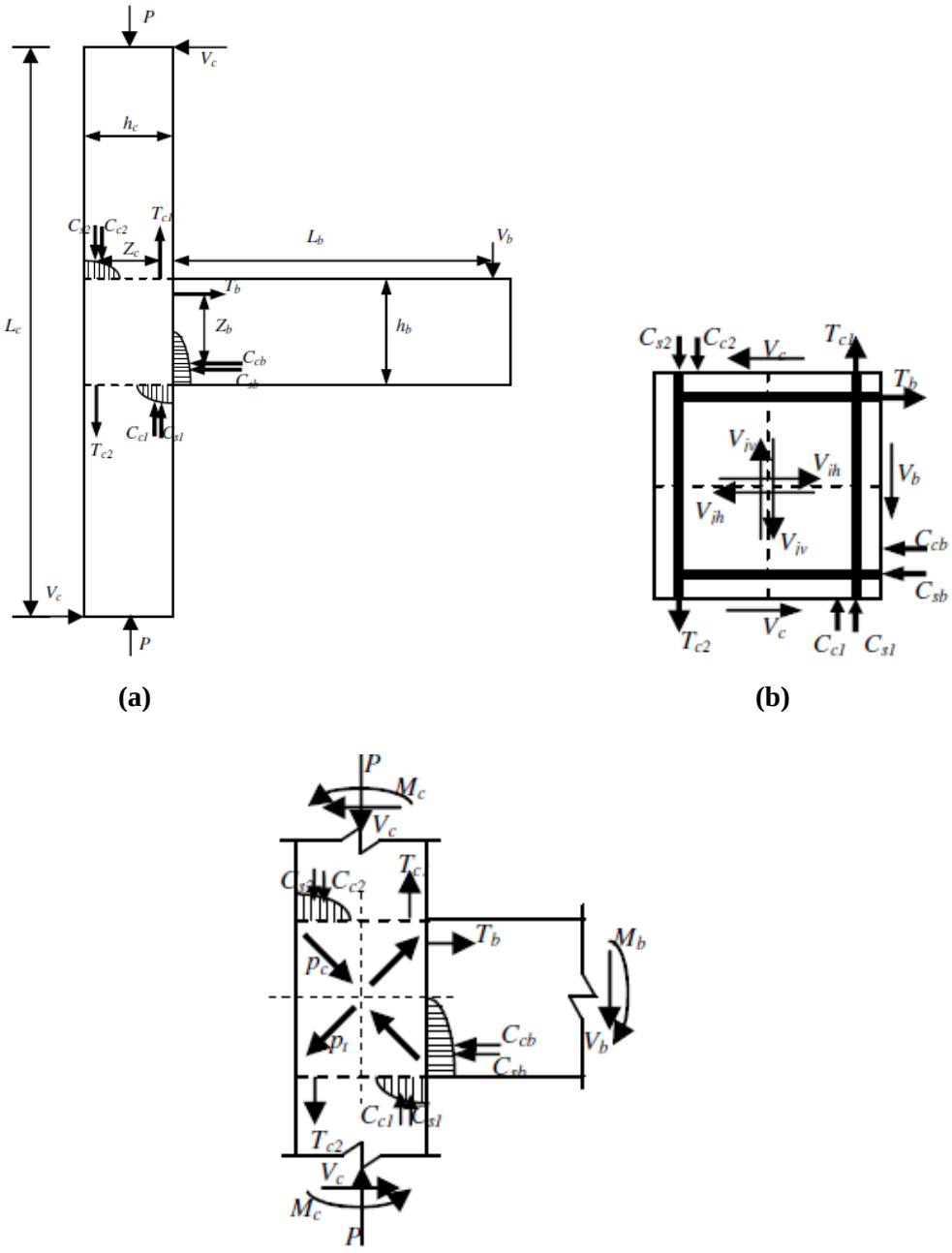

Fig. 1.4: Mechanics of exterior joint under seismic actions: (a) External actions and forces in beams and columns; (b) Horizontal and vertical joint shear; (c) Principal stresses in joint.

Other forces transmitted to the joint core from beam and column bars by means of bond, necessitate a truss mechanism. The strength of the diagonal strut controls the joint strength before cracking. The transverse reinforcement in the joint helps confine the concrete diagonal strut in the joint core thereby contributing to increased joint strength after the first diagonal cracking. If the joint shear forces are large, diagonal cracking in the joint core occurs followed by the crushing of concrete in the joint core.

The joint reinforcement alone is not sufficient to avoid undesirable pinching in hysteretic loops at this stage (**Murty et al., 2003**). Standards (**ACI 318-08**; **NZS 3101:1995**; **EC8:1998**) recommend keeping the stresses in the joint below permissible limits. **ACI 318-08** and **EC8:1998** specify this limit based on the tensile strength of concrete by specifying the value of maximum permissible horizontal joint shear stress as $k\sqrt{f_c'}$, where, f_c' is the cylinder compressive strength of concrete and k is a parameter that depends on the confinement provided by the members framing into the joint. **NZS 3101:1995** recommends that the horizontal shear stress shall not exceed a value of $0.2f_c'$. Other authors recommend that principal stresses that consider the contribution of axial forces also, provide better criteria for the damage in the joint (**Priestley, 1997**; **Pampanin et al., 2003**). The values are suggested as $k\sqrt{f_c'}$, where, f_c' is the cylinder compressive strength of concrete and k is a parameter that depends on the type of joint, type of reinforcement and end anchorage details of the beam longitudinal bars in the core. **Priestley (1997)** suggested the critical principal tensile stress values for exterior and corner beam-column joints with deformed bars with bent-in and bent-out type end anchorages and **Pampanin et al. (2003)** proposed the same for exterior beam-column joints with plain round bars and end hooks.

Once, the joints are analyzed based on the formulations given above, the decision on whether a joint needs retrofitting or not, and to what extent, can be made.

1.3 SEISMIC RETROFIT STRATEGIES FOR BEAM-COLUMN JOINTS

In order to prevent devastating failures of structures not designed as per the current seismic design procedures and not having special seismic detailing, retrofitting is often required. At the global structural level the retrofitting can be performed by strengthening techniques such as addition of shear walls or stiffeners, or by response control techniques such as using base isolation system or installing dampers. Sometimes, these techniques alone may be suitable enough to redistribute the forces (e.g. in case of adding shear walls) or reduce the forces (e.g. in case of base isolation) to an extent that no further retrofitting at member level is required. However, often it may be more suited because of technical or economic reasons to retrofit single members only or in addition to global retrofitting. Such techniques usually target an increase of the ductility of the structure more than a strengthening.

At the member level (i.e. for beams and columns), various retrofitting techniques are available such as concrete jacketing, steel jacketing, wrapping with fiber reinforced polymer (FRP) sheets, external prestressing etc. These techniques have proved over the years to be quite effective with each of the above having its own advantages, disadvantages and limitations. However, retrofitting of beam-column joints is still a major topic of concern. Many researchers have investigated different techniques, with varying degree of success, for retrofitting of the reinforced concrete beam-column joints. One of the major challenges is to practically implement a retrofitting scheme, because there is only a restricted access, if any, to the real joint core to perform any retrofitting technique.

Engindeniz et al (2005) presented a comprehensive up-to-date literature search pertaining to the performance of, as well as to the repair and strengthening techniques for, nonseismically designed RC beam-column joints, reported between 1975 and 2003.

These techniques included: 1) epoxy repair; 2) removal and replacement; 3) concrete jacketing; 4) concrete masonry unit jacketing; 5) steel jacketing and addition of external steel laminates; and 6) strengthening with fiber-reinforced polymeric (FRP) composite applications. Each method of repair or strengthening was reviewed with emphasis on its application details, required labour, range of applicability, and performance. Relative advantages and disadvantages of each method were discussed.

The results of the epoxy repair applications on one-way joints have showed that the reliability of this technique in restoring the original characteristics of damaged joints was questionable. The bond around the reinforcing bars, once destroyed, did not seem to be completely restored by epoxy injection. This was evidenced by the partial recovery of stiffness and by the pinching in the hysteresis loops. It was also observed that the effectiveness of the epoxy repair was limited by the access to the joint and that epoxy cannot be effectively introduced into the joints surrounded by transverse beams and floor slab.

Partial or total removal and replacement of concrete is used for heavily damaged joints with crushed concrete, buckled longitudinal bars, or ruptured ties. Depending on the amount of concrete removed, some additional ties or longitudinal reinforcement may be added. This technique can be used for strengthening if high-strength non-shrink concrete was used for replacement. However the damaged joint should be readily accessible for effective use of this technique.

Concrete jacketing involves encasing the existing column, along with the joint region, in new concrete with additional longitudinal and transverse reinforcement. The continuity of the added longitudinal bars through the joint requires opening the slab at the column corners. It was observed that this technique was effective but at the same time the most labour-intensive strengthening method due to difficulties in placing additional joint transverse reinforcement. Also the increase in member size, reduced the available floor space and the construction procedures disrupted building occupants.

Joint strengthening using reinforced concrete masonry units (CMUs) led to desirable ductile beam failures and reduction of interstory drifts; however, no experimental data were available to validate their performance.

Various configurations of steel jackets, plates, or shapes have been used to increase the strength and ductility of deficient beam-column joints. In one of the study, cracking near the joint before retrofit was successfully moved to the end of the enlarged joint region after retrofit, and there was no evidence of damage in the column or its external reinforcement. The strength, initial stiffness, and energy dissipation of the exterior joint were increased by approximately 18, 12 and 2%, respectively. The corresponding increases for the interior joint were 21, 34 and 13% respectively. Use of steel jackets significantly reduced the construction time due to prefabrication, but has the disadvantages, such as the potential for corrosion, difficulty in handling the heavy steel plates, objectionable aesthetics, and loss of floor space. Also these are difficult to apply in cases where floor members are present.

Since 1998, research efforts on upgrading existing beam-column joints have focused on the use of FRP composites in the form of epoxy-bonded flexible sheets, shop-manufactured strips, or near-surface-mounted rods. The relatively higher initial cost of FRPs is purportedly outweighed by their advantages such as high strength-weight ratio, corrosion resistance, ease of application (including limited disruption to building occupancy), low labour costs, and no significant increase in member size. Externally bonded FRP composites could eliminate some important limitations of other strengthening techniques, and still improve the joint shear capacity and shift the failure towards ductile beam hinging mechanisms.

1.4 EXTERNALLY BONDED FRP REINFORCEMENT

Recent developments related to materials, methods and techniques for structural strengthening have been enormous. One of today's state-of-the-art techniques is the use of fibre reinforced polymer (FRP) composites, which are currently viewed by structural engineers as "new" and highly promising materials in the construction industry. Composite materials for strengthening of civil engineering structures are available today mainly in the form of:

- thin unidirectional *strips* (with thickness in the order of 1 mm) made by pultrusion,
- flexible *sheets* or *fabrics*, made of fibres in one or at least two different directions, respectively (and sometimes pre-impregnated with resin).

For comparison with steel, typical stress-strain diagrams for unidirectional composites under short-term monotonic loading are given in **Fig. 1.5**.

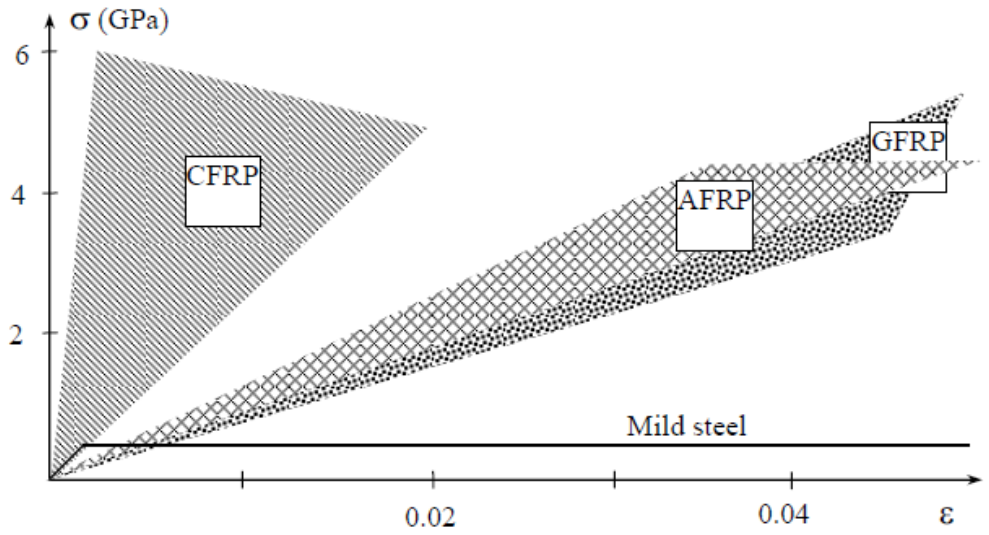

Fig. 1.5: Uniaxial tension stress-strain diagrams for different unidirectional FRPs and steel. CFRP = carbon FRP, AFRP = aramid FRP, GFRP = glass FRP.

The three main components, namely adhesives, resin matrices and fibres of an FRP strengthening material system are discussed briefly here.

The purpose of the adhesive is to provide a shear load path between the concrete surface and the composite material, so that full composite action may develop. The most common type of structural adhesive used in structural applications is epoxy adhesive, which is the result of mixing an epoxy resin (polymer) with a hardener. When using epoxy adhesives there are two different time concepts that need to be taken into consideration. The

first is the ***pot life*** and the second is the ***open time***. Pot life represents the time one can work with the adhesive after mixing the resin and the hardener before it starts to harden in the mixture vessel; for an epoxy adhesive, it may vary between a few seconds up to several years. Open time is the time that one can have at his/her disposal after the adhesive has been applied to the adherents and before they are joined together. Another important parameter to consider is the ***glass transition temperature***, T_g. Most synthetic adhesives are based on polymeric materials, and as such they exhibit properties that are characteristic for polymers. Polymers change from relatively hard, elastic, glass-like to relatively rubbery materials at a certain temperature. This temperature level is defined as glass transition temperature, and is different for different polymers.

The matrix for a structural composite material can either be of thermosetting type or of thermoplastic type, with the first being the most common one. The function of the matrix is to protect the fibres against abrasion or environmental corrosion, to bind the fibres together and to distribute the load. The matrix has a strong influence on several mechanical properties of the composite, such as the transverse modulus and strength, the shear properties and the properties in compression. Epoxy resins, polyester and vinylester are the most common polymeric matrix materials used with high-performance reinforcing fibres. They are thermosetting polymers with good processibility and good chemical resistance. Epoxies have, in general, better mechanical properties than polyesters and vinylesters, and outstanding durability, whereas polyesters and vinylesters are cheaper.

A great majority of materials are stronger and stiffer in the fibrous form than as a bulk material. A high fibre aspect ratio (length/diameter ratio) permits very effective transfer of load via matrix materials to the fibres, thus enabling full advantage of the properties of the fibres to be taken. Therefore, fibres are very effective and attractive reinforcement materials. Fibres can be manufactured in continuous or discontinuous (chopped) form, but here only continuous fibres are considered. Such fibres have a diameter in the order of 5-20 μm, and can be manufactured as unidirectional or bi-directional reinforcement. The fibres used for strengthening all exhibit a linear elastic behaviour up to failure and do not have a pronounced yield plateau as for steel. There are mainly three types of fibres that are used for strengthening of civil engineering structures, namely glass, aramid and carbon fibres. It should be recognised that the physical and mechanical properties can vary a great for a given type of fibre as well of course the different fibre types. Typical properties of various types of fiber materials are provided in **Table 1.1**.

Table 1.1: Typical properties of fibers (**FIB Bulletin No. 14**)

Material	Elastic modulus (GPa)	Tensile strength (MPa)	Ultimate tensile strain (%)
Carbon			
❖ High strength	215-235	3500-4800	1.4-2.0
❖ Ultra high strength	215-235	3500-6000	1.5-2.3
❖ High modulus	350-500	2500-3100	0.5-0.9
❖ Ultra high modulus	500-700	2100-2400	0.2-0.4
Glass			
❖ E	70	1900-3000	3.0-4.5
❖ S	85-90	3500-4800	4.5-5.5
Aramid			
❖ Low modulus	70-80	3500-4100	4.3-5.0
❖ High modulus	115-130	3500-4000	2.5-3.5

FRP materials consist of a large number of small, continuous, directionalized, non-metallic fibres with advanced characteristics, bundled in a resin matrix. Depending on the type of fibre, they are referred to as AFRP (aramid fibre based), CFRP (carbon fibre based) or GFRP (glass fibre based). Typically, the volume fraction of fibres in FRPs equals about 50-70% for strips and about 25-35% for sheets. Hence fibres are the principal stress bearing constituents, while the resin transfers stresses among fibres and protects them. Basic mechanical properties of FRP materials may be estimated if the properties of the constituent materials (fibres, matrix) and their volume fraction are known. This may be accomplished by applying the "rule of mixtures" simplification as follows:

$$E_f = E_{fib}V_{fib} + E_mV_m$$

$$f_f = f_{fib}V_{fib} + f_mV_m$$

where E_f = Young's modulus of FRP in fibre direction, E_{fib} = Young's modulus of fibres, E_m = Young's modulus of matrix, V_{fib} = volume fraction of fibres, V_m = volume fraction of matrix, f_f = tensile strength of FRP in fibre direction, f_{fib} = tensile strength of fibres and f_m = tensile strength of matrix. Note that in the above equations $V_{fib} + V_m = 1$. Also, typical values for the volume fraction of fibres in prefabricated strips are in the order of 0.50 – 0.65.

Typical FRP commercial products in the form of prefabricated strips have the properties given in **Table 1.2**, where the properties for mild steel area also given for comparison.

Table 1.2: Typical properties of prefabricated FRP strips and comparison with steel (**FIB Bulletin No. 14**)

Material	Elastic modulus (GPa)	Tensile strength (MPa)	Ultimate tensile strain (%)
Prefabricated strips	E_f	f_f	ε_{fu}
❖ Low modulus CFRP strips	170	2800	1.6
❖ High modulus CFRP strips	300	1300	0.5
Mild steel	200	400	25*

* Yield strain = 0.2%

Different systems of externally bonded FRP reinforcement exist, related to the constituent materials, the form and the technique of the FRP strengthening. In general, these can be subdivided into “wet lay-up” (or “cured in-situ”) systems and “prefab” (or “precured”) systems.

The basic FRP strengthening technique, which is most widely applied, involves the manual application of either wet lay-up (so-called hand lay-up) or prefabricated systems by means of cold cured adhesive bonding. Common in this technique is that the external reinforcement is bonded onto the concrete surface with the fibres as parallel as practically possible to the direction of principal tensile stresses. Typical applications of the hand lay-up and prefabricated systems are illustrated in **Fig. 1.6**.

(a) **(b)**

Fig. 1.6: (a) Hand lay-up of CFRP sheets or fabrics; (b) Application of prefabricated strips.

1.5 FINITE ELEMENT METHOD (FEM)

The Finite Element Analysis (FEA) method, originally introduced by **Turner et al. (1956)**, is a powerful computational technique for approximate solutions to a variety of "real-world" engineering problems having complex domains subjected to general boundary conditions. FEA has become an essential step in the design or modelling of a physical phenomenon in various engineering disciplines. A physical phenomenon usually occurs in a continuum of matter (solid, liquid, or gas) involving several field variables. The field variables vary from point to point, thus possessing an infinite number of solutions in the domain.

The basis of FEA relies on the decomposition of the domain into a finite number of subdomains (elements) for which the systematic approximate solution is constructed by applying the variational or weighted residual methods. In effect, FEA reduces the problem to that of a finite number of unknowns by dividing the domain into elements and by expressing the unknown field variable in terms of the assumed approximating functions within each element. These functions (also called interpolation functions) are defined in terms of the values of the field variables at specific points, referred to as nodes. Nodes are usually located along the element boundaries, and they connect adjacent elements.

The ability to discretize the irregular domains with finite elements makes the method a valuable and practical analysis tool for the solution of boundary, initial, and eigenvalue problems arising in various engineering disciplines.

The finite element analysis method requires the following major steps:

- Discretization of the domain into a finite number of subdomains (elements).
- Selection of interpolation functions.
- Development of the element matrix for the subdomain (element).
- Assembly of the element matrices for each subdomain to obtain the global matrix for the entire domain.
- Imposition of the boundary conditions.
- Solution of equations.
- Additional computations (if desired).

In matrix notation, the global system of equations can be cast into

$$\mathbf{Ku} = \mathbf{F}$$

where **K** is the system stiffness matrix, **u** is the vector of unknowns, and **F** is the force vector. Depending on the nature of the problem, **K** may be dependent on **u**, i.e., **K = K(u)** and **F** may be time dependent, i.e., **F = F (t)**.

As shown in **Fig. 1.7**, the transformation of the practical engineering problem to a mathematical representation is achieved by discretizing the domain of interest into elements (subdomains). These elements are connected to each other by their "common" nodes. A node specifies the coordinate location in space where degrees of freedom and actions of the physical problem exist. The nodal unknown(s) in the matrix system of equations represents one (or more) of the primary field variables. Nodal variables assigned to an element are called the degrees of freedom of the element. The common nodes shown in **Fig. 1.7** provide continuity for the nodal variables (degrees of freedom). Degrees of freedom (DOF) of a node are dictated by the physical nature of the problem and the element type. **Table 1.3** presents the DOF and corresponding "forces" used in FEA for different physical problems.

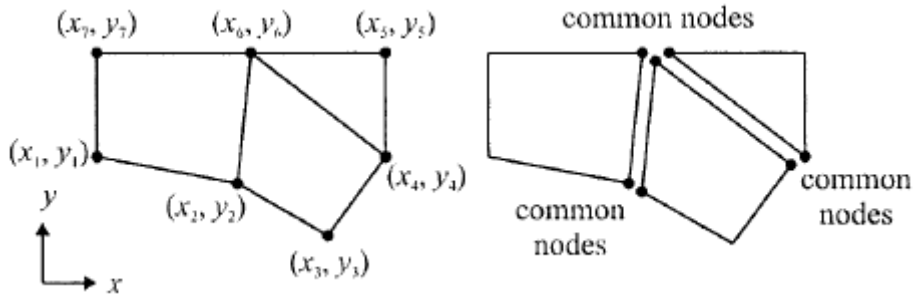

Fig. 1.7: Division of a domain into subdomains (elements).

Table 1.3: Degrees of freedom and force vectors in FEA for different engineering disciplines

Discipline	DOF	Force vector
Structural/solids	Displacement	Mechanical forces
Heat conduction	Temperature	Heat flux
Acoustic fluid	Displacement potential	Particle velocity
Potential flow	Pressure	Particle velocity
General flows	Velocity	Fluxes
Electrostatics	Electric potential	Charge density
Magnetostatics	Magnetic potential	Magnetic intensity

Depending on the geometry and the physical nature of the problem, the domain of interest can be discretized by employing line, area, or volume elements. Some of the common elements in FEA are shown in **Fig. 1.8**.

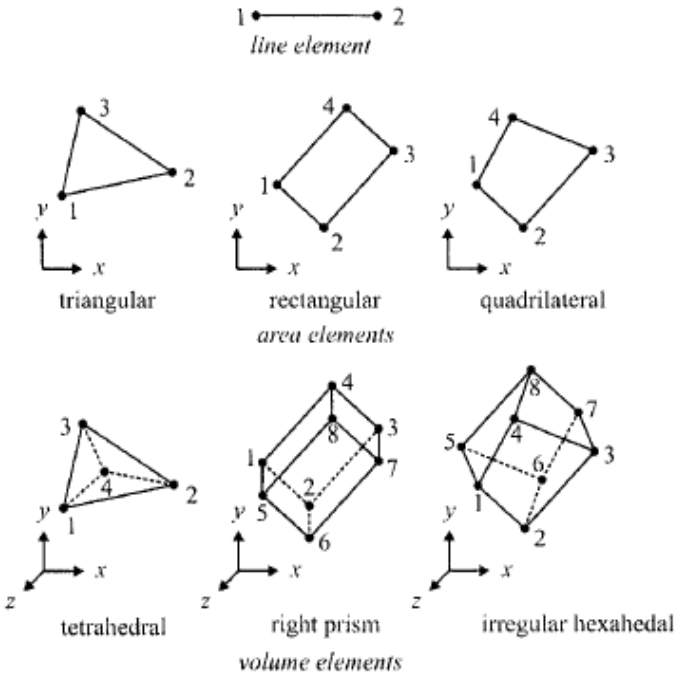

Fig. 1.8: Description of line, area, and volume elements with node number at the element level.

Willam and Warnke (1975) developed a widely used model for the triaxial failure surface of unconfined plain concrete. The failure surface in principal stress-space is shown in **Fig. 1.9**. The mathematical model considers a sextant of the principal stress space because the stress components are ordered according to $\sigma_1 \geq \sigma_2 \geq \sigma_3$. These stress components are the major principal stresses. The failure surface is separated into hydrostatic (change in volume) and deviatoric (change in shape) sections as shown in **Fig. 1.10**. The hydrostatic section forms a meridional plane which contains the equisectrix $\sigma_1 = \sigma_2 = \sigma_3$ as an axis of revolution (see **Fig. 1.9**). The deviatoric section in **Fig. 1.10** lies in a plane normal to the equisectrix (dashed line in **Fig. 1.10**).

The deviatoric trace is described by the polar coordinates r and θ, where r is the position vector locating the failure surface with angle, θ. The failure surface is defined as:

$$\frac{1}{z}\frac{\sigma_a}{f_{cu}} + \frac{1}{r(\theta)}\frac{\tau_a}{f_{cu}} = 1$$

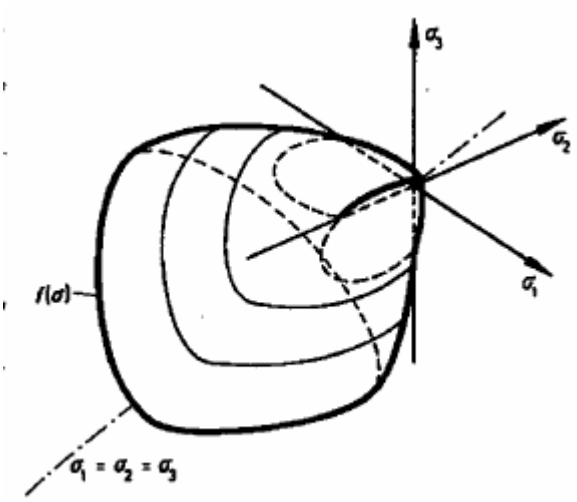

Fig. 1.9: Failure surface of plain concrete under triaxial conditions by **Willam and Warnke (1975)**.

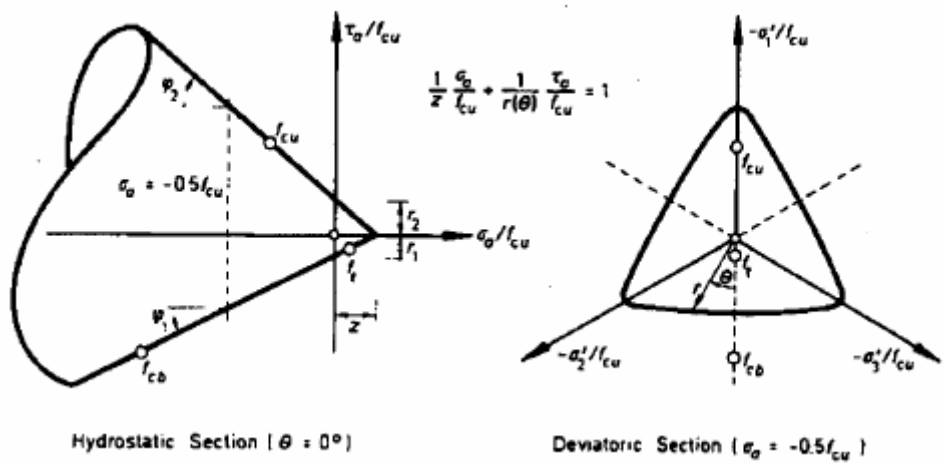

Fig. 1.10: Three parameter model by **Willam and Warnke (1975)**.

where: σ_a and τ_a = average stress components,

z = apex of the surface,

f_{cu} = uniaxial compressive strength.

The opening angles of the hydrostatic cone are defined by φ_1 and φ_2. The free parameters of the failure surface z and r, are identified from the uniaxial compressive strength (f_{cu}), biaxial compressive strength (f_{cb}), and uniaxial tension strength (f_t).

This mathematical model of the failure surface for the concrete has the following advantages:

- Close fit of experimental data in the operating range;
- Simple identification of model parameters from standard test data;
- Smoothness (e.g. continuous surface with continuously varying tangent planes);
- Convexity (e.g. monotonically curved surface without inflection points).

Based on the above criteria, a constitutive model for the concrete suitable for FEA implementation was formulated.

This constitutive model for concrete assumes an appropriate description of the material failure. The yield condition be approximated by three or five parameter models distinguishing linear from non-linear and elastic from inelastic deformations using the failure envelope defined by a scalar function of stress $f(\sigma)=0$ through a flow rule, while using incremental stress-strain relations. The parameters for the failure surface can be seen in **Fig. 1.10**.

During transition from elastic to plastic or elastic to brittle behavior, two numerical strategies were recommended: proportional penetration, which subdivides proportional loading into an elastic and inelastic portion which governs the failure surface using integration, and normal penetration, which allows the elastic path to reach the yield surface at the intersection with the normal therefore solving a linear system of equations. Both of these methods are feasible and give stress values that satisfy the constitutive constraint condition. From the standpoint of computer application the normal penetration approach is more efficient than the proportional penetration method, since integration is avoided.

Tavarez (2001) discussed three techniques that exist to model steel reinforcement in finite element models for reinforced concrete (**Fig. 1.11**): the discrete model, the embedded model, and the smeared model.

The reinforcement in the discrete model (**Fig. 1.11a**) uses bar or beam elements that are connected to concrete mesh nodes. Therefore, the concrete and the reinforcement mesh share the same nodes and concrete occupies the same regions occupied by the reinforcement. A drawback to this model is that the concrete mesh is restricted by the location of the reinforcement and the volume of the mild-steel reinforcement is not deducted from the concrete volume.

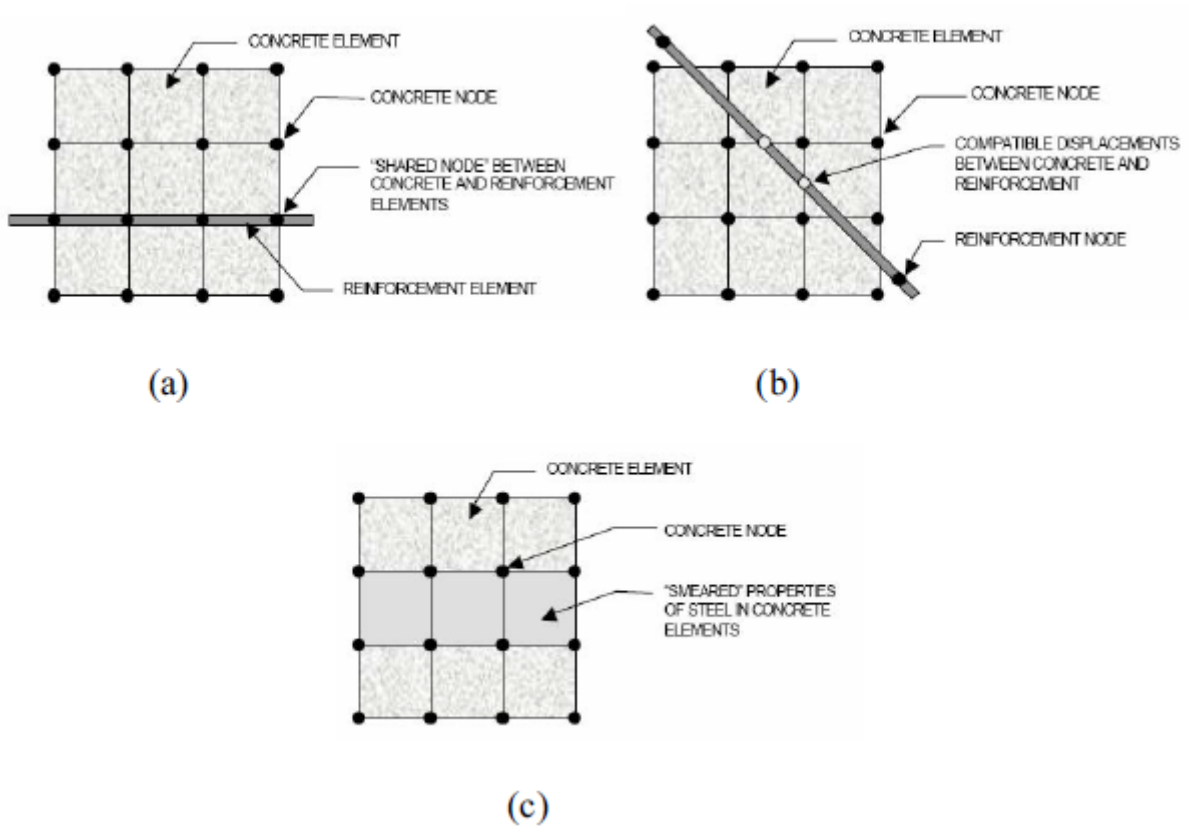

Fig. 1.11: Models for reinforcement in reinforced concrete: (a) discrete; (b) embedded; and (c) smeared by **Tavarez (2001)**.

The embedded model (**Fig. 1.11b**) overcomes the concrete mesh restriction(s) because the stiffness of the reinforcing steel is evaluated separately from the concrete elements. The model is built in a way that keeps reinforcing steel displacements compatible with the surrounding concrete elements. When reinforcement is complex, this model is very advantageous. However, this model increases the number of nodes and degrees of freedom in the model, therefore, increasing the run time and computational cost.

The smeared model (**Fig. 1.11c**) assumed that reinforcement is uniformly spread throughout the concrete elements in a defined region of the FE mesh. This approach is used for large-scale models where the reinforcement does not significantly contribute to the overall response of the structure.

Fanning (2001) modelled the response of the reinforcement using the discrete model and the smeared model for reinforced concrete beams. It was found that the best modelling strategy was to use the discrete model when modelling reinforcement.

1.6 OBJECTIVE AND ORGANIZATION OF THESIS

The objective of the thesis is to perform finite element modelling of a reinforced concrete exterior beam-column joint retrofitted with externally bonded fiber reinforced polymer (FRP).

The thesis has been organised into the following five chapters.

Chapter-1 deals with the general introduction about the topic of thesis.

Chapter-2 deals with the review of literature conducted to evaluate previous experimental and analytical procedures related to retrofitting of concrete structures. Past research on use of finite element modelling for concrete structures is also taken.

Chapter-3 deals with the FEM modelling of beam-column joint. First a beam-column joint model is set up using a commercial finite element analysis package ANSYS 12.1 (**SAS, 2009**) and evaluated with an experimental study from the literature. Then the beam-column joint is retrofitted with externally bonded FRP and analysed. These results are then compared with the controlled specimen.

Chapter-4 deals with the results and discussion related to the present work.

Chapter-5 presents the conclusions drawn from the present study. Future scope of work is also presented.

Extensive research has been carried out in the last two decades to improve the seismic performance of reinforced concrete beam-column joints. This has resulted in the use of materials such as fiber-reinforced polymer (FRP) and ferrocement as external laminates for retrofitting of structures. These materials provide continuous confinement of the joint area thereby enhancing yield load, initial stiffness and energy dissipation capacity considerably. In recent years, the use of finite element analysis to analyze concrete structural components has also increased. The finite element analysis provides a powerful tool to investigate the complex behaviour of beam-column joints in addition to being much faster, and extremely cost-effective as compared to the experimental based testing.

In this chapter, the literature review is presented on the following topics: (1) Retrofitting of Concrete Structures – Experimental studies; (2) Retrofitting of Concrete Structures – Analytical Modelling & Design; and (3) Finite Element Modelling of Concrete Structures.

2.1 RETROFITTING OF CONCRETE STRUCTURES – EXPERIMENTAL STUDIES

Bansal et al. (2011) studied the effects of number of layers of wire mesh in the ferrocement jackets, type of section (balanced or under reinforced) and initial stress level on the strength of retrofitted stressed reinforced cement concrete beams.

In the study, 28 prototype beams of size 127 mm x 227 mm x 4100 mm were cast using M20 grade concrete. Fourteen (under reinforced) beams were reinforced with two bars of 10 mm diameter in tension and two bars of 8 mm diameter in compression, while fourteen (balanced) beams were reinforced with three bars of 12 mm diameter in tension and two bars of 8 mm diameter in compression. A set of two beams each for balanced and under reinforced sections, were stressed to three stress levels of 60, 75, and 90% of the experimentally obtained safe load. These were then retrofitted with a 25 mm thick U-shaped ferrocement jacket. The ferrocement jacket for the first set of beams was reinforced with two layers of GI

woven wire mesh of wire diameter 2.4 mm, whereas the other set was reinforced with three layers of GI woven wire mesh. The beams were then tested under a two-point loading system with simply supported end conditions having an effective span of 3.75 m.

The results showed that there was higher increase in the maximum load, safe load carrying capacity, ductility and toughness for beams with three layers woven wire mesh ferrocement jackets as compared to beams reinforced with two layers of woven wire mesh. It was further seen that the percentage improvement in above properties decreased with increase in initial stress level and change in type of section from under reinforced to balanced.

Dar (2011) studied the effect of different wrapping techniques on retrofitting of RCC beam column joints using ferrocement. Five external beam column joint specimens were cast using M-20 grade concrete and Fe-500 grade steel.

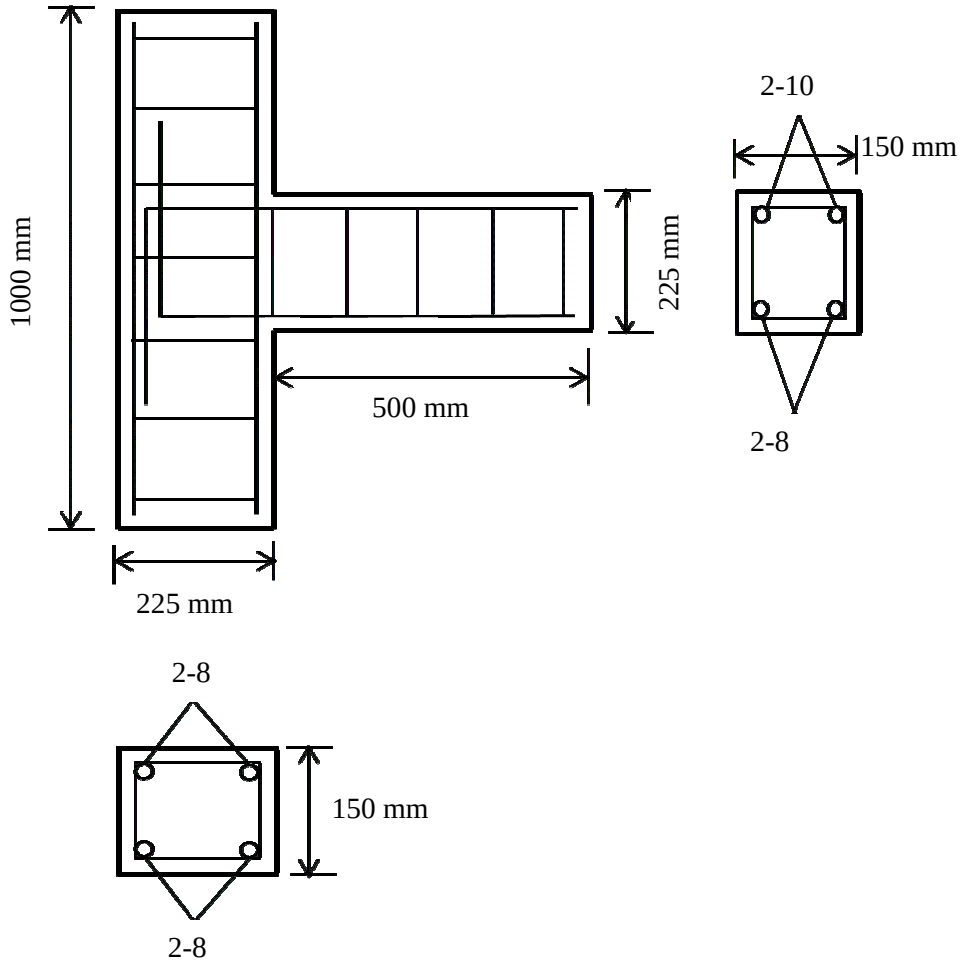

Fig. 2.1: Dimensions and Reinforcement Detailing of Beam-Column Joint by **Dar (2011)**

The column was rectangular in shape with dimensions 225 x 150 mm and a length of 1000 mm. The beam had dimensions 225 x 150 mm and length of 500 mm. The column main reinforcement consisted of 4 No. 8 mm diameter bars whereas the beam reinforcement consisted of 2 No. 10 mm diameter bars in tension zone and 2 No. 8 mm diameter bars in the compression zone. From the face of the column, an anchorage length of 600 mm on both sides was provided. The ties consisted of rectangular hoops of 6 mm diameter placed 100 mm c/c in both column and beam portion. **Fig. 2.1** shows the dimensions and reinforcement of the specimens.

The specimen was fixed on loading frame and was subjected to a point load at a distance of 300 mm from the face of the column. The value of deflection was taken with the help of three LVDT's, one at the beam free end, second at a distance of 150 mm from beam free end and third at 100 mm from column face. Out of the five specimens, one specimen was taken as the control specimen and was loaded to ultimate capacity. The rest four specimens were loaded to 80% of the ultimate load and then were retrofitted using different wrapping techniques.

For the control specimen, the load-deflection results were plotted and it was found that in the beginning the deflections were very less. After the first crack load of 10 kN, non-linear behaviour was obtained upto a load of 55 kN and after that yielding of reinforcement took place. Displacements increased at a much higher rate till the ultimate load of 64.1 kN was reached. After that the joint failed. These results were taken as a basis in the present study.

The retrofitted joints were loaded upto 80% of the ultimate load before retrofitting. Two different retrofitting schemes were adopted. Type one retrofitting consisted of two L-shapes of wire mesh on the lower and upper faces of the beam at the joint. Type two retrofitting consisted of extra mesh on the diagonal of the joint in addition to the mesh as in type one retrofitting. It was found that the load carrying capacity of retrofitted beam-column joints increased significantly as compared to the control joint with specimen with type two retrofitting showing maximum improvement in terms of yield load, ultimate strength, ductility ratio and energy absorption.

Mehta (2011) studied the effect of initial stress levels on retrofitting of beams using pre-stressed carbon fibre sheets. For this, beams of size 600 x 300 mm were used which were stressed to three different initial stress levels taken respectively from elastic zone, elasto-plastic zone and plastic zone from the load-deflection plot of the beam taken as control specimen. Through this study it was observed that load carrying capacity of the retrofitted beams was remarkably improved compared to that of fresh control beam. The control specimen failed at 94.35 kN and the retrofitted beams were seen to be failed in the range of 125 kN to 136 kN. Subsequent decrease in the deflection was also seen as compared to that of the fresh control beam at all the stress levels. The 53% stressed beam showed the maximum deflection whereas the 100% stressed beam showed the minimum deflection with overall decrease of around 65% of that of control beam. Stiffness had also increased after retrofitting at all stressed levels as compared to the control beam. The 53% and 89% stressed beams showed almost same stiffness but the 98% stressed beam showed the maximum stiffness with increase of around 25% of that of control specimen.

Akguzel and Pampanin (2010) examined the effects of axial load variation on the column due to the frame lateral sway on the performance of retrofitted beam-column joints. For this purpose, four 2/3-scale exterior beam-column joint subassemblies including one as-built (2D1) and three retrofitted configurations (2D2, 2D3 and 2D4) were tested under varying axial load. All specimens were designed and constructed according to pre-1970s construction practice. Beam-column joints were retrofitted using glass fiber reinforced polymer (GFRP) sheets.

Schematic views of GFRP retrofit configurations with top view layouts along with the implementation sequence in alphabetical order are given in **Fig. 2.2**. Apart from vertical and horizontal FRP layers applied on the beam and columns, additional smaller strips were also used to provide better anchorage to the main FRP laminates in the beam and column.

In retrofitted specimen 2D2, which was tested under constant axial load, some hairline cracks occurred in both column faces and the beam-column joint intersection. Apart from these, no debonding, damage in the joint or delamination of the GFRP sheet was observed. Stable hysteresis behaviour without any degradation of bearing capacity was achieved until the end of the experiment.

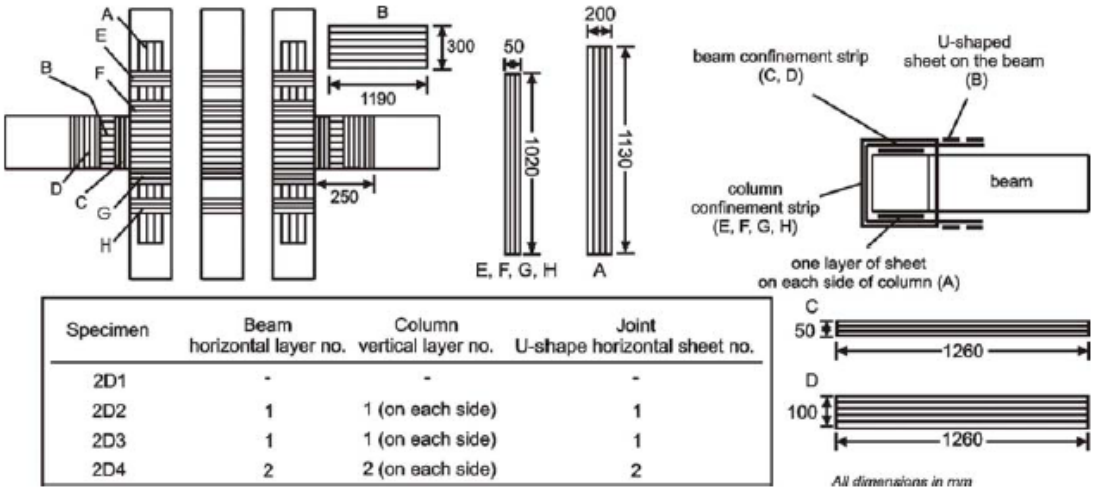

Specimen	Beam horizontal layer no.	Column vertical layer no.	Joint U-shape horizontal sheet no.
2D1	-	-	-
2D2	1	1 (on each side)	1
2D3	1	1 (on each side)	1
2D4	2	2 (on each side)	2

Fig. 2.2: GFRP retrofit configuration with top view layout by **Akguzel and Pampanin (2010)**

In specimen 2D3 (retrofitted with the same layout as specimen 2D2), which was tested under the varying axial load regime, a hybrid failure mechanism occurred. This consisted of gradual debonding of the GFRP sheet in the vicinity of the joint, bond deterioration and damage to the joint concrete core resulting in a lower load capacity at peak displacements. In addition, reloading cycles exhibited softening and pinching which led to a reduction of about 17% in terms of energy dissipation capacity when compared with the specimen 2D2. Although similar ductility levels were achieved, however the failure mode shifted from ductile (for specimen 2D2) to the brittle mode (for specimen 2D3). Also, the gradual debonding of the FRP sheets was initiated at a lower level drift (2.5%) in the beams compared to the specimen 2D2 in which no debonding was observed.

Thus it was shown that the retrofit solution designed under constant load conditions could be inadequate under varying axial load condition. The alternative retrofit scheme that was applied in the specimen 2D4 was proved to be sufficient enough to produce a satisfactory mode of failure.

Alsayed et al. (2010) studied the efficiency and effectiveness of carbon fiber-reinforced polymer (CFRP) sheets in upgrading the shear strength and ductility of four half-scale seismically deficient (inadequate joint shear strength with no transverse reinforcement) exterior beam-column joints. Out of these four as-built specimens, two specimens were used as control specimens (EC1 and EC2) and the other two were strengthened with CFRP sheets under two different schemes (ES1 and ES2). In the first scheme (Scheme #1, **Fig. 2.3**), CFRP sheets were epoxy bonded to joint, beams, and part of the column regions. In the second scheme (Scheme #2, **Fig. 2.4**), however, sheets were epoxy bonded to joint region only but

they were effectively prevented against any possible debonding through mechanical anchorages.

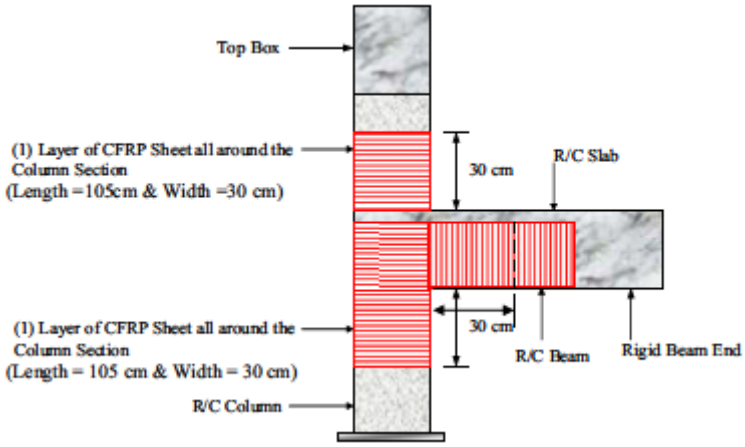

Fig. 2.3: Schematic representation of FRP Scheme #1 by **Alsayed et al. (2010)**

All these four subassemblages were subjected to cyclic lateral load histories so as to provide the equivalent of severe earthquake damage. The damaged control specimens were then repaired by filling their cracks through epoxy and externally bonding them with CFRP sheets under the same above two schemes. These repaired specimens (ER1 and ER2) were subjected to similar cyclic lateral load history and their response histories were obtained.

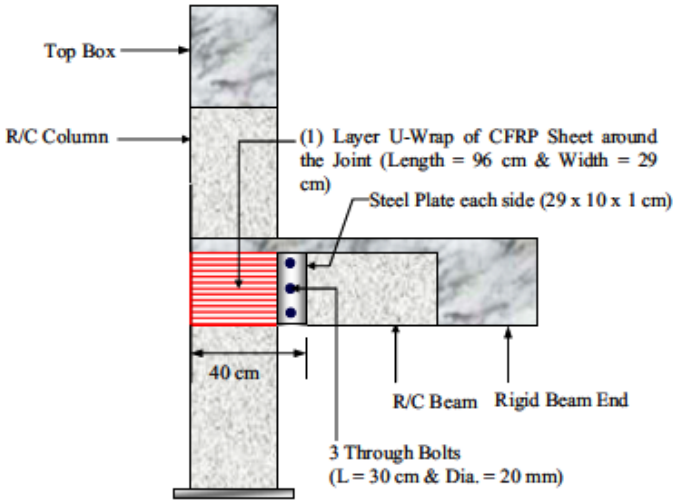

Fig. 2.4: Schematic representation of FRP Scheme #2 by **Alsayed et al. (2010)**

The hysteretic behaviour of exterior joints was examined in terms of shear strength (measured in terms of ultimate load) and deformation capacity. The ultimate load and deformation capacity for specimens ER1 and ER2 were significantly higher than their corresponding control specimens EC1 and EC2. This was primarily due to the increased confinement of joint resulting from externally bonded CFRP sheets.

Using the envelopes of load-displacement hysteretic curves, the peak load, ultimate displacements, and ductility for control, repaired, and strengthened specimens were obtained and are listed in **Table 2.1**. The table showed that the increase in average peak loads for repaired specimens ER1 and ER2 was substantially higher than their corresponding as-built control specimens EC1 and EC2. Further, a comparison of repaired specimens with their corresponding strengthened specimens showed that for Scheme #1, there was a considerable higher peak load for repaired specimen ER1 than strengthened specimen ES1. For Scheme #2, however, there was no remarkable difference between strengthened and repaired specimens peak load.

Table 2.1: Peak Test Load and Maximum Ductility by **Alsayed et al. (2010)**

Group	Specimen	Peak load (average) (kN)	Disp. at first yield of steel, Δ_y (mm)	Disp. at 10% drop of peak load, Δ_{10} (mm)	Disp. at 20% drop of peak load, Δ_{20} (mm)	Ductility factor Δ_{10}/Δ_y	Ductility factor Δ_{20}/Δ_y
1	EC1	47.08	18.67	28.7	30.0	1.54	1.61
	ER1	81.79	18.67[a]	36.7	40.7	1.97	2.24
	ES1	62.34	15.02	30.7	32.5	2.05	2.16
2	EC2	45.80	16.01	27.5	27.9	1.71	1.75
	ER2	58.63	16.01[a]	37.5	45.0	2.34	2.81
	ES2	58.11	18.69	33.7	36.5	1.80	1.95

[a]Taken same as respective control values.

Table 2.1 also showed that the application of CFRP sheets had improved the ductility of repaired and strengthened specimen significantly. For ER1 the increase in ductility was up to 39% and for ER2 it was up to 61% with respect to their respective control specimens. For specimens ES1 and ES2, however, the increase in ductility with respect to their corresponding control specimens was up by 34% and 11.4%, respectively.

A plot of stiffness degradation with lateral displacement showed that for Scheme #1, the initial stiffness of repaired or strengthened specimens were significantly higher than those of their corresponding control specimen. This high initial stiffness was attributed to external bonding of CFRP sheets on beams, joint, and column regions. However, for Scheme #2, as CFRP sheets were attached only on joint region, the initial stiffness of repaired and strengthened specimens was not substantially higher than those of their control specimens. It was also revealed that, in CFRP repaired or strengthened specimens, the degradation of

stiffness with lateral movement was slow compared to that of the corresponding control specimens. This is a desirable property in earthquake like situations.

Bansal et al. (2010) studied the effect of fiber orientation and stress level on the strength of stressed beams retrofitted with GFRP jackets. In the investigation 28 prototype beams of size 127 x 227 x 4100 mm reinforced with two bars of 10 mm diameter in tension and two bars of 8 mm diameter in compression for under-reinforced beams, and three bars of 12 mm diameter in tension and two bars of 8 mm diameter in compression for balanced beams were cast using M20 grade concrete. Out of these 28 beams, a set of four beams from each type (balanced and under-reinforced) were stresses to three stress levels 60, 75 and 90% of the safe load and then retrofitted with GFRP jackets with fibers oriented at 0 and 45^0 to the longitudinal axis of the beam.

It was observed from the experimental results that the beams retrofitted using GFRP jackets with fibers at 45^0 to the longitudinal axis yielded a higher increase in the maximum load carrying capacity. Also, it was felt that there was a need to consider initial stress level in order to calculate the maximum load carrying capacity of retrofitted beams. It was observed that there was lesser increase in ductility ratio for the balanced sections as compared to the under-reinforced sections. The toughness of the under-reinforced beams increased on average by 30.16%, and for the balanced beams the toughness increased on average by 66.4%. The increase in toughness was attributed to the increase in the stiffness of the section after the retrofitting.

Bousselham (2010) presented a comprehensive review and synthesis of published experimental studies on the seismic rehabilitation of RC frame beam-column joints with FRP. A total of 54 tests carried out worldwide were considered in the review, and a database of the published studies, encompassing all relevant design parameters, was assembled. The following observations were drawn by the author from the previous reported laboratory work. Firstly, the test results indicated substantial enhancement due to FRP in terms of strength, ductility, and energy dissipation. On the other hand, the test results showed that the stiffness degradation was significantly reduced in the presence of FRP. It was felt that it was not judicious to directly compare the efficiency of the various schemes proposed in the literature because the joint behaviour involved several parameters, such as the ratio of the flexural strength of column to that of the beam, the concrete strength, the joint reinforcement ratio, the bond conditions, that were not necessary similar in all the reported tests.

Secondly, most studies showed that the failure due to, or initiated by, debonding of the FRP sheets, including delamination, represented a potential scenario of rupture. On the other hand, the test results clearly demonstrated the important role of mechanical anchorage systems in limiting such undesirable mode of failure.

Thirdly, the test results confirmed that the performance increases significantly with, but not proportionally, to the FRP ratio, and the FRP sheets were more effective than strips. As for the effectiveness of carbon versus glass fibers, the study concluded that, for the same axial stiffness, glass fibers sheets proved marginally more effective than carbon fiber sheets.

Fourthly, other observations that were covered were: the positive effect of the column axial load as its intensity increased, and the decrease in the gain in strength due to FRP as the transverse reinforcement ratio increased.

Lee et al. (2010) proposed an effective rehabilitation strategy to enhance the strength and stiffness of the beam-column joint using carbon fiber reinforced polymer (CFRP). Three interior beam-column joints were tested in this study. JI0 represented the prototype, while JI1 and JI2 represented the strengthened specimens. The specimens were designed to represent the pre-seismic code design construction devoid of any transverse reinforcement. Rehabilitation scheme for specimens JI1 and JI2 are shown in **Fig. 2.5** and **Fig. 2.6** respectively. Note that to prevent debonding of the CFRP, no anchorage was used for specimen JI1 while it was used for specimen JI2.

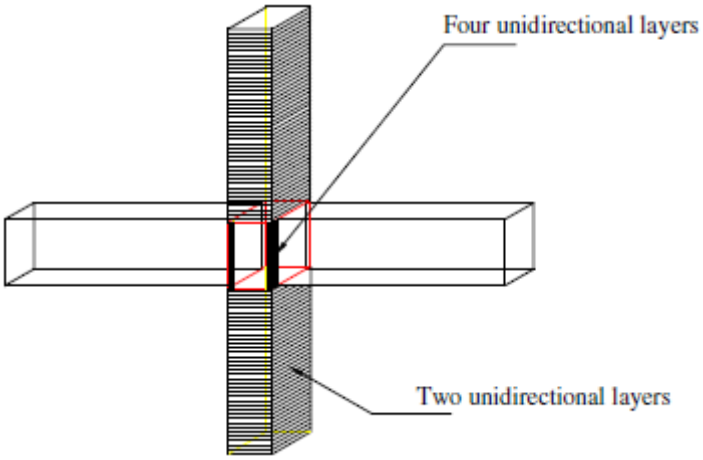

Fig. 2.5: Rehabilitation scheme for specimen JI1 by **Lee et al. (2010)**

The load-displacement loop of specimen JI1 showed that it was similar to that of specimen JI0 suggesting that the CFRP did not contribute much to the column shear of joint if the joint was strengthened with CFRP without anchoring. The first diagonal crack was observed in the joint core, and the crack progress was also similar to the control specimen. Specimen JI1 reached a maximum load of 139 kN at a 1.5% drift ratio, and the test was continued until a 3.0% drift ratio, when the load reached 80% peak load. The failure mode of the CFRP for this specimen was debonding.

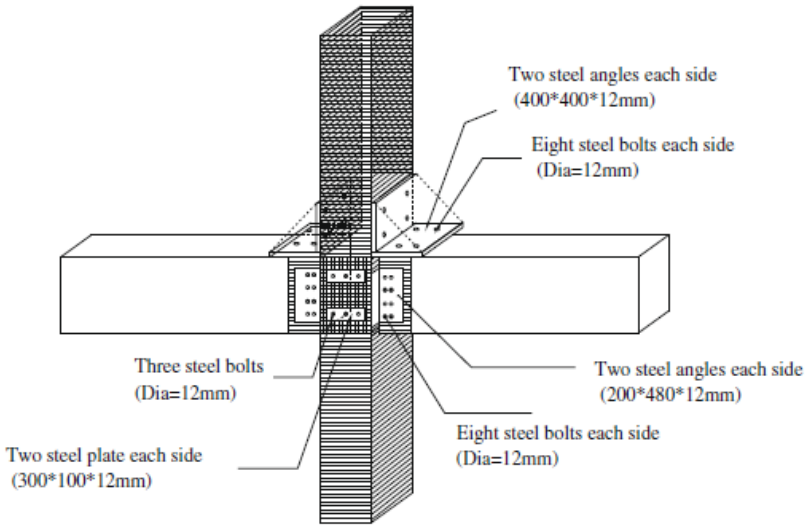

Fig. 2.6: Rehabilitation scheme for specimen JI2 by **Lee et al. (2010)**

The load-displacement loop of specimen JI2 showed that when the drift ratio was between 0% and 0.25%, the specimen behaved almost elastically. Strain field at 0.5% suggested that the CFRP began to work effectively to resist the deformation of the beam-column joint. Several cracks occurred in the beam at a 1% drift ratio, and specimen reached a peak load of 182 kN at a 2.0% drift ratio. No CFRP debonding was observed around the bolted plate in the joint zone. The test was continued until a 3.5% drift ratio, when the load reached 80% peak load.

The test results showed that the behaviour of the specimen JI1 strengthened with CFRP without anchoring was similar to that of specimen JI0. The ultimate strength of specimen JI1 increased only about 4%, which suggested that the CFRP without anchoring did not contribute much to the column shear of the joint. The appropriate anchoring in specimen JI2 had an important role in preventing the premature debonding of CFRP and upgrading the shear resistance of the beam-column joint.

Sharma et al. (2010) reported the results of a full scale RC structure repaired and retrofitted using a combination of CFRP and GFRP sheets (**Fig. 2.7**). The structure had been tested earlier under pushover loads till failure. Now the structure was retrofitted and re-tested. The FRP design criterion was set as to bring back the structure to almost at same level as original structure. It was found that the structure could reach 90% of the base shear as was recorded for original structure (**Fig. 2.8**), but the stiffness of the retrofitted structure was reduced and delamination was quite pronounced due to surface unevenness in locations that were critical but difficult to reach in practise. Although, in general the joint behaviour was improved due to prevention of spalling of concrete, the failure could not be prevented.

(a) **(b)**

Fig. 2.7: Full scale structure being tested under pushover loads (a) As-built; (b) Retrofitted by **Sharma et al. (2010)**

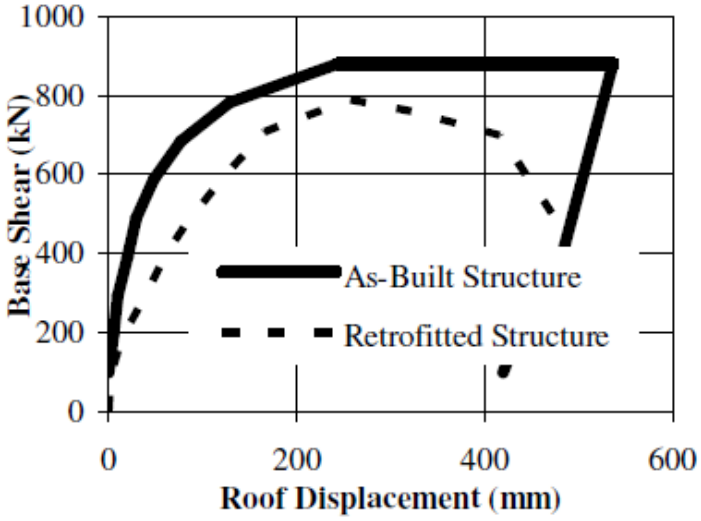

Fig. 2.8: Pushover curves by **Sharma et al. (2010)**

Li and Chua (2009) undertook experimental studies at Nanyang Technological University, Singapore to better understand the effects of different configurations of GFRP and CFRP strips and sheets on strengthening nonseismically detailed interior beam-column joints subjected to seismic loadings. The specimens were designed with column longitudinal bars just lap spliced above the floor level, beam bottom bars lap spliced within the joint, and with no transverse reinforcement within the joint core.

Fig. 2.9 illustrates the proposed FRP strengthening scheme for each of the three specimens SE1C, SC1C and SC2C.

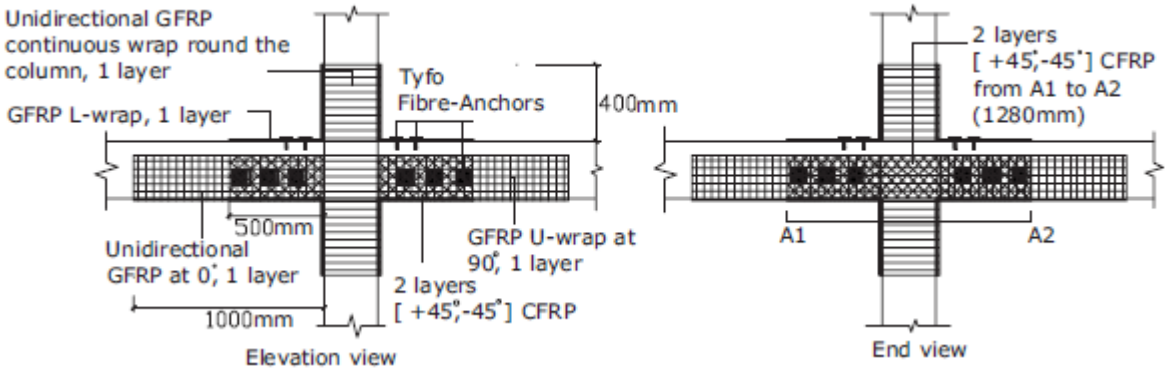

(a)

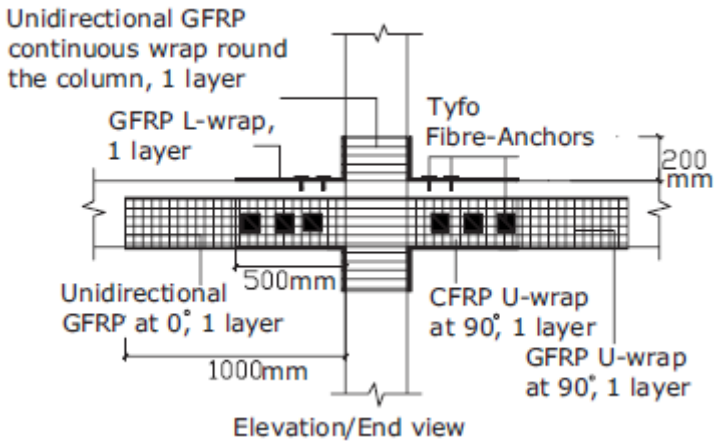

(b)

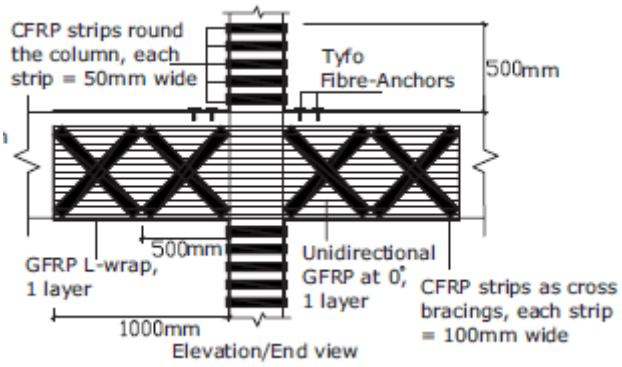

(c)

Fig. 2.9: Wrapping scheme for: (a) Specimen SE1C; (b) Specimen SC1C; (c) Specimen SC2C by **Li and Chua (2009)**

A comparison between the performance of original specimens and strengthened ones showed a tremendous increase in strength, stiffness and energy dissipation capacity. This was attributed to the following reasons: the use of two layers of $\pm 45^0$ CFRP strips at the joint and beam area was effective in strengthening eccentric joint. The use of CFRP strips on strong-column weak-beam was effective in flexural strength: CFRP strips round the column and CFRP strips as cross bracings on the beam and column face. Good anchorage in the form of fiber anchors was effective in anchoring FRP sheets and strips; they contributed much to the shear strengthening of beam-column joint and beam. To develop the strength of the fiber, it was recommended that the anchorages be installed at beam bottom near the beam-column interface and at the edges of FRP strips and sheets near the joint core. On the other hand, it was noted that beam jacketing in the form of FRP U-wrapping was necessary in preventing shear failure in the beam and allowed a flexural hinge to develop.

The proposed strengthening schemes were successful in eliminating or delaying the shear mode of failure. Instead, flexural hinging of the beam, a ductile mode of failure, occurred in the form of cracks near the joint corners for specimen SE1C and delamination of FRP strips at beam-column interface near joint core region for specimen SC1C and specimen SC2C.

Bansal et al. (2008) studied the effect of wire mesh orientation on the strength of stressed beams retrofitted with ferrocement jackets. To carry out the investigation, eight prototype beams of size 127 x 227 x 4100 mm reinforced with two bars of 10 mm diameter in tension and two bars of 8 mm diameter in compression were cast using the proportioned mix.

Out of these, six beams are stresses up to 75% of safe load and then retrofitted with 15 mm thick ferrocement jackets with wire mesh at different orientations viz. 0, 45, and 60 degree.

The results showed that the percent increase in load carrying capacity for beam retrofitted with ferrocement jackets with wire mesh at 0, 45, 60 degree angle with longitudinal axis of beam, varied from 45.87 to 52.29 percent. Also a considerable increase in energy absorption was observed for all orientations. However, orientation at 45 degree showed higher percentage increase in energy absorption followed by 60 and 0 degree respectively. After retrofitting, all the test specimens showed reduced crack widths, large deflection at the ultimate load and a significant increase in the ductility ratio.

Ludovico et al. (2008) performed an experimental program on the seismic behaviour of a full-scale RC structure retrofitted using GFRP laminates to assess the effectiveness of different retrofit methodologies. The structure was designed in order to represent a typical housing building in most earthquake-prone areas of Europe in which issues related to plan irregularity, poor local detailing, scarcity of rebars, insufficient confinement and weak joints, combined with old construction practice, were commonly found.

For the seismic retrofit of the structure, GFRP column confinement was undertaken to increase the ductility of the plastic hinges at column ends with two plies of GFRP uniaxial laminates for a length of 800 mm from the beam-column interface (**Fig. 2.10a**) greater than the plastic hinge length of about 380 mm. In order to prevent brittle shear failure of the connections due to increased ductility of the columns, further FRP retrofit was designed on beam-column joints corresponding to corner columns according to the approach proposed by **Antonopoulos and Triantafillou (2002)** using two plies of quadriaxial GFRP laminates that were extended on the beams by 200 mm on each side (**Fig. 2.10b**).

Despite the similarity in terms of base shear and top displacement at the PGA level equal to 0.20 *g*, it was observed that the retrofitted structure was almost undamaged after the test, while the as-built structure showed significant damage on the structural members, especially columns. At the seismic level intensity of 0.30 *g*, the maximum displacement recorded on the retrofitted structure was significantly enhanced confirming the effectiveness of the retrofit technique.

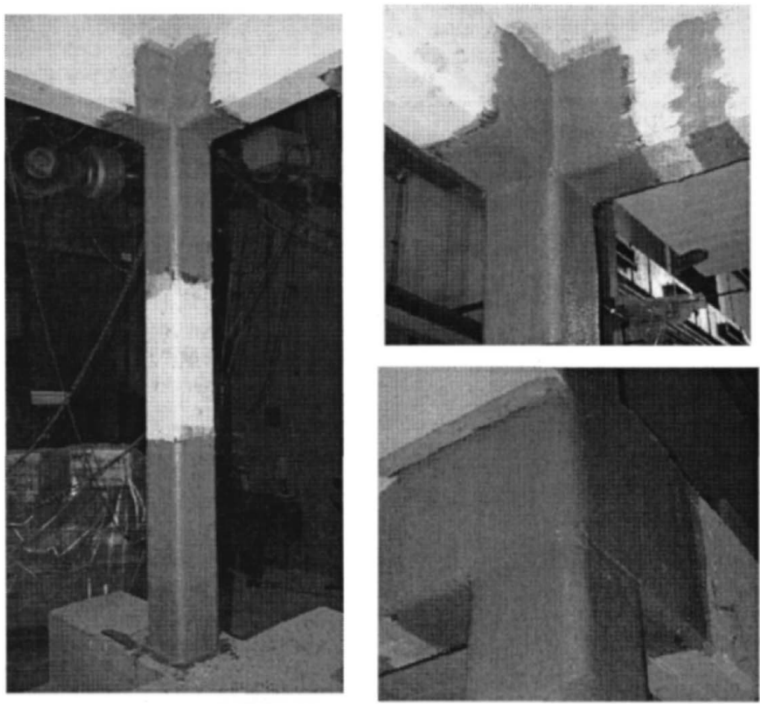

(a) **(b)**

Fig. 2.10: GFRP retrofit of the structure: (a) column confinement; (b) unconfined joint retrofit by **Ludovico et al. (2008)**

Mahini and Ronagh (2007) performed an experimental study to evaluate the ability of CFRP sheets in preventing the plastic hinge formation at the face of the column in exterior RC joints. Five plain/CFRP-retrofitted scaled down joints of a typical OMRF were tested under monotonic/cyclic loads to failure. CSM0 and CSC1 represented plain specimens while RSM1, RSM2 and RSC1 represented CFRP retrofitted specimens. FRP sheets of specific lengths (**Table 2.2**) were stuck to the sides of the beams of the joint (i.e. web-bonded FRP) and extended over the joint to act as an anchor.

Table 2.2 also shows the maximum strengths and the estimated ductility of all specimens. As was seen, the maximum load recorded in these tests was about 24.64, 24.70, and 21.12; for specimens CSM0, RSM1 and RSM2 all in kN respectively. The maximum load strength recorded for specimen RSM1 was about that of the plain specimen CSM0 whereas that for specimen RSM2 was only 86% of the maximum strength of plain specimen CSM0. This was attributed to the fact that the retrofitting length of this specimen was not sufficient enough to carry loads at the early stages of the test.

Table 2.2: Summary of the test results by **Mahini and Ronagh (2007)**

Specimen	Loading type	No. of CFRP piles	CFRP wrapping length (mm)	Maximum strength (kN)	Displacement ductility factor	Failure mechanism	Failure location
CSM0	Monotonic	-	-	24.64	5.8	Ductile	Beam end
RSM1	Monotonic	1	350	24.70	-	Sudden	Beam end
RSM2	Monotonic	3	200	21.12	5.7	Ductile	Within the beam
CSC1	Cyclic	-	-	19.52	6.5	Ductile	Beam end
RSC1	Cyclic	3	200	21.32	6	Ductile	within

Specimen RSC1 was subjected to cyclic loading regime as plain specimen CSC1. During the first few cycles of displacement control, no crack was observed at the column face. In fact all cracks shifted beyond the cut-off of CFRP. First signs of debonding of FRP sheets were observed at the seventh cycle of loading. In the cycles that followed, steel bars started to carry the developed tensile force and in the ninth cycle, the top steel bars of the beam started to buckle. This buckling occurred around 150 mm away from the column face and was considered as the centre of plastic hinge. Thus, it was concluded that FRPs have been able to shift the location of plastic hinge 150 mm away from the column face which was about 65% of the section depth and three quarter of the length of FRP coverage.

Another evidence which indicated the satisfactory behaviour of the retrofitted specimens was their displacement ductility. Specimen RSM1 with only one ply of CFRP sheet failed by concrete crushing and did not allow for adequate ductility (**Table 2.2**). Specimen RSM2 exhibited a ductile failure with a ductility factor of 5.7 which was about that of the plain specimen CSM0. Also similar displacement ductility were calculated for specimens CSC1 and RSC1 but the failure of specimen RSC1 was located further from the beam end and joint core indicating that the plastic hinge in this specimen was relocated from the joint core towards the beam under cyclic loading regime and therefore the performance of the frame was converted into a ductile manner.

Ghobarah and El-Amoury (2005) compared the performance of rehabilitated reinforced concrete beam-column joints with the response of existing joints designed to pre-seismic codes to assess proposed rehabilitation techniques. Six beam-column subassemblies with non-ductile reinforcement detailing were subjected to simulated seismic forces.

Specimens T-B12 and T-B11 having inadequate anchorage length of the bottom beam bars were strengthened by using carbon-fiber-reinforced polymer (CFRP) sheets attached to the bottom beam face (**Fig. 2.11a** and **Fig. 2.11b** respectively) while specimens T-SB8 and T-SB7 having no steel ties installed in the joint zone, in addition to inadequate anchorage length of the beam bars were strengthened by glass-fiber-reinforced polymer (GFRP) jackets of the joint zone and steel rods or plates (**Fig. 2.11c** and **Fig. 2.11d** respectively).

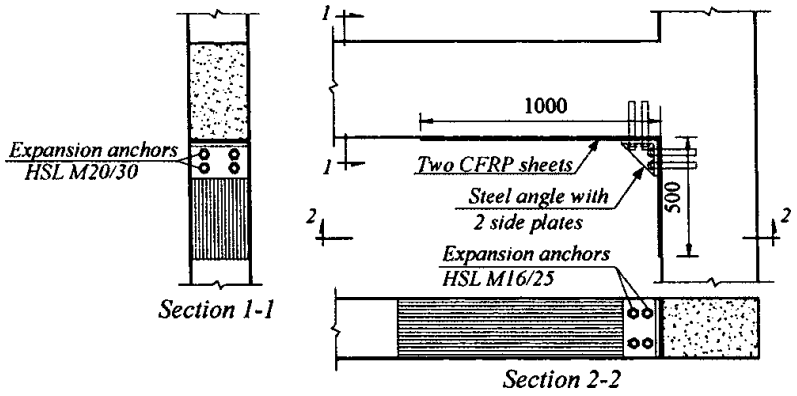

(a)

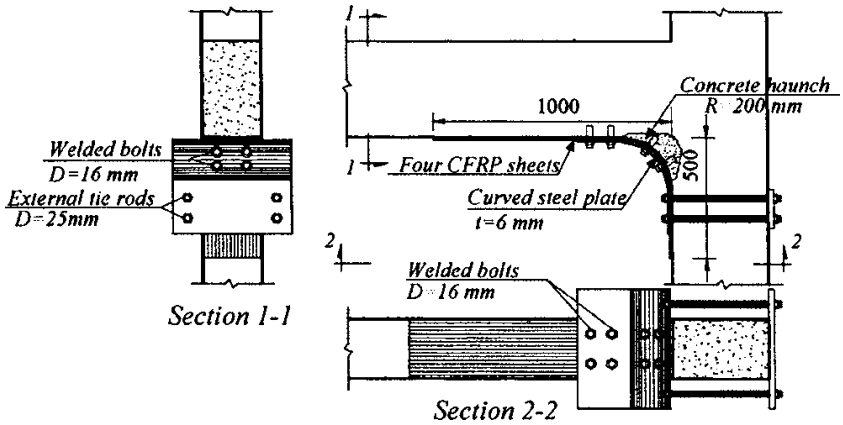

(b)

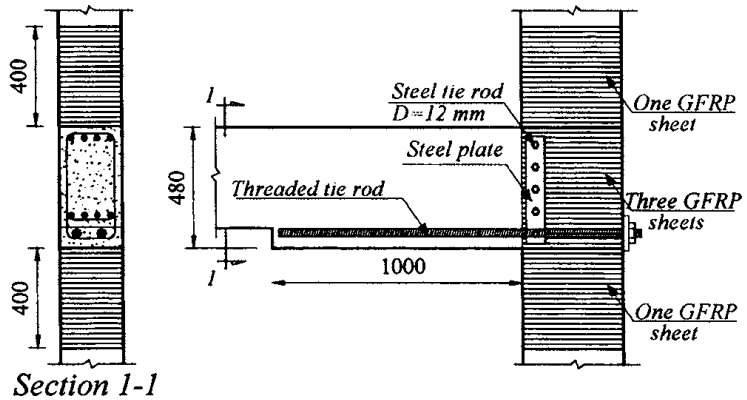

(c)

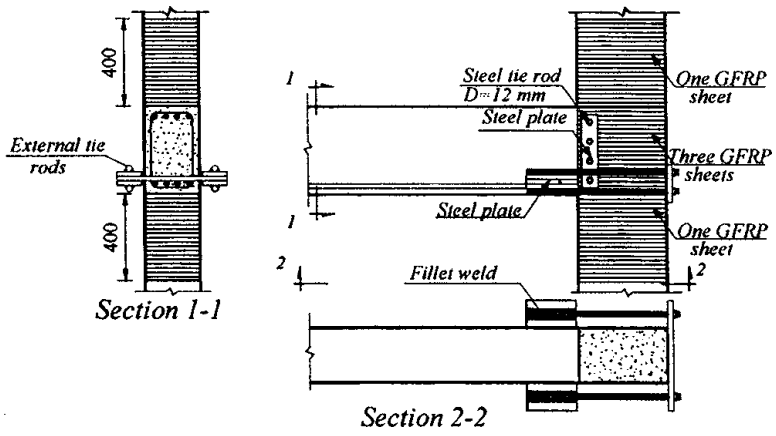

(d)

Fig. 2.11: Strengthening joint (a) T-B12; (b) T-B11; (c) T-SB8; (d) T-SB7 by **Ghobarah and El-Amoury (2005)**

The rehabilitation techniques were found effective in eliminating the brittle joint shear and steel bar bond-slip failure modes, and instead ductile beam hinging occurred. For specimens TB-12 and TB-11, CFRP sheets were found effective in replacing the anchorage-deficient beam bars, when an adequate anchorage system of these sheets was provided. For specimens T-SB8 and T-SB7, GFRP jacket was found to be an effective system to provide confinement and shear strength to shear-deficient joints. External steel tie-rods welded to the existing deficient beam reinforcement were found to be a simple and effective technique to improve the anchorage conditions of these bars so that the bars' tensile strength could be fully developed.

Mukherjee and Joshi (2005) examined the performance of fiber reinforced polymer composites (FRP) in upgradation of healthy beam-column joints with adequate and deficient reinforcements and also in rehabilitation of damaged joints. One set of joints had adequate steel reinforcements with proper detailing of reinforcements at the critical sections called "Ductile specimens". The other set of specimens had deficient bond lengths of the beam reinforcements at the junctions with the columns and were called "Non-Ductile specimens". The specimens were also strengthened by using carbon and glass FRP materials. The schematic arrangement for two typical systems used in the study; L-overlays and precured carbon plates is shown in **Fig. 2.12** and **Fig. 2.13** respectively. The control specimens without FRP were used after testing to evaluate the rehabilitation of joints with FRP called "Rehabbed specimens".

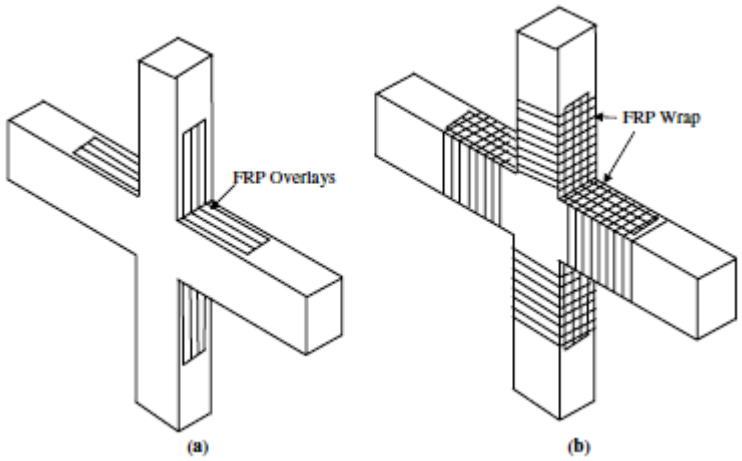

Fig. 2.12: Type A strengthening system – use of composite overlays by **Mukherjee and Joshi (2005)**

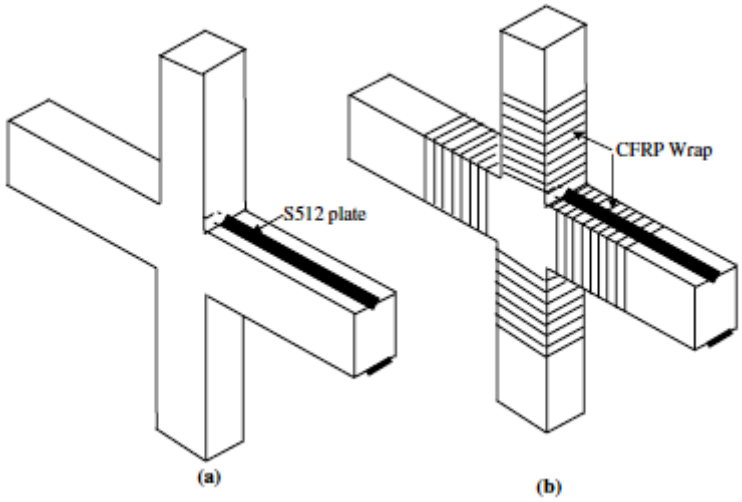

Fig. 2.13: Type B strengthening system – use of precured carbon plate by **Mukherjee and Joshi (2005)**

It was observed that for ductile specimens the load at yield was considerably higher in the FRP reinforced specimens than the control specimen. For the same tip load, the tensile force in steel was lower in the carbon reinforced specimen than in the glass reinforced specimens. Thus, the steel in the carbon reinforced specimens yielded at higher tip loads. The displacement at yield increased to a much lesser extent than the load due to FRP reinforcements. The load-displacement envelopes showed that all the FRP reinforced specimens had higher peak loads than the control specimen.

Stiffness degradation plots showed that all the FRP reinforced specimens had a total loss of stiffness at a higher displacement level than the control specimen. The carbon specimens had higher initial stiffness and slower rate of degradation. The cumulative energy dissipation graphs showed that the energy dissipation of the FRP reinforced specimens

followed closely that of the control specimen because FRPs remain elastic until failure and not much dissipation of energy was expected through the deformation of the FRP. However, the FRPs had increased the ultimate deformation of the structure to a large extent. The photographs of the failed specimens showed that the confinement provided by the FRP reinforced joints impeded the creation of hinge through the spalling of concrete.

The load versus displacement envelops for the rehabbed specimens showed that the use of composite system not only restored the original capacity of damaged specimen, but also upgraded the ultimate load capacity by 55%. Also displacement at ultimate load was increased by 30%. Stiffness versus displacement curve showed that there was 48% increase in initial stiffness. An increment of 57% was observed in energy dissipation capacity of structure after the rehabilitation.

The photographs of the failed non-ductile specimens showed that the beam had failed at the joint by pull out of steel reinforcement. Lack of development length prevented the formation of plastic hinge. The FRP reinforced specimens, however, did not have the reinforcement pull out. The difference in the failure mode was due to the confinement provided by the FRP overlays and wraps to the joint. They held the beam in its position. As a result, the cracked concrete surfaces closed and they could react against each other at subsequent cycles. Therefore, the moment resistance of the beam was not lost. This offered higher collapse loads and displacement.

Prota et al. (2004) used CFRP rods in combination with externally bonded sheets (**Fig. 2.14**) to upgrade and test eleven one-way interior joints with three different levels of column axial load in an attempt to shift the failure first from the column to the joint, then from the joint to the beam. The CFRP rods were placed in epoxy-filled grooves prepared near the surface.

The failure modes could not be controlled as intended, and a ductile beam failure was not achieved. The Type 2 scheme moved the failure from the compression to the tension side of the column for low column axial load while, for high axial load, a combined column-joint failure occurred. The addition of CFRP rods as flexural reinforcement along the column (Type 3) led to a joint shear failure. When the joint panel was also strengthened (Type 4), the column-joint interface failed, which was attributed to termination of the FRP sheet reinforcement at that location to account for the presence of a floor system.

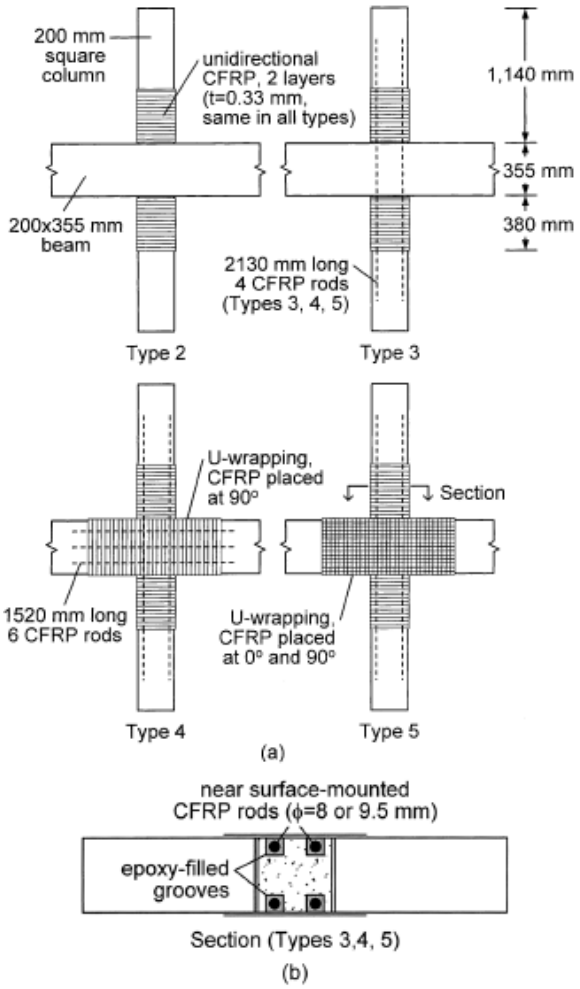

Fig. 2.14: Specimens strengthened with CFRP sheets and/or rods tested: (a) elevation; and (b) plan by **Prota et al. (2005)**

The increases in strength were 7 to 33% for Type 2, 39 and 62% for Type 3, and 37 and 83% for Type 4. The changes in the maximum story drift for low and high column axial load were -11 and 25% for Type 2, 6 and -14% for Type 3, and 73 and 51% for Type 4, where negative values indicate loss of ductility. The Type 5 scheme with U-wrapping of the beam and joint resulted in a failure mode similar to that of Type 4.

Antonopoulos and Triantafillou (2003) conducted 2/3-scale reverse-cycle tests on 18 exterior joints strengthened with various configurations of pultruded carbon strips and with flexible carbon or glass fiber sheets. The investigated variables were the following: area fraction and distribution of FRP, column axial load, internal joint reinforcement, initial damage, carbon versus glass fibers, sheets versus strips, and the effect of transverse stub beams.

All 18 specimens were designed to fail in joint shear both before and after strengthening so that the contribution of FRP to the joint shear capacity could be evaluated. Consequently, the failures were preceded by partial or complete debonding of composites (either at the unanchored ends or near the joint corners), leading to substantial pinching in the hysteresis loops. An increase in column axial load from 4 to 10% of its axial load capacity improved the strength increase from 65 to approximately 85% and the energy increase from 50 to 70%. The increase in stiffness varied in each loading cycle and reached values around 100%.

The conclusions of this research highlighted the need for mechanical anchorage, better performance of flexible sheets over strips, the positive effect of increased column axial load on shear capacity of FRP-strengthened joints, better energy dissipation due to glass fibers than carbon fibers, increased effectiveness of FRP due to less internal joint reinforcement, and the negative effect of transverse stubs on the effectiveness of FRPs.

El-Amoury and Ghobarah (2002) modified the GFRP schemes used by **Ghobarah and Said (2002)**, as shown in **Fig. 2.15**, for strengthening joints with both inadequate anchorage of beam bottom bars and no hoop shear reinforcement.

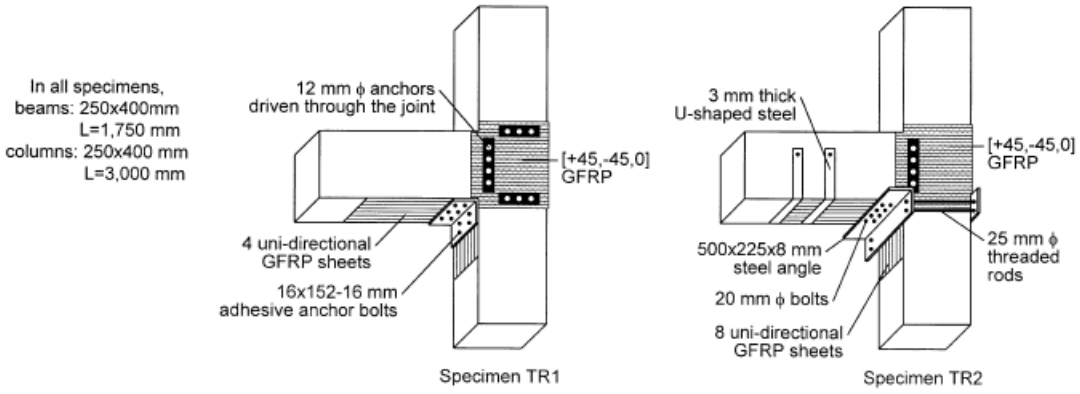

Fig. 2.15: GFRP-strengthened specimens tested by **El-Amoury and Ghobarah (2002)**

Both schemes resulted in an approximate 100% increase in load-carrying capacity; specimen TR1 and TR2 dissipated three and six times the energy dissipated by the reference specimen, respectively. The failure of Specimen TR1 was due to complete debonding of the composites from the beam and column surfaces, and pullout of the beam bottom bars led by fracture of the weld around the bolt heads. In Specimen TR2, the use of two U-shaped steel plates eliminated debonding of the GFRP and reduced the strength degradation; this specimen eventually failed in joint shear.

Ghobarah and Said (2002) tested four, one-way exterior joints (**Fig. 2.16**), originally designed to fail in joint shear, with or without strengthening by unidirectional or bidirectional (±45 degrees) glass fiber-reinforced polymer (GFRP) sheets.

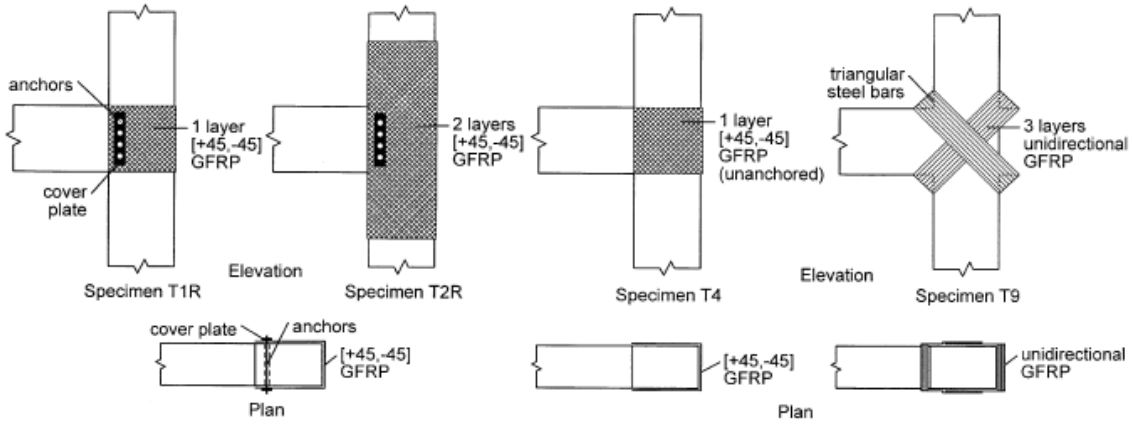

Fig. 2.16: GFRP-strengthened specimens tested by **Ghobarah and Said (2002)**

Specimens T1R and T2R, previously damaged in the joint region and repaired, were provided with mechanical anchorage using steel plates and threaded rods core-drilled through the joint. While the GFRP sheet anchored through the joint in Specimen T1R was effective until it failed in tension, it provided no improvement in Specimen T4 due to lack of threaded-rod anchorage and the resulting early delamination. No debonding or joint shear cracking was observed in Specimen T2R; the failure was due to a beam plastic hinge. The placement of the diagonal unidirectional strips in Specimen T9 was felicitated by the triangular steel bars fitted at the four corners of the joint panel. This scheme could not prevent expansion of the joint concrete, which led to delamination and a simultaneous failure of the beam and joint. Overall, this study highlighted the importance of anchorage of composite sheets in developing the full fiber strength in a small joint area.

Ghobarah and Said (2001) presented an innovative and practical technique for the seismic rehabilitation of beam-column joints using FRP to upgrade their shear capacity and thus allow the ductile flexural hinge to form in the beam. The beam-column joint specimen designated as T1 was designed with no transverse reinforcement and tested as control specimen. The joint was repaired and rehabilitated using one layer of bidirectional (in 45^0 degree) GFRP laminate in the form of a "U" (**Fig. 2.17**). The free ends of the "U" were tied together using threaded steel rods driven through the joint section and a steel plate. This specimen was designated as T1R and re-tested.

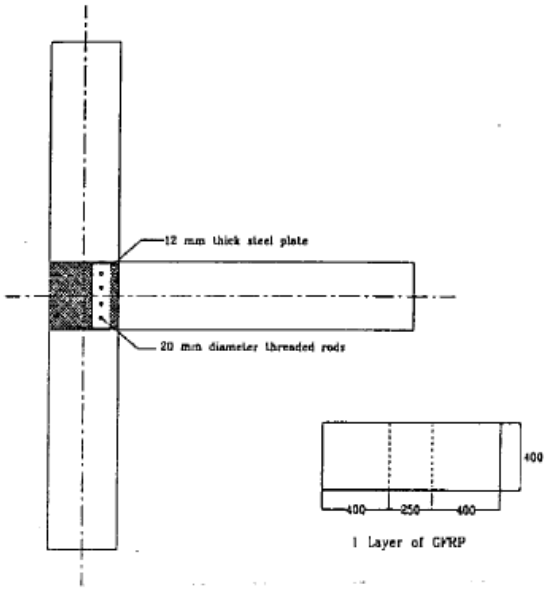

Fig. 2.17: Proposed joint rehabilitation scheme using FRP by **Ghobarah and Said (2001)**

A comparison of the load-deflection plots showed a slightly higher yield load for specimen T1R as compared to specimen T1. The envelopes of the beam tip load-displacement curves indicated that a lower rate of deterioration of strength, a higher ductility up to failure (increased by 60%) and a slightly higher initial stiffness in the repaired specimen T1R. A plot of the cumulative energy dissipation with the loading cycles showed that the total energy dissipation of specimen T1R was three times higher than that of specimen T1. Plots of story shear-joint shear deformation showed that for specimen T1 the joint shear deformation increased with increasing story drift, while the plot was different for specimen T1R as the joint showed a stiffer behaviour.

Gergely et al. (2000) presented the experimental results of 14 1/3-scale tests of concrete beam-column T-joints using FRP composite materials. There were four baseline specimens tested in the as-built condition. The remaining specimens were externally reinforced using composite woven sheets. The variables considered were the composite curing process, the CFRP layout, and the surface preparation of the concrete specimens.

Fig. 2.18 gives a general composite layout. For each specimen, the dimensions L_i, the fiber orientations, the curing temperatures, and the surface preparation are summarized in **Table 2.3**.

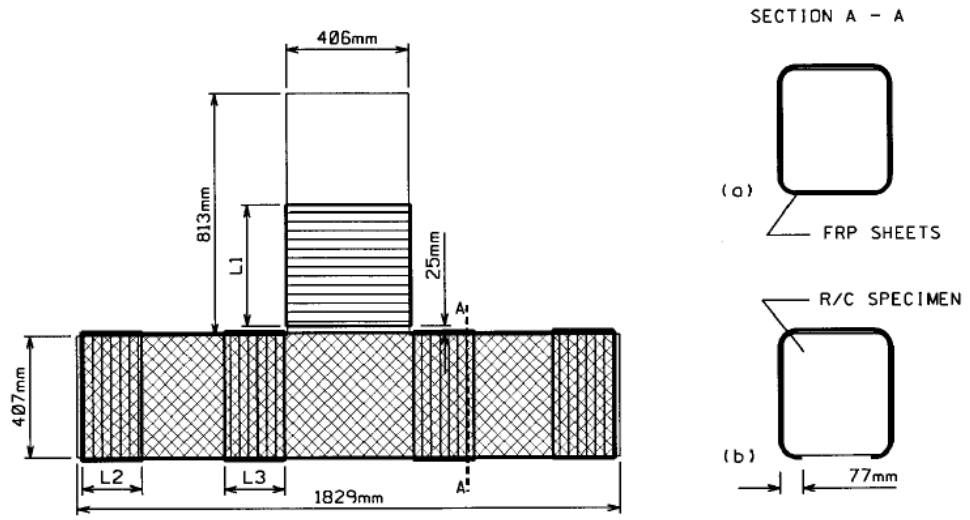

Fig. 2.18: CFRP layout on: (a) Four sides of Beam; (b) Three sides of beam by **Gergely et al. (2000)**

Table 2.3: Beam-Column Joint Specimen CFRP layout by **Gergely et al. (2000)**

Phase	Specimen	Surface preparation	CFRP layout[a]	Curing temperature	L_1 (mm)	L_2 (mm)	L_3 (mm)
I	1[b]	N/A	N/A	N/A	N/A	N/A	N/A
	2[b]	N/A	N/A	N/A	N/A	N/A	N/A
	3	Wire brush	[45]	350^0F	0	178	0
	4	Wire brush	[±45]	350^0F	0	178	0
	5	Wire brush	[45]	Room	0	229	0
	6	Wire brush	[45]	Room	432	229	406
	7	Wire brush	[45]	Room	432	229	406
	8	Wire brush	[±45]	Room	0	203	0
	9	Wire brush	[±45]	Room	406	229	203
II	10[b]	N/A	N/A	N/A	N/A	N/A	N/A
	11[b]	N/A	N/A	N/A	N/A	N/A	N/A
	12	Water jet and structural adhesive	[±45]	Room	406	203	406[c]
	13	Water jet and structural adhesive	[±45]	Room	406	203	406[c]
	14	Water jet and structural adhesive	[±45]	Room	406	203	406[c]

Note: N/A/ = not available
[a]CFRP layout on each vertical face of beam.
[b]Baseline specimens.
[c]Only on three sides.

From the joint tests performed, it was observed that the failure of the baseline specimens was identical, with extensive diagonal tension cracks in the joint region, which extended into the beam at the level of the bottom longitudinal reinforcement. The FRP reinforced specimens reached their peak load, but as the composite delaminated, this load level could not be sustained. This caused specimen failures at lower loads and corresponding bending moments more than the element's capacity.

Superior performance was achieved by water jetting the concrete surface and using a high strength adhesive. There was no evidence of better joint shear improvement by using an elevated temperature cure system versus room temperature. The most effective fibers in the joint region were inclined at 45^0, the direction of the principal planes. Delamination of the inclined FRP sheets was observed to start from the top and bottom of the joint, which reinforced the importance of proper anchorage.

The performance of the specimens was a function of the concrete-composite bond. Delamination occurred at stress levels of only a fifth of the composite's capacity. There were no significant compression stresses in the inclined composite layers, because the concrete in the joint could resist the diagonal compression forces.

2.2 RETROFITTING OF CONCRETE STRUCTURES – ANALYTICAL MODELLING & DESIGN

Akguzel and Pampanin (2012) presented an analytical procedure for the evaluation of the expected performance of existing reinforced concrete (RC) beam-column joints before and after being retrofitted using FRP composite materials. The contribution aimed at proposing a rational step-by-step procedure, relatively simple to implement in a spreadsheet program, for the assessment of RC beam-column joints in their as-built and retrofit configurations.

A detailed assessment of each joint component within the beam-column joint subassembly was firstly performed in its as-built configuration. The components capacities were compared within a M-N (moment-axial load) performance domain in order to establish the internal hierarchy of strength and the sequence of events before the retrofit intervention while accounting for the correct demand conditions. The total shear strength of the retrofitted joint was evaluated as sum in parallel (for the same joint shear deformation) of the strength contributions of the as-built plain concrete and the composite material attached to the plain concrete.

In **Fig. 2.19** and **Fig. 2.20**, a schematic illustration of the average stresses, the external and internal actions, with the nomenclature used in the design and assessment of exterior RC joint strengthened with FRP, are shown with the idealization of the joint as a three-dimensional element.

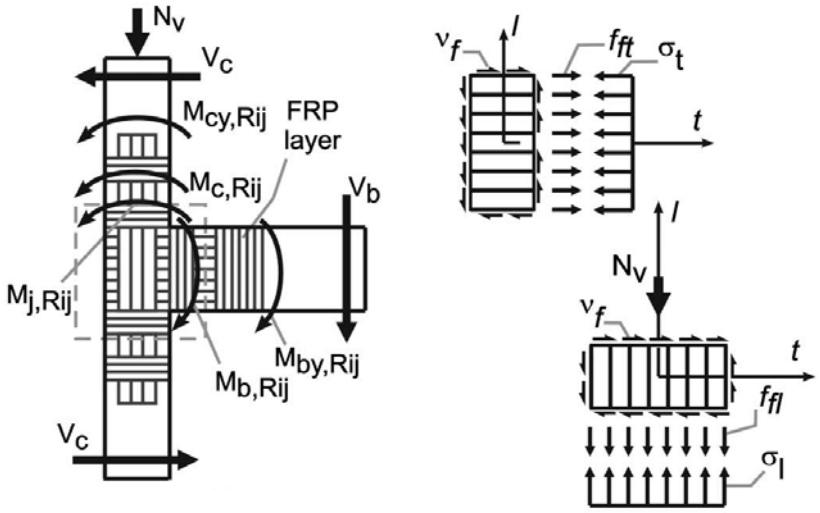

(a) **(b) and (c)**

Fig. 2.19: Exterior RC joint shear resisting mechanisms: a) forces acting on a retrofitted joint; b) horizontal force equilibrium; c) vertical force equilibrium by **Akguzel and Pampanin (2012)**

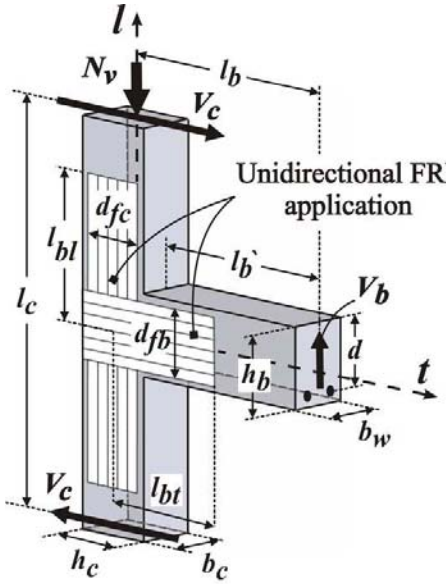

Fig. 2.20: Exterior RC joint strengthening with FRP: schematic illustration of design dimensions by **Akguzel and Pampanin (2012)**.

The authors developed an iterative procedure to evaluate the joint shear capacity after FRP strengthening which is reproduced below:

The input consisted of:

1. *Geometric data:* h_b, b_w, h_c, b_c;
2. *Material properties:* compressive strength of concrete, $f_c^{'}$; elastic modulus of concrete, E_c; tensile strength of concrete, f_{ct}; FRP thickness per layer, t_f; design rupture strain in the FRP, ε_{fu}; and elastic modulus of the fibers, E_f,
3. *FRP application scheme details:* depth of FRP sheet on beam surface, d_{fb}; depth of FRP sheet on column surface, d_{fc}; number of sheet on beam, n_{fb}; number of sheets on column, n_{fc}; number of beam sides covered with FRP , $n_{sf,b}$;
   number of column sides covered with FRP, $n_{sf,c}$. FRP reinforcement ratio in the transverse or longitudinal direction was found as follows:

$$\rho_{ft} = \frac{n_{fb} n_{sf,b} t_f d_{fb}}{h_b b_w}$$

$$\rho_{ft} = \frac{n_{fc} n_{sf,c} t_f d_{fc}}{h_c b_c}$$

At the end of each iteration step, two failure conditions were checked:

1. *Debonding or failure of FRP*: The FRP will fail by tensile fracture when the tensile stress reaches the tensile strength, f_{fu} or corresponding ultimate strain, ε_{fu}. The maximum tensile stress in an FRP strip of thickness, t_f, in mm when debonding occurs, (i.e. on beam side) was given by

$$f_{f,max} = f_{f,deb} = c_1 \sqrt{\frac{E_f f_{ct}}{t_f n_{fb}}} \quad \text{for} \quad l_{bt} \geq l_{b,max}$$

   where c_1 was an empirical coefficient taken as 0.64 for CFRP and l_{bt} was FRP development length along the direction t (in mm).

$$l_{b,max} = \sqrt{\frac{E_f t_f}{c_2 f_{ct}}}$$

   where c_2 is taken as 2.

2. *Diagonal compression failure of the concrete in the joint panel zone*: In order to satisfy capacity design considerations, the diagonal compression stress in the joint

panel zone was to be limited ($p_c \leq 0.3f_c'$) to prevent premature brittle failure of the compression strut especially after the development of multiple diagonal cracks.

By employing the aforementioned relationships, the FRP contribution to the increase in the joint shear capacity of poorly detailed beam-column joint could be adequately estimated in terms of principal tensile stress, p_{tf}, as a function of the amount and layout of the externally bonded reinforcement.

The authors compared the analytical model predictions with experimental test results available from the past literature and confirmed the validity of the proposed design procedure.

Mahini and Ronagh (2010) developed an analytical model to calculate the first yield load, the ultimate load and the corresponding ductility of the web-bonded FRP beam using the first principles. The following major flexural failure modes of concrete beams strengthened with web-bonded FRP reinforcement were considered:

- De-bonding;
- Yielding of reinforcing steel in tension followed by the rupture of FRP (FRP rupture);
- Yielding of reinforcing steel in tension followed by concrete crushing (tension failure);
- Crushing of concrete in compression before yielding of the reinforcing steel (compression failure).

Since de-bonding was not observed in experimental tests, it was not considered in the derivation. A trial and error procedure was established to quantify the moment-curvature graph into pre-cracking, cracking and post-cracking stage. In line with the classical approach, it started with the estimation of the neutral axis depth and ended with a calculated value based on the force equilibrium using the constitutive laws of the materials and the strain compatibility in the section. If the differences between the two values were small, the estimated values were accepted; otherwise they were modified using the bisection method until convergence occurred.

A typical rectangular RC beam strengthened with web-bonded FRP was considered with b and h being the width and height of the section (**Fig. 2.21**). The fiber composite was considered to have a thickness t_f and stress f_f, the tensile steel reinforcement, an area A_s and

stress f_s and the compressive reinforcement, an area A'_s and stress f'_s. The concrete was considered to have a compressive strength f'_c.

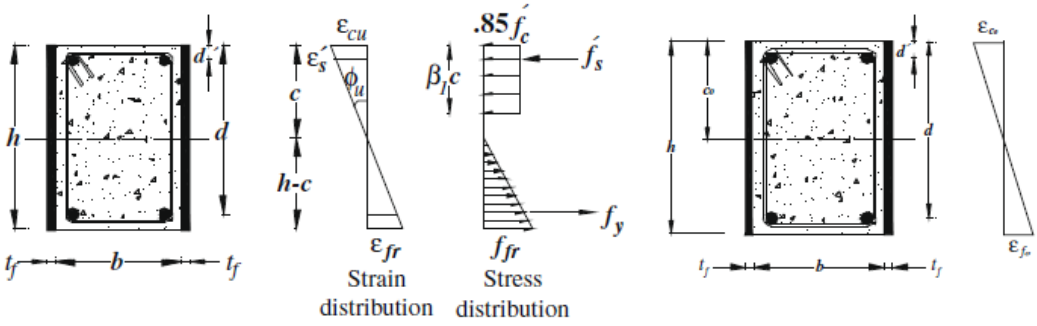

Fig. 2.21: (a) General stress and strain distributions of web-bonded FRP beams and (b) strain compatibilities of beam before retrofitting by **Mahini and Ronagh (2010)**

The two possibilities at ultimate were "FRP rupture" and "tension failure": if $\varepsilon_{fr} + \varepsilon_{f_o} < \varepsilon_{cu}((h-c)/c)$, then the failure was governed by "FRP rupture", and if $\varepsilon_{fr} + \varepsilon_{f_o} > \varepsilon_{cu}((h-c)/c)$, then the failure was governed by "tension failure". In these, ε_{fr} and ε_{f_o}, were the ultimate strain of FRP and the initial strain of the unstrengthened beam at the extreme tensile level of the RC section respectively, ε_{cu} was the ultimate compressive strain in the concrete (**Fig. 2.21**). $\varepsilon_{ft} = \varepsilon_{fr} + \varepsilon_{f_o}$ was the total strain at the extreme tensile level of the FRP wrap and c was the neutral axis depth at ultimate conditions.

The following expression of c was obtained from equilibrium:

$$c = \frac{A_s f_s - A'_s f'_s + f_f(h-c)t_f}{0.85 f'_c \beta_1 b}$$

This value was checked against the estimated neutral axis depth and changed until convergence occurred.

The ultimate flexural capacity of the FRP web-bonded beam was calculated by considering both the failure modes. The maximum attainable curvature of the web-bonded FRP beam was expressed as: $\phi_u = \varepsilon_{cu}/c$ with the maximum dependable concrete compression strain in the extreme fiber ε_{cu} assumed as 0.003 when normal strength concrete was used.

Based on the above trial and error procedure, the authors suggested to develop comprehensive set of design graphs for the selection of the type and amount of FRP that was required for upgrading an existing member to a specified moment and ductility capacity.

Antonopoulos and Triantafillou (2002) presented analytical models for the analysis of reinforced concrete joints strengthened with composite materials in the form of externally bonded reinforcement comprising unidirectional strips or flexible fabrics. The models provide equations for stresses and strains at various stages of the response before or after yielding of the beam or column reinforcement until the ultimate capacity is reached, defined by concrete crushing or fiber-reinforced polymer (FRP) failure due to fracture or debonding.

In this study, the authors had extended the model proposed by **Pantazopoulou and Bonacci (1992)** to account for the effect of externally bonded FRP. The models provided equations for stresses and strains at various stages of the response until the ultimate capacity was reached, defined by concrete crushing or FRP failure due to fracture or debonding. Solutions to these equations were obtained numerically.

The models provided useful information on the shear capacity of FRP-strengthened joints in terms of the quantity and configuration of the externally bonded reinforcement. Shear-strength predictions provided by the analytical models were found in extremely good agreement with the experimental results found in the literature.

Ghobarah and Said (2001) proposed a design methodology for fiber jacketing to upgrade the shear capacity of existing beam-column joints in reinforced concrete moment resisting frames. The fiber was designed to replace the missing transverse reinforcement in the beam-column joint. The joint shear force, V_j, was calculated based on the expression given by **Park and Paulay (1974)** as the difference between the maximum force in the bottom steel, allowing a 25% over strength in steel, and the shear force in the column, V_{col},

$$V_j = 1.25A_s f_y - V_{col}$$

where A_s is the area of the longitudinal tension steel reinforcement in the beam and f_y is the yield strength of the steel

The total joint shear resistance of the rehabilitated joint was assumed to consist of the concrete shear resistance, V_c, the transverse reinforcement contribution, V_s, and resistance provided by the fiber, V_f.

$$V_j = V_c + V_s + V_f$$

The force carried by the steel ties V_s, is zero if there is no transverse reinforcement in the beam-column joint. The shear resistance of concrete considering the applied axial stress is:

$$V_c = 0.2\sqrt{f_c'}\left(1 + \frac{3f_{col}}{f_c'}\right) bd_j$$

where f_{col} is the nominal stress in the column due to the axial load, b is the width of the joint and d_j is the effective depth of the joint.

The required area of fiber in the joint height was then calculated as:

$$A_f = \frac{V_f s}{\phi_f d_j f_u}$$

where A_f is the area of fiber einforcement required over the jointregion designed to replace the transverse steel, f_u is the tensile strength of the fiber, s is the joint height, and ϕ_f is a resistance factor for the GFRP material suggested to be 0.8. If bidirectional FRP laminate is used, the joint shear force was to be analysed into two perpendicular components making 45^0 with the vertical column axis.

Gergely et al. (2000) gave a design equation for the retrofit of beam-column joints based on the experimental results by the same authors.

Firstly, the forces acting at the face of the column and the beam were reduced to tension-compression couples to calculate the horizontal and vertical shear forces in the joint region. The relationship between the increase in the joint shear forces/stresses and composite properties was expressed as

$$V_f = nt\varepsilon_f E_f d_e \frac{\sin\beta}{\cos\beta}$$

where V_f = increase in the joint shear force provided by the CFRP sheets; n = total number of composite layers inclined by the same angle β with respect to the member's longitudinal axis; t = calculated thickness of the composite sheets; ε_f = average axial strain in the fiber direction at the peak horizontal load calculated for each group; E_f = elastic modulus of the composite material; and d_e = effective joint depth.

Fig. 2.22 shows the column-cap beam joint with the composite layer perpendicular to the crack. The direction of the crack is parallel to the principal compression stresses. The force *F* acting normal to crack was the total force resisted by the composite layers stressed in the fiber direction. As was seen, the dimension of the joint and the inclination of the principal planes control the value of the joint effective depth, d_e. The magnitude of the force *F*, expressed as a function of the number of composite layers *n*, was calculated as

$$F = nt\varepsilon_f E_f \frac{d_e}{\cos\beta}$$

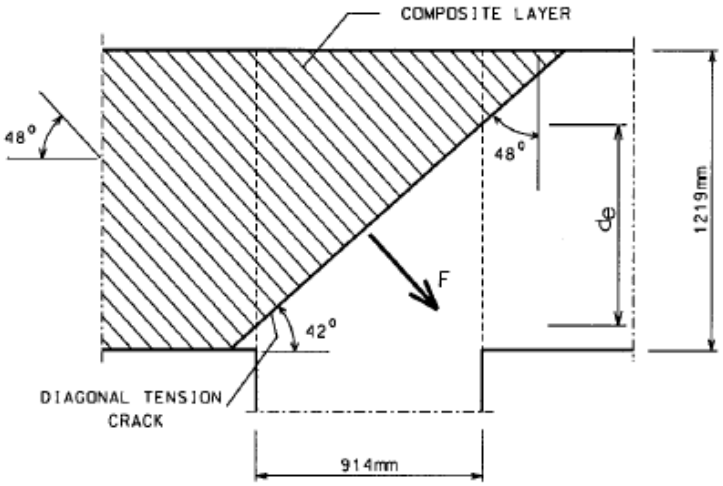

Fig. 2.22: Composite tensile forces by **Gergely et al. (2000)**

To find the principal tensile stress in the composite, the value of the force *F* was divided by the width of the joint and by the inclined length (along the crack) bordered by the effective depth.

$$\sigma_f = \frac{F\cos\beta}{bd_e}$$

The total number of layers required was given by

$$n = \frac{\Delta\sigma_t}{\sigma_f}$$

2.3 FINITE ELEMENT MODELLING OF CONCRETE STRUCTURES

Ravi and Arulraj (2010) carried out the finite element analysis of beam-column joints retrofitted with carbon fiber reinforced polymer sheets (CFRP) using the package ANSYS. Three exterior reinforced concrete beam-column joint specimens were modelled. The first two specimens were the control specimens. The first specimen had reinforcement as

per code **IS 456: 2000** while the second specimen had reinforcement as per **IS 13920-1993**. The third specimen had reinforcement as per the first specimen and was retrofitted with carbon fiber reinforced polymer (CFRP) sheets.

The beam-column joint considered for analysis consisted of a cantilever portion and column portion. The column had a cross section of 200 mm x 200 mm with an overall length of 1500 mm and the beam had a cross section of 200 mm x 200 mm and the length of the cantilevered was 600 mm.

Meshing was done for both control and retrofitted specimens using ANSYS (**Fig. 2.23**). Both ends of the column were hinged. The concrete was modelled using Solid65 element. The reinforcement was modelled using Link8 element. The wrapping was modelled using Solid45 element. The static load was applied at the free end of the cantilever beam at a regular interval of 5 kN for the control and retrofitted reinforced concrete beam column joint models.

It was found from that the deflection of the beam-column joint specimen detailed as per code **IS 13920-1993** was 23.53% less than that of the specimen detailed as per code **IS 456: 2000**.

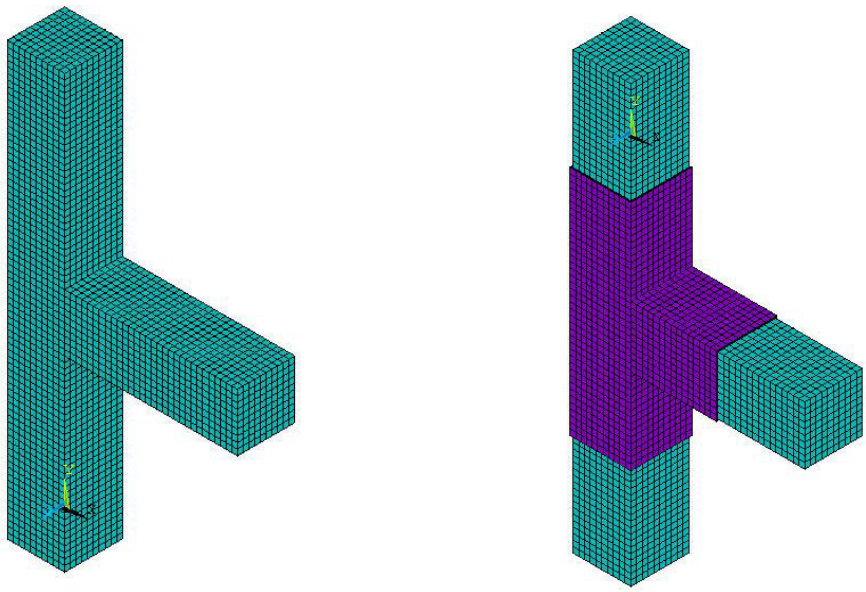

(a) **(b)**

Fig. 2.23: (a) Meshed control specimen; (b) Meshed retrofitted specimen by **Ravi and Arulraj (2010)**

Deflection of the beam-column joint specimen retrofitted with carbon reinforced polymer sheet was 75.29 % less than that of the specimen detailed as per code **IS 456: 2000**.

It was also observed that the energy absorption capacity of the specimen beam-column joint specimen detailed as per code **IS 13920-1993** was 42.86 % more than that of the specimen detailed as per code **IS 456: 2000** and energy absorption capacity of the beam-column joint specimen retrofitted with carbon reinforced polymer sheet was 114.29 % more than that of the specimen detailed as per code **IS 456: 2000**.

Ibrahim and Mahmood (2009) presented an analysis model for reinforced concrete beams externally reinforced with fiber reinforced polymer (FRP) laminates using finite elements method. Six beams with different conditions (all were deficient shear reinforcement) were analysed using ANSYS. The results obtained were compared with the experimental data from the literature.

The finite element used a smeared cracking approach to model the reinforced concrete and three dimensional layered elements to model the FRP composites. Solid65 element was used to model the concrete. The following properties of concrete were entered in ANSYS: elastic modulus E_c, ultimate uniaxial compressive strength f_c', ultimate uniaxial tensile strength (modulus of rupture f_r), Poisson's ratio v, shear transfer coefficient β_t, and compressive uniaxial stress-strain relationship for concrete.

Link8 element was used to model steel reinforcement. The steel reinforcing was connected between nodes of each adjacent concrete solid element, so the two materials shared the same nodes. Elastic modulus, yield stress and Poisson's ratio were entered as the design material properties for steel reinforcement. A Solid46 layered element was used to model FRP composites.

Due to symmetry in cross-section of the concrete beam and loading, symmetry was utilized in the finite element analysis and only one quarter of the beam was modelled. The finite element mesh, boundary condition and loading region is shown in **Fig. 2.24**.

The ANSYS program recorded the crack pattern at each applied load step. The failure modes of the finite element models showed good agreement with observations and data from the experimental full-scale beams. The addition of FRP reinforcement to the control beam shifted the behaviour of the beams from a shear failure near the ends of the beam to flexure failure at the midspan.

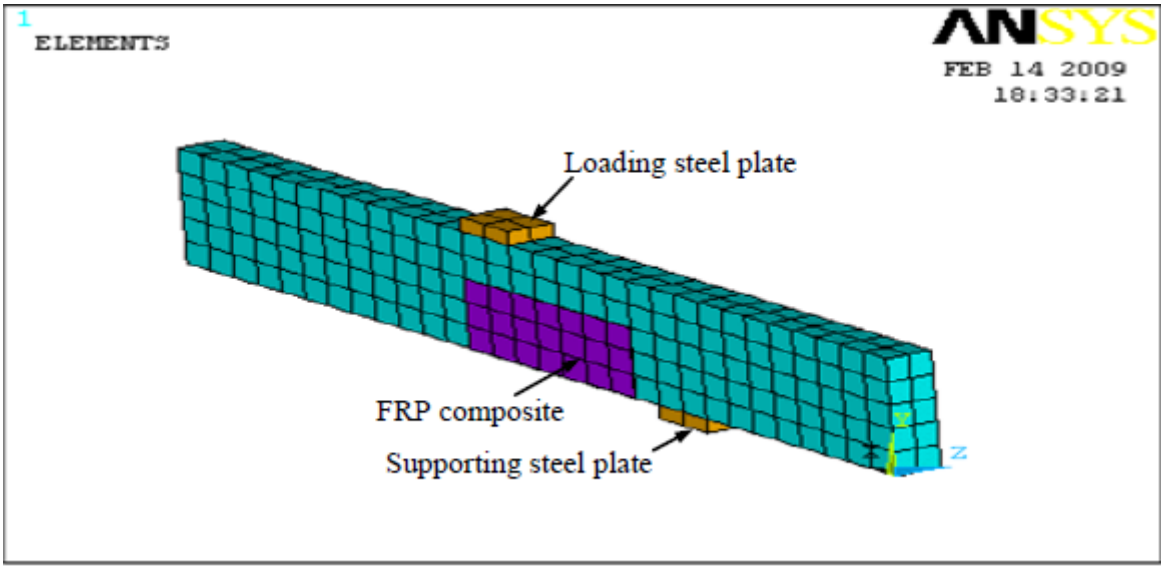

Fig. 2.24: Finite element modelling by **Ibrahim and Mahmood (2009)**

The failure load obtained from the numerical solution for all beams was slightly smaller than experimental load. The final loads for the finite element models were the last applied load step before the solution diverges due to numerous cracks and large deflections.

Haach et al. (2008) studied the behaviour of exterior beam-column joints under the influence of column axial load through numerical simulations. The numerical study was performed through the software ABAQUS, based on Finite Element Method. A comparison of the numerical and experimental results was presented in order to validate the simulation.

The numerical simulation used two-dimensional planar solid (continuum) elements with 2 active degrees of freedom to represent the concrete. The longitudinal and transversal bars were represented by truss elements whose nodes were embedded in the concrete elements. The column was meshed for elements with 19 mm x 20 mm and the beam was meshed for elements with 20 mm x 20 mm. Some triangle elements were used in regions of stress concentration in the structure to avoid an early failure.

A monotonic loading was defined in two steps. Firstly, the column axial load was applied up to the required level. In the second step, a vertical displacement (δ) was applied in the beam extremity. Analysis of numerical specimens with the material properties same as that of the experimental specimens was done. Joint behaviour was studied under the influence of (1) different levels of column axial load (v): 0.0, 0.2, 0.4, 0.6 and 0.8; (2) eccentricity of column axial load (e): -50 mm to 50 mm; (3) stirrup ratio variation (ρ_w): 0.0%, 0.14%, 0.29%,

0.43% and 0.57%. In addition, study of the beam behaviour near to the joint region, where Bernoulli's hypothesis was not valid was done numerically.

Numerical results confirmed the experimental observations and allowed analyzing other aspects that could not be evaluated in the tests. **Fig. 2.25** and **Fig. 2.26** showed the confrontation of numerical and experimental result for the behaviour of the stirrup in the joint and the tensioned bar of the beam, for specimen with v = 0.85 and v = 0.64 respectively. The numerical results represented the experimental specimen in an intact condition only before the maximum load. In the experimental specimen, when the loading reached the maximum value, a rearrangement in the load resisting mechanism occurred. When one of the load resisting mechanism reached its capacity, the rearrangement occurred again and the load decreased. The numerical model could not represent this phenomenon, thus near to this maximum level of loading, numerical instabilities appeared in some areas of the mesh and the model cannot continue converging.

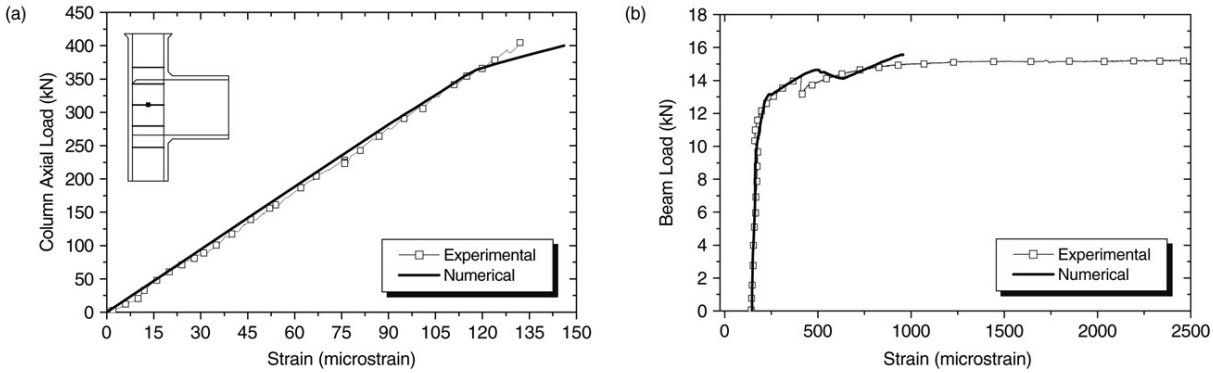

Fig. 2.25: Strain of stirrup inside the joint for specimen with v = 0.85: (a) Column load; and (b) Beam load by **Haach et al. (2008)**.

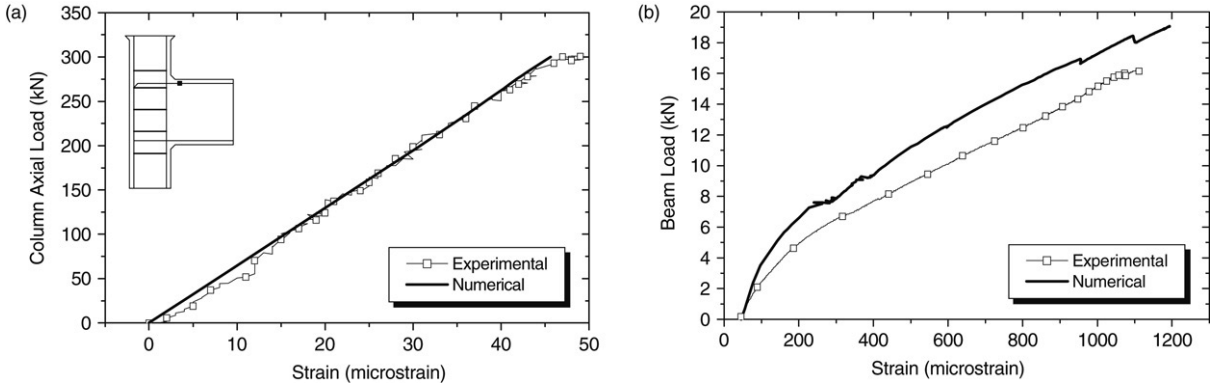

Fig. 2.26: Strain of tensioned bar of beam for specimen with v = 0.64: (a) Column load; and (b) Beam load by **Haach et al. (2008)**.

Significant values of strain in stirrups inside the joint region were observed earlier in specimens with low column axial loads than in specimens with high column axial loads. The eccentricity of column axial load did not produce significant changes in the joint stress behaviour. An increase in the stirrup ratio made the stress distribution in the joint more regular, independent of the level of column axial load. Stirrups located in the upper region of the joint absorbed part of the tension proceeding from beam longitudinal reinforcement and improved their anchorage. Also, column axial load generated tension stress on beam longitudinal reinforcement, hence shear force in the joint was increased by this variable.

Mahini et al. (2008) presented the results of a study on the capability of nonlinear quasistatic finite element modelling in simulating the hysteretic behaviour of CFRP-retrofitted RC exterior beam-column joints under cyclic loads. Two exterior beam-column connections tested by the authors in an earlier study were modelled using nonlinear finite element method, and the hysteretic curves of these connections were extracted and compared with experiments. Cyclic loads were applied with a step by step strategy in a displacement control regime similar to the tests. An automatically reforming stiffness matrix was employed in order to simulate cracking and crushing of the concrete and steel yielding during cyclic loading.

To model the characteristics of concrete, the Solid65 element was used. This element was capable of simulating the cracking and crushing of concrete. The Willam-Warnke criterion was used for fracture modelling in concrete. Parameters used to perform the failure envelope in the model were the compressive strength if concrete, the modulus of rupture, and the shear transfer coefficients for open and closed cracks. For modelling the compressive strength of concrete, the Hognested model was used. To model the longitudinal reinforcement and the FRP composites, Link8 and Solid45 elements were used, respectively.

For the control specimen, the plastic hinge was formed at the face of the column in the analytical modelling similar to the experimental observation. Also, the hysteresis curves of the specimen obtained from experimental and analytical studies were found to be reasonably similar. For the retrofitted specimen, the plastic hinge was formed beyond the cut-off point of the CFRP, similar to the experimental results. Comparison between the hysteresis curves obtained from the analytical and experimental showed that the energy absorption was maintained as the maximum load was held to the end.

Hegger et al. (2004) conducted a nonlinear finite element analysis to investigate the behaviour of exterior and interior beam-column joints. The model was validated by one of the author's experimental data, and an extensive parametric study was conducted to investigate the behaviour as well as the critical parameters influencing the shear capacity of such connections. The nonlinear finite element analysis program ATENA was used in the study. The concrete was modelled with nine-node isoparametric shell elements, while discrete bars were used to model the reinforcement. **Fig. 2.27** shows the meshes for the exterior and interior connections.

The connections investigated had a beam and column thickness of 150 mm. Inside the joint, the element size is 10 x 10 mm. For the beam and the column, a coarser mesh was used. The program assumes full bond between the reinforcement and the concrete. In some of the connections, the beam tensile reinforcement was anchored by anchor plates at their ends.

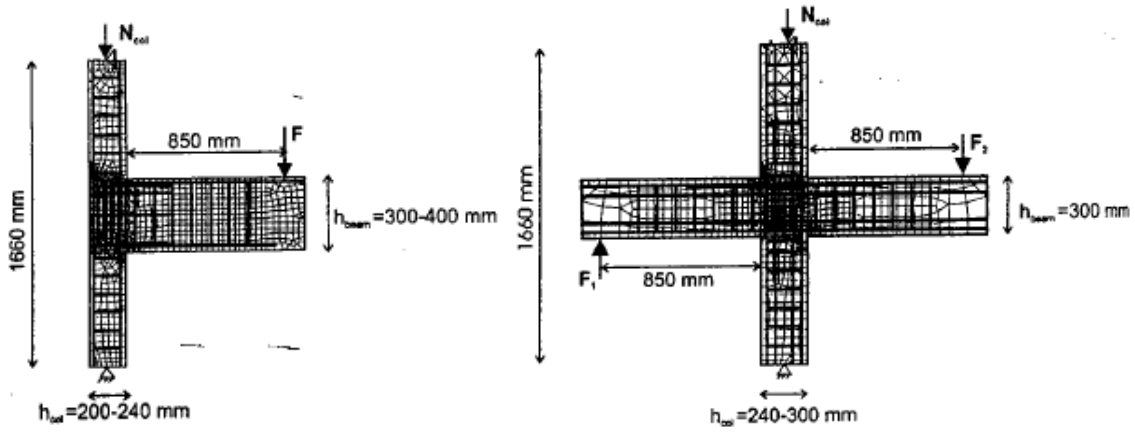

(a) **(b)**

Fig. 2.27: Finite element model used in analysis (a) Exterior beam-column joint; (b) Interior beam-column joint by **Hegger et al. (2004)**.

There was a good agreement between the theoretical and experimental load-deflection curves for both the exterior as well as the interior connections. Also, the FEM was capable of distinguishing between the failure types of the connections, i.e., bending failure in the beam or shear failure of inside the joint.

Wolanski, A.J.B.S. (2004) investigated the use of the finite element method for the analysis of reinforced and pre-stressed concrete beams. A mild-steel reinforced concrete beam with flexural and shear reinforcement was analysed to failure and compared to experimental results of **Buckhouse (1997)** to calibrate the parameters in ANSYS 2003 for later analyses.

In ANSYS, only one quarter of the beam was modelled, due to the symmetry in cross-section of the concrete beam and loading. The model was 2.36 m long, with a cross-section of 125 x 450 mm. The FE mesh for the beam model consisted of rectangular Solid65 element for concrete and Link8 element for the steel reinforcement. No mesh of the reinforcement was done as its individual elements were created through the nodes created by the mesh of the concrete volume.

To ensure that the model acted in the same way as the experimental beam, boundary conditions were applied at points of symmetry, and where the supports and loadings exist.

The FE analysis of the model was set to examine three different behaviours: initial cracking of the beam, yielding of the steel reinforcement, and the strength limit state of the beam. The application of the loads up to failure was done incrementally. After each load increment was applied, the restart option was used to go to the next step after convergence.

The analysis of the linear region was made to ensure deflections and stresses were consistent with the FE model and the beam before cracking occurred. Once cracking occurred, deflections and stresses become more difficult to predict. The stresses in the concrete and steel immediately preceding initial cracking were analysed. The load at step 5210 was analysed and it coincides with a load of 5210 lbs. applied on the steel plate. A comparison of values obtained from the FE model and hand calculations can be seen in **Table 2.4**. The maximums existed in the constant-moment region of the beam during load application. This is it were expected to occur.

Table 2.4: Deflection and Stress Comparisons at first cracking by **Wolanski, A.J.B.S. (2004)**

Model	Extreme Tension Fiber Stress (psi)	Reinforcing Steel Stress (psi)	Centerline Deflection (in.)	Load at First Cracking (lbs.)
Hand-Calculations	530	3024	0.0529	5118
ANSYS	536	2840	0.0534	5216

The results in **Table 2.4** indicated that the FE analysis of the beam prior to cracking was acceptable. The initial cracking of the beam in the FE model corresponded to a load of 5216 lbs that created stress just beyond the modulus of rupture of the concrete (520 psi) as shown. This compared well with the load of 5118 lbs as per hand calculations.

In the non-linear region of the response, subsequent cracking occurred as more load was applied to the beam. Cracking increased in the constant moment region and the beam began cracking out towards the supports at a load of 8,000 lbs. Significant flexural cracking occurred in the beam at 12,000 lbs. Also, diagonal tension cracks began to form in the model.

Yielding of steel reinforcement occurred when a force of 13,400 lbs. was applied. At this point in the response, the displacements of the beam began to increase at a higher rate as more load was applied. At 15,000 lbs., the beam had increased flexural cracks, and diagonal tension cracks. Also, more cracks were formed in the constant moment region.

Table 2.5: Deflections at ultimate load by **Wolanski, A.J.B.S. (2004)**

Beam	Load (lb.)	Centerline Deflection (in.)
Buckhouse (1997)	16310	3.65
ANSYS	16310	3.586

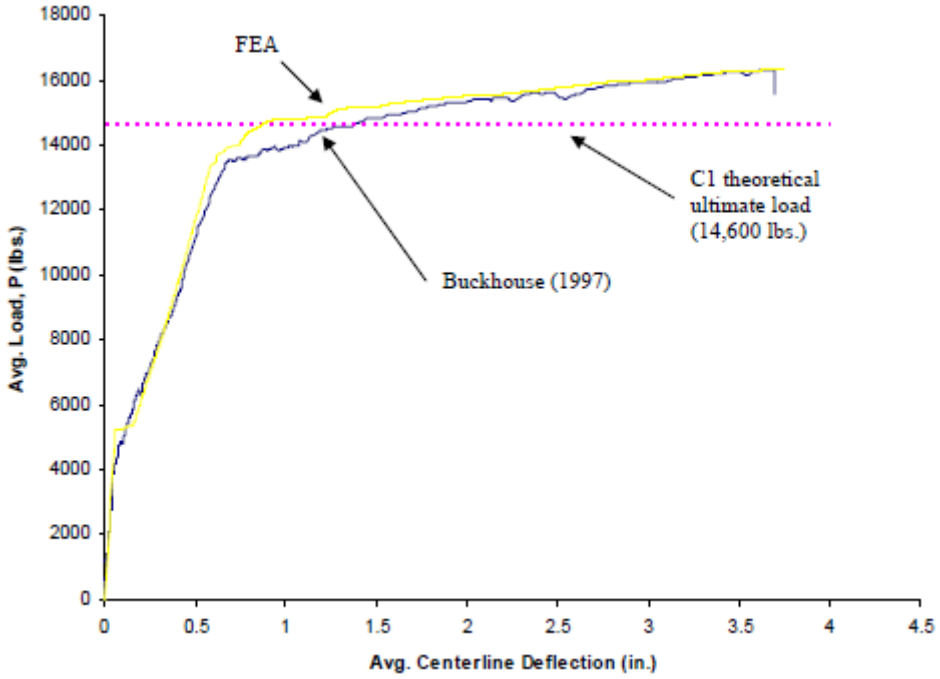

Fig. 2.28: Load vs. Deflection curve comparison of ANSYS and Buckhouse by **Wolanski, A.J.B.S. (2004)**

At 16,000 lbs., cracking reached the top of the beam. At load 16,382 lbs., the beam no longer supported additional load as indicated by an insurmountable convergence failure. Severe cracking throughout the entire constant moment region occurred. The deflections at the analytical failure load of the control beam were compared with the finite element model

as shown in **Table 2.5**. The deflection of the finite element model was within 2% of the control beam at the same load at which the control beam failed.

The entire load-deformation response of the model produced compared well with the response from Buckhouse (1997) (**Fig. 2.28**). This gave confidence in the use of ANSYS (SAS 2003) and the model developed.

Kachlakev et al. (2001) performed the finite element modelling of the Horsetail Creek Bridge strengthened with FRP laminates for the Oregon Department of Transportation. Finite element method (FEM) models were developed to simulate the behaviour of four full-size beams from linear through non-linear response and up to failure, using the ANSYS program (1998). Comparisons between finite element results and those from the experimental beams were shown.

The load-carrying capacity of the bridge was increased by applying FRP sheets to the transverse and longitudinal beams. In the case of the transverse beams, both shear and flexural strengthening were required, while only shear strengthening was needed for the longitudinal beams. For flexural strengthening, carbon FRP (CFRP) composite was attached to the bottom of the beam with the fibers oriented along the length of the beam. For shear strengthening, glass FRP (GFRP) composite was wrapped from the bottom of the deck down the side of the beam around the bottom and up the other side to the deck. The fibers were oriented perpendicular to the length of the beam.

Solid65 element was used to model the concrete. A Link8 element was used to model the steel reinforcement. A layered solid element, Solid46, was used to model the FRP composites. For concrete, the input data required by ANSYS was: elastic modulus E_c, ultimate uniaxial compressive strength f_c', ultimate uniaxial tensile strength (modulus of rupture f_r), Poisson's ratio v, shear transfer coefficient β_t, and compressive uniaxial stress-strain relationship. Material properties for the steel reinforcement were: elastic modulus E_s, yield stress f_y, and Poisson's ratio v.

The general behaviour of the finite element models represented by the load-deflection plots at midspan showed good agreement with the test data from the full-scale beam tests. Also, the crack patterns at the final loads from the finite element models corresponded well with the observed failure modes of the experimental beams.

The literature review has suggested that limited work is done on the use of FEM to analyse retrofitted beam-column joint. Thus it has been decided to use ANSYS 12.1 (**SAS, 2009**) software for the finite element modelling of beam-column joint retrofitted with externally bonded FRP.

Modelling of beam-column joint presented in this chapter pertains to the joint detail, material properties and loading conditions as taken in the experimental study conducted by **Dar (2011)**. The control specimen is taken and analysed by finite element method (FEM) using the commercial available software ANSYS 12.1 **(SAS, 2009)**. Then, the specimen is retrofitted with externally bonded fiber reinforced polymer (FRP) and analysed using the same software.

3.1 CONTROL SPECIMEN

3.1.1 Assumptions

The assumptions made in the FEM modelling of the control specimen are summarized below:

- Concrete and steel are modelled as isotropic and homogeneous materials.
- Steel is assumed to be an elastic-perfectly plastic material and identical in tension and compression.
- Initially plane sections remain plane after loading (that is, the strain in the concrete and the reinforcement is proportional to the distance from the neutral axis).
- The maximum compressive strain in the concrete is assumed to be 0.0035 mm/mm as suggested by **IS 456: 2000**.
- The tensile strength of the concrete is ignored.
- Perfect bond exits between concrete and steel reinforcement.

3.1.2 Failure Criteria for Concrete

The model is capable of predicting failure for concrete materials. Both cracking and crushing failure modes are accounted for. The two input strength parameters – i.e. ultimate uniaxial tensile and compressive strengths – are needed to define a failure surface for the

concrete. Consequently, a criterion for failure of the concrete due to a multiaxial stress state can be calculated **(Willam and Warnke, 1975)**.

A three-dimensional failure surface for concrete is shown in **Fig. 3.1**. The most significant non-zero principal stresses are in the *x* and *y* directions, represented by σ_{xp} and σ_{yp} respectively. Three failure surfaces are shown as projections on the σ_{xp}-σ_{yp} plane. The mode of failure is a function of the sign of σ_{zp} (principal stress in the *z* direction). For example, if σ_{xp} and σ_{yp} are both negative (compressive) and σ_{zp} is slightly positive (tensile), cracking would be predicted in a direction perpendicular to σ_{zp}. However, if σ_{zp} is zero or slightly negative, the material is assumed to crush (**SAS, 2009**).

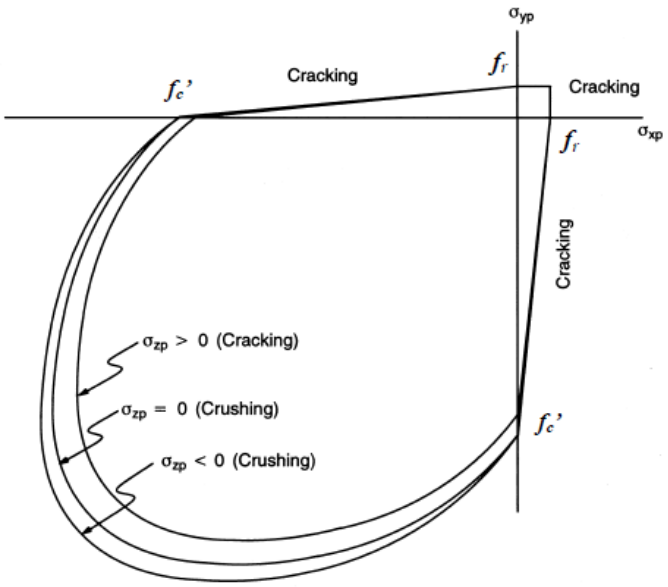

Fig. 3.1: 3-D failure surface for concrete **(SAS, 2009)**

In a concrete element, cracking occurs when the principal tensile stress in any direction lies outside the failure surface. After cracking, the elastic modulus of the concrete element is set to zero in the direction parallel to the principal tensile stress direction. Crushing occurs when all principal stresses are compressive and lie outside the failure surface; subsequently, the elastic modulus is set to zero in all directions (**SAS, 2009**), and the element effectively disappears.

During this study, it was found that if the crushing capability of the concrete is turned on, the finite element beam models fail prematurely. Crushing of the concrete started to develop in elements located directly under the loads. Subsequently, adjacent concrete elements crushed within several load steps as well, significantly reducing the local stiffness.

Finally, the model showed a large displacement, and the solution diverged. Therefore, in this study, the crushing capability was turned off and cracking of the concrete controlled the failure of the finite element models. Same behaviour is observed by past researchers such as **Ibrahim and Mahmood (2009)**, **Wolanski (2004)** and **Kachlakev et al. (2001)**.

3.1.3 Element Types

The Solid65 element is used to model concrete. This element has eight nodes with three degrees of freedom at each node – translations in the nodal *x*, *y*, and *z* directions. This element is capable of plastic deformation, cracking in three orthogonal directions, and crushing. A schematic of the element is shown in **Fig. 3.2**.

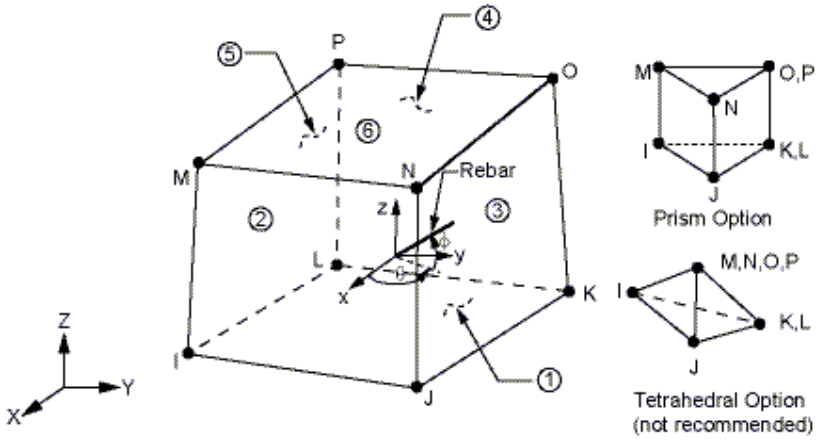

Fig. 3.2: Solid65 Element **(SAS, 2009)**

A Link180 element is used to model steel reinforcement. This element is a 3D spar element and it has two nodes with three degrees of freedom at each node – translations in the nodal *x*, *y* and *z* directions. This element is also capable of plastic deformation. This element is shown in **Fig. 3.3**. Link180 is a current-technology element and is preferred over the legacy element, Link8, as suggested by ANSYS **(SAS, 2009)**.

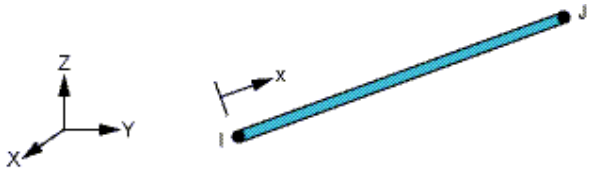

Fig. 3.3: Link180 Element **(SAS, 2009)**

The Solid185 element is used for the modelling of steel plate for application of load. This element is defined by eight nodes having three degrees of freedom at each node –

translations in the nodal *x*, *y*, and *z* directions. The element is capable of plasticity, hyperelasticity, stress stiffening, creep, large deflection, and large strain capabilities.

SOLID185 is available in two forms:

- Homogeneous Structural Solid (default); and
- Layered Structural Solid.

Homogeneous Structural Solid with simplified enhanced strain formulation is used to model steel plate for application of load. This element is shown in **Fig. 3.4**. Solid185 is a current-technology element and is preferred over the legacy element, Solid45, as suggested by ANSYS **(SAS, 2009)**.

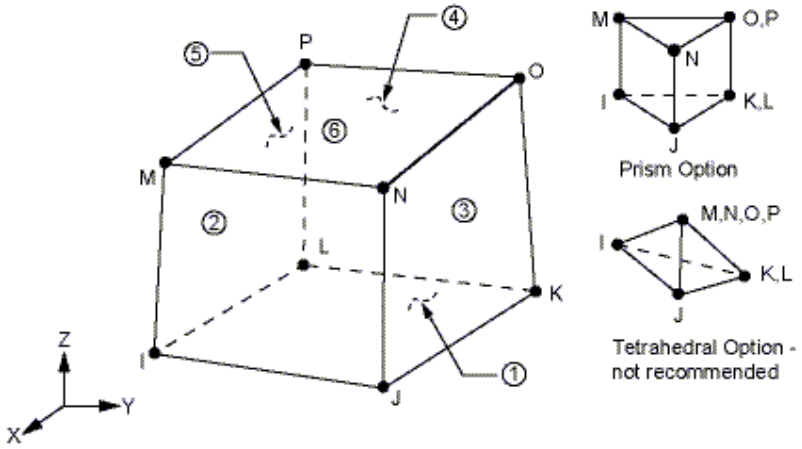

Fig. 3.4: Solid185 Element (Homogeneous Structural Solid) **(SAS, 2009)**

The element types for the control specimen are tabulated in **Table 3.1**.

Table 3.1: Element types for the Control Specimen

Material Type	ANSYS Element
Concrete	Solid65
Steel Reinforcement	Link180
Steel Plate	Solid185 (Homogeneous Structural Solid)

3.1.4 Real Constants

The real constants for this model are shown in **Table 3.2**. Note that individual elements contain different real constants.

Table 3.2: Real Constants for the Control Specimen

Real Constant Set	Element Type	Constants			
1	Solid65		Real Constant for Rebar 1	Real Constant for Rebar 2	Real Constant for Rebar 3
		Material Number	0	0	0
		Volume Ratio	0	0	0
		Orientation Angle	0	0	0
		Orientation Angle	0	0	0
2	Link180	Cross-sectional area (mm^2)	78.5		
		Initial strain (mm/mm)	0		
3	Link180	Cross-sectional area (mm^2)	50.3		
		Initial strain (mm/mm)	0		
4	Link180	Cross-sectional area (mm^2)	28.3		
		Initial strain (mm/mm)	0		

Real Constant Set 1 is used for the Solid65 element. It requires real constants for rebar assuming a smeared model. Values can be entered for Material Number, Volume Ratio, and Orientation Angles. The material number refers to the type of material for the reinforcement. The volume ratio refers to the ratio of steel to concrete in the element. The orientation angles refer to the orientation of the reinforcement in the smeared model. ANSYS 12.1 **(SAS, 2009)** allows the user to enter three rebar materials in the concrete. Each material corresponds to *x*, *y*, and *z* directions in the element **(Fig. 3.2)**. The reinforcement has uniaxial stiffness and the directional orientation is defined by the user. In the present study the joint is modelled using discrete reinforcement as suggested by **Fanning (2001)**. Therefore, a value of zero was entered for all real constants which turned the smeared reinforcement capability of the Solid65 element off as suggested by past researchers (**Ibrahim and Mahmood, 2009**; **Wolanski, 2004**; **Kachlakev et al., 2001**).

Real Constant Sets 2, 3, and 4 are defined for the Link180 element. Values for cross-sectional area and initial strain are entered. Cross-sectional areas in sets 2 and 3 refer to the reinforcement of 10 mm and 8 mm diameter bars respectively. Cross-sectional areas in set 4 refer to the 6 mm diameter stirrups. A value of zero was entered for the initial strain because there was no initial stress in the reinforcement.

No real constants set exist for the Solid185 element.

3.1.5 Material Properties

Parameters needed to define the material models for the control specimen are listed in **Table 3.3**. Note that there are multiple parts of the material model for each element.

Material Model Number 1 refers to the Solid65 element. The Solid65 element requires linear isotropic and multilinear isotropic material properties to properly model concrete. The multilinear isotropic material uses the von Mises failure criterion along with the **Willam and Warnke (1975)** model to define the failure of the concrete (refer **3.1.1.2**). EX is the modulus of elasticity of the concrete (E_c), and PRXY is the Poisson's ratio (v). The modulus is based on the equation (as per Cl. 6.2.3.1 of **IS 456: 2000**),

$$E_c = 5000\sqrt{f_{ck}} \qquad (\mathbf{3.1})$$

with a value of f_{ck} equal to 20 MPa. Poisson's ratio is taken as 0.2 **(Kachlakev et al., 2001)**.

As suggested by past researchers (**Ibrahim and Mahmood, 2009**; **Wolanski, 2004**; **Kachlakev et al., 2001**), the compressive uniaxial stress-strain relationship for the concrete model is obtained using the following equations to compute the multilinear isotropic stress-strain curve for the concrete.

$$f = \frac{E_c \varepsilon}{1 + \left(\frac{\varepsilon}{\varepsilon_0}\right)^2} \qquad (\mathbf{3.2})$$

$$\varepsilon_0 = \frac{2f_{ck}}{E_c} \qquad (\mathbf{3.3})$$

$$E_c = \frac{f}{\varepsilon} \qquad (\mathbf{3.4})$$

where:

f = stress at any strain ε, MPa

ε = strain at stress f

ε_0 = strain at the ultimate compressive strength f_{ck}

The multilinear curve is used to help with convergence of the nonlinear solution algorithm.

Table 3.3: Material Models for the Control Specimen

Material Model Number	Element Type	Material Properties		
1	Solid65	Linear Isotropic		
		EX	22360.68 MPa	
		PRXY	0.2	
		Multilinear Isotropic		
			Strain	Stress (MPa)
		Point 1	0.0002683	6
		Point 2	0.0006485	13
		Point 3	0.0010286	17
		Point 4	0.0014087	19
		Point 5	0.0017889	20
		Concrete		
		ShrCf-Op	0.3	
		ShrCf-Cl	1.0	
		UnTensSt	3.13 MPa	
		UnCompSt	-1	
		HydroPrs	Default	
		BiCompSt	Default	
		UnTensSt	Default	
		TenCrFac	Default	
2	Link180	Linear Isotropic		
		EX	200000 MPa	
		PRXY	0.3	
		Bilinear Isotropic		
		Yield stress	500 MPa	
		Tangent Modulus	0	
3	Link180	Linear Isotropic		
		EX	200000 MPa	
		PRXY	0.3	
		Bilinear Isotropic		
		Yield stress	250 MPa	
		Tangent Modulus	0	

4	Solid185 (Homogeneous Structural Solid)	Linear Isotropic	
		EX	200000 MPa
		PRXY	0.3

Fig. 3.5 shows the stress-strain relationship used for this study as suggested by **Ibrahim and Mahmood (2009)**, **Wolanski (2004)** and **Kachlakev et al. (2001)**. The curve starts at zero stress and strain. Point 1, defined as $0.30f_{ck}$, is calculated in the linear range (**Eq. 3.4**). Points 2, 3, and 4 are calculated from **Eq. 3.2** with ε_0 obtained from **Eq. 3.3**. Strains are selected and the stress is calculated for each strain. Point 5 is at f_{ck} of 20 MPa and ε_0 of 0.00179 mm/mm. After Point no. 5, perfectly plastic behaviour of concrete is assumed.

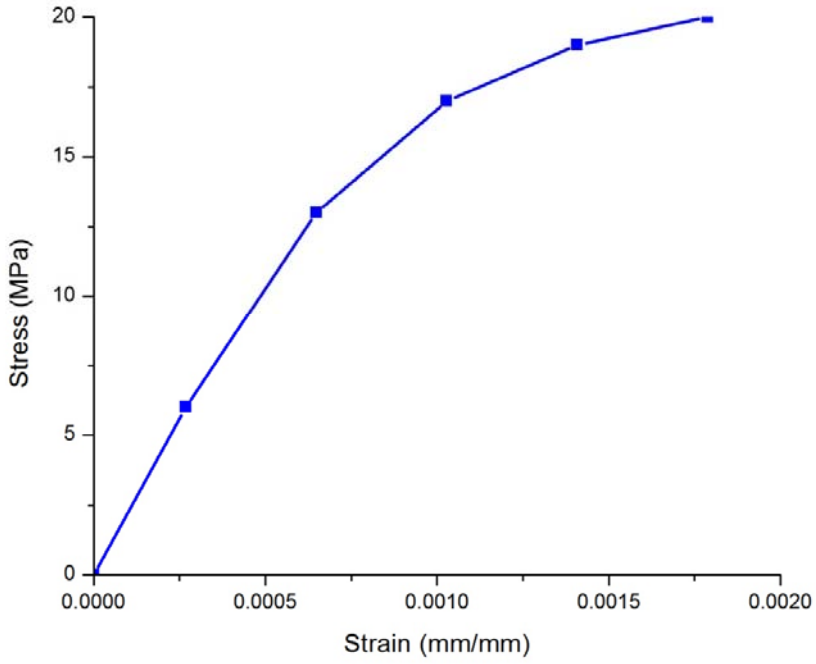

Strength

Fig. 3.5: Uniaxial stress-strain curve for concrete

Implementation of the **Willam and Warnke (1975)** material model in ANSYS 12.1 requires that different constants be defined. These 9 constants are (**SAS, 2009**):

1. Shear transfer coefficients for an open crack;
2. Shear transfer coefficients for a closed crack;
3. Uniaxial tensile cracking stress;
4. Uniaxial crushing stress (positive);

5. Biaxial crushing stress (positive);
6. Ambient hydrostatic stress state for use with constants 7 and 8;
7. Biaxial crushing stress (positive) under the ambient hydrostatic stress state (constant 6);
8. Uniaxial crushing stress (positive) under the ambient hydrostatic stress state (constant 6);
9. Stiffness multiplier for cracked tensile condition.

Typical shear transfer coefficients range from 0.0 to 1.0, with 0.0 representing a smooth crack (complete loss of shear transfer) and 1.0 representing a rough crack (no loss of shear transfer). The shear transfer coefficients for open and closed cracks are determined using the work of **Kachlakev et al. (2001)** as a basis. Convergence problem occurs when the shear transfer coefficient for the open crack drops below 0.2. No deviation of the response occurs with the change of the coefficient. Therefore, the coefficient for the open crack is set to 0.3 (**Table 3.3**). The uniaxial cracking stress is based upon the modulus of rupture. This value is determined using the following equation (as per Cl. 6.2.2 of **IS 456: 2000**).

$$f_r = 0.7\sqrt{f_{ck}} \qquad (\mathbf{3.5})$$

The uniaxial crushing stress in this model was based on the uniaxial unconfined compressive strength (f_{ck}) and is denoted as f_t. It was entered as -1 to turn off the crushing capability of the concrete element as suggested by past researchers (**Ibrahim and Mahmood, 2009**; **Wolanski, 2004**; **Kachlakev et al., 2001**).

The biaxial crushing stress refers to the ultimate biaxial compressive strength (f'_{cb}). The ambient hydrostatic stress state is denoted as σ_h. This stress state is defined as:

$$\sigma_h = \frac{1}{3}(\sigma_{xp} + \sigma_{yp} + \sigma_{zp}) \qquad (\mathbf{3.6})$$

where σ_{xp}, σ_{yp}, and σ_{zp} are the principal stresses in the principal directions. The biaxial crushing stress under the ambient hydrostatic stress state refers to the ultimate compressive strength for a state of biaxial compression superimposed on the hydrostatic stress state (f_1). The uniaxial crushing stress under the ambient hydrostatic stress refers to the ultimate compressive strength for a state of uniaxial compression superimposed on the hydrostatic stress state (f_2). The failure surface can be defined with a minimum of two constants, f_t and

f_c'. The remainder of the variables in the concrete model are left to default based on these equations:

$$f_{cb}' = 1.2f_c' \qquad (\mathbf{3.7})$$

$$f_1 = 1.45f_c' \qquad (\mathbf{3.8})$$

$$f_2 = 1.725f_c' \qquad (\mathbf{3.9})$$

These stress states are only valid for stress states satisfying the condition $|\sigma_h| \leq \sqrt{3}f_c'$.

Material Model Number 2 and 3 refers to the Link180 element. Material Model Number 2 is used to model the reinforcement while Material Model Number 3 is used to model the stirrups. These materials are assumed to be bilinear isotropic and are based on the von Mises failure criteria. The bilinear model requires the yield stress (f_y), as well as the hardening modulus of steel to be defined. The yield stress is defined as 500 MPa for Material Model Number 2 while it is 250 MPa for Material Model Number 3. The tangent modulus (of the plastic region) is defined as 0. Elastic modulus (EX) is defined as 2,00,000 MPa and Poisson's ratio (PRXY) as 0.3. **Fig. 3.6** shows the assumed stress-strain curve for steel reinforcement.

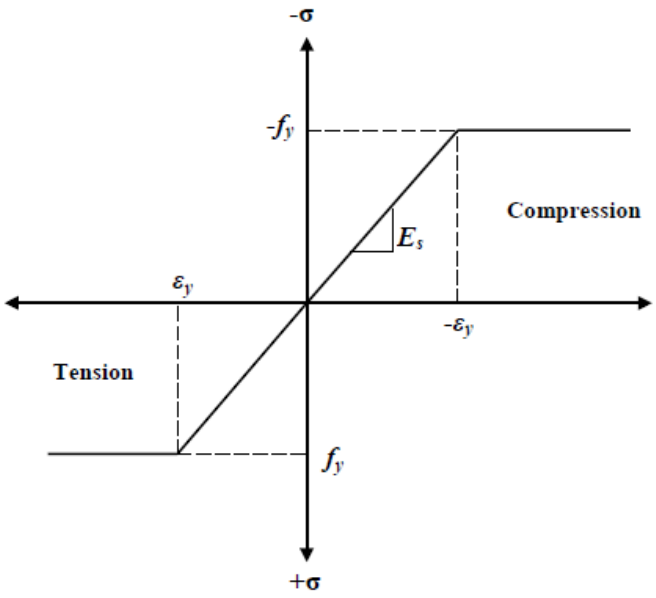

Fig. 3.6: Stress-strain curve for steel reinforcement

Material Model Number 4 refers to the Solid185 element. This element is modelled as a linear isotropic element with a modulus of elasticity for the steel (EX) as 2,00,000 MPa and Poisson's ratio (PRXY) as 0.3.

3.1.6 Modelling

The joint is modelled as volume. The dimensions are shown in **Table 3.4**. The combined volumes created in ANSYS are shown in **Fig. 3.7**.

Table 3.4: Dimensions of Column and Beam for the Control Specimen

ANSYS	Column (mm)		Beam (mm)		Steel Plate (mm)	
	Volume 1		Volume 2		Volume 3	
X1, X2 X-coordinates	0	225	225	725	475	575
Y1, Y2 Y-coordinates	0	1000	375	600	600	625
Z1, Z2 Z-coordinates	0	150	0	150	0	150

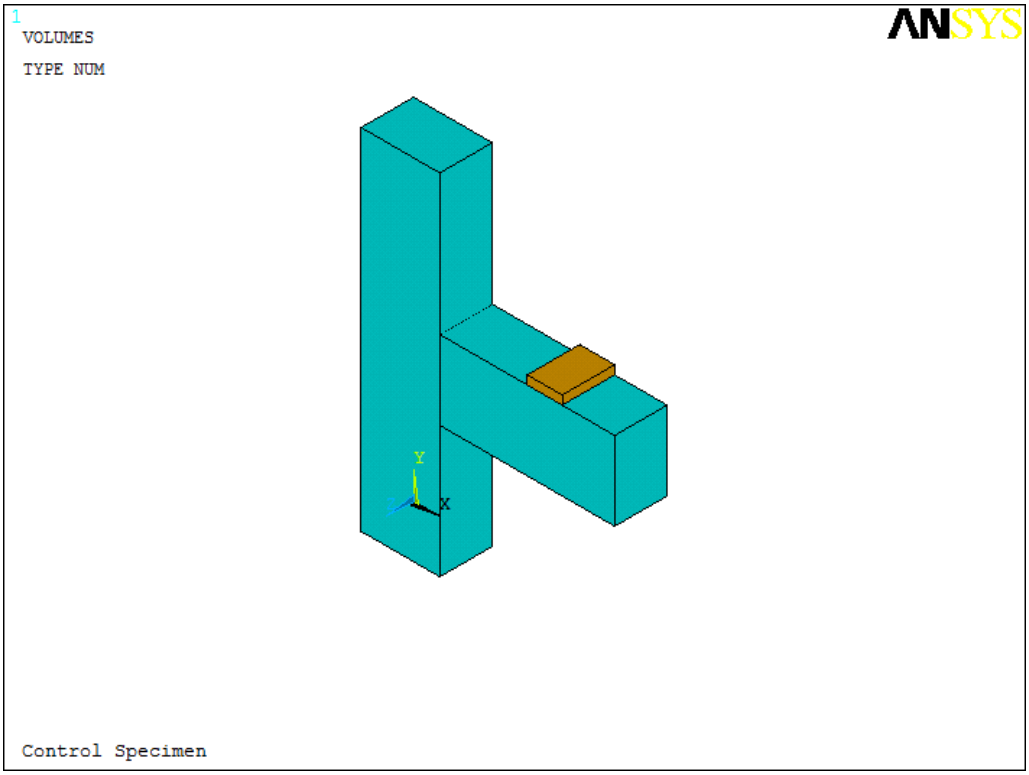

Fig. 3.7: Volumes Created in ANSYS for the Control Specimen

3.1.7 Meshing

To obtain good results from the Solid65 element, the use of a rectangular mesh is recommended (**Wolanski, 2004**; **Kachlakev et al., 2001**). Therefore, the mesh is set up such that square or rectangular elements are created. The overall mesh of the control specimen created in ANSYS is shown in **Fig. 3.8**. The necessary element divisions are noted.

The meshing of the reinforcement is a special case compared to the concrete volumes. No mesh of the reinforcement is needed because individual elements are created in the

modelling through the nodes created by the mesh of the concrete volumes (**Fig. 3.9**). However, the necessary mesh attributes as described in **Table 3.5** need to be set before each section of the reinforcement is created. **Fig. 3.10** illustrates the reinforcement configuration modelled in ANSYS. The command 'merge items' is used to merge separate entities that have the same location.

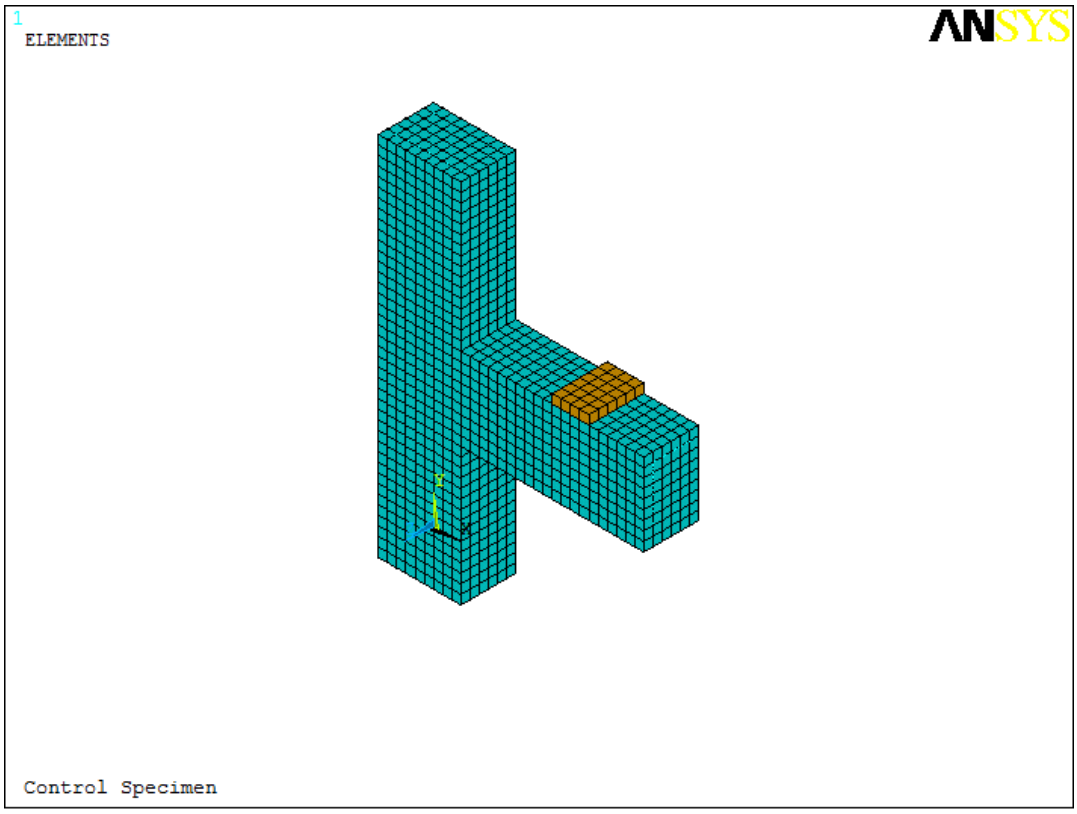

Fig. 3.8: Mesh Created in ANSYS for the Control Specimen

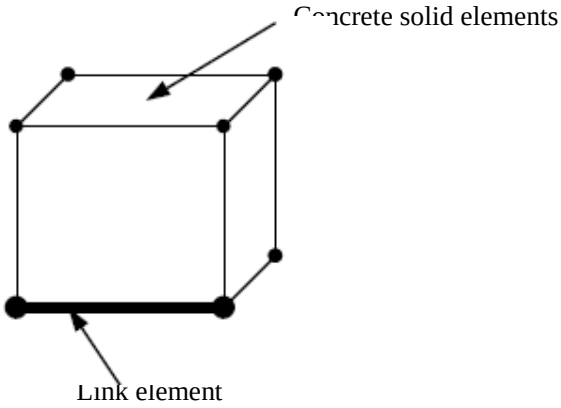

Fig. 3.9: Element connectivity: concrete solid and link elements

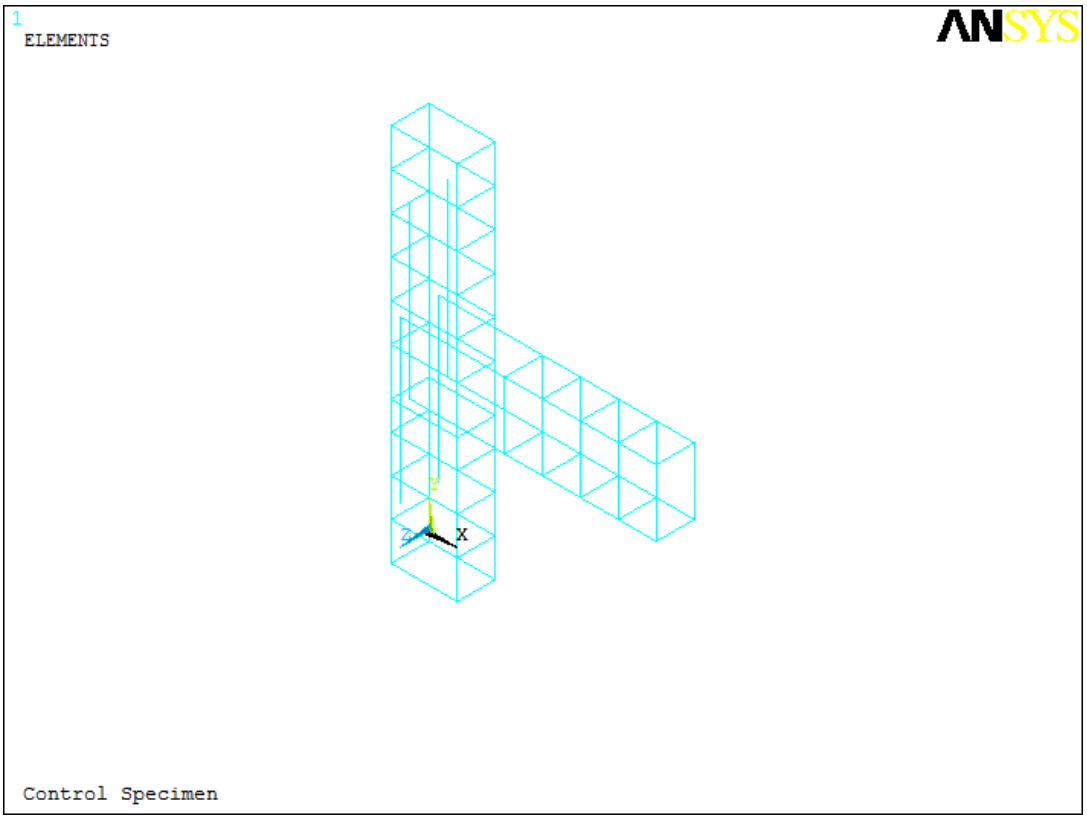

Fig. 3.10: Reinforcement Configuration modelled in ANSYS for the Control Specimen

The element type number, material number, and real constant set number for the control specimen are set for each mesh as shown in **Table 3.5**.

Table 3.5: Mesh Attributes for the Model of Control Specimen

Model Parts	Element Type	Material Number	Real Constant Set
Column	1	1	1
Beam	1	1	1
Rebar in Column	2	2	3
Top Rebar in Beam	2	2	2
Bottom Rebar in Beam	2	2	3
Stirrups	2	3	4
Steel plate	3	4	N/A

3.1.8 Loads and Boundary Conditions

Displacement boundary conditions are needed to constrain the model to get a unique solution. To achieve this, the translations at the nodes (UX, UY and UZ) are given constant values of 0. The support conditions at the bottom of the column are shown in **Fig. 3.11**. Similar support

conditions are given at the top of the column. The force, F, is applied at a distance of 300 mm from the face of the column. **Fig. 3.12** illustrates the applied loading.

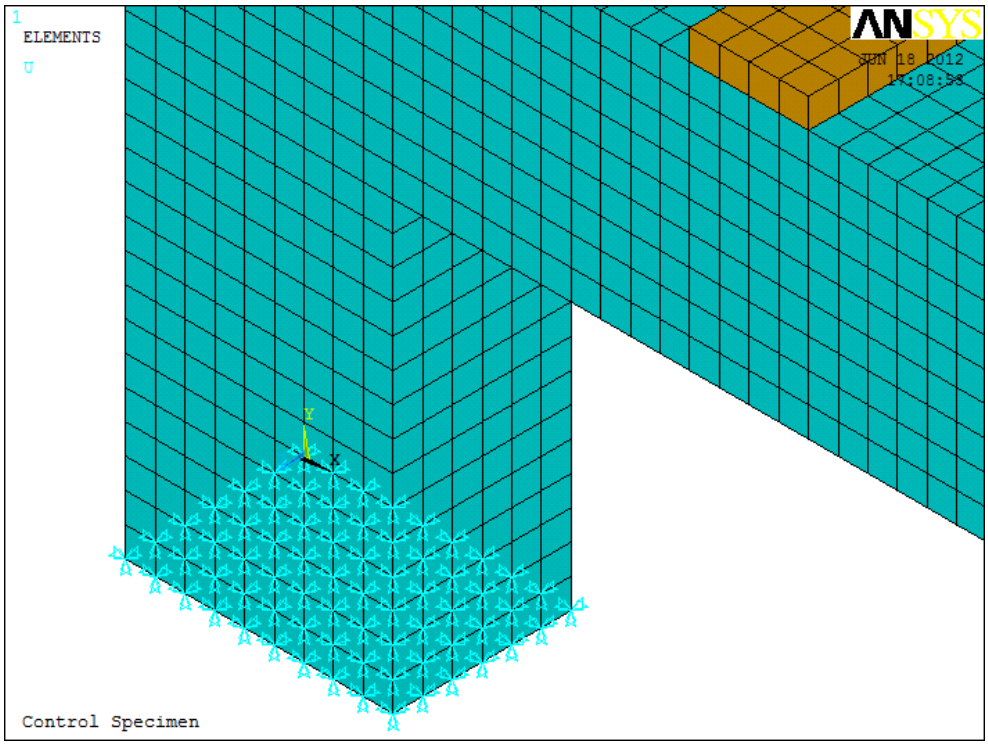

Fig. 3.11: Boundary Conditions for the Control Specimen

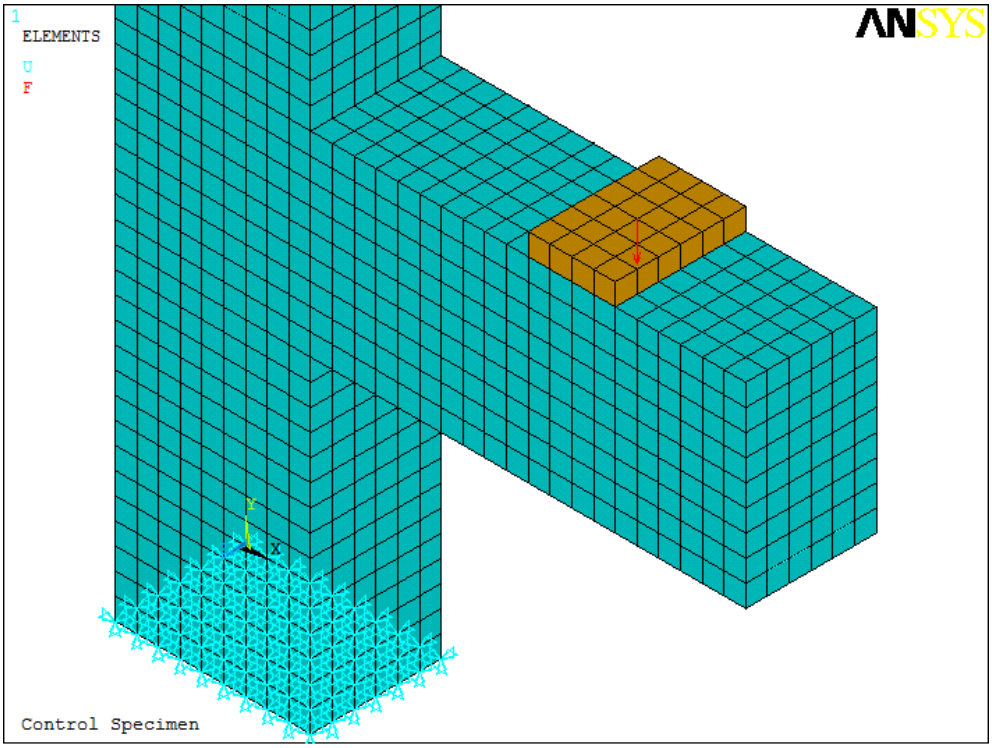

Fig. 3.12: Loading Conditions for the Control Specimen

3.1.9 Analysis Type

For the purpose of this model, the Static analysis type is utilized. The Restart command is utilized to restart an analysis after the initial run or load step has been completed.

The Sol'n Controls command dictates the use of a linear or non-linear solution for the finite element model. Typical commands utilized in a nonlinear static analysis are shown in **Table 3.6**.

Table 3.6: Commands Used to Control Nonlinear Analysis

Analysis Options	Small Displacement
Calculate Prestress Effects	No
Time at End of Loadstep	5000
Automatic Time Stepping	On
Number of Substeps	1
Max no. of Substeps	2
Min no. of Substeps	1
Write Items to Results File	All Solution items
Frequency	Write Every Substep

In the particular case considered in this thesis, the analysis is small displacement and static. The time at the end of the load step refers to the ending load per load step. **Table 3.6** shows the first load step taken. The sub steps are set to indicate load increments used for this analysis. The commands used to control the solver and output are shown in **Table 3.7**.

Table 3.7: Commands Used to Control Output

Equation Solvers	Sparse Direct
Number of Restart Files	1
Frequency	Write Every Substep

All these values are set to ANSYS 12.1 **(SAS, 2009)** defaults. The commands used for the nonlinear algorithm and convergence criteria are shown in **Table 3.8**. All values for the nonlinear algorithm are set to defaults.

Table 3.8: Nonlinear Algorithm and Convergence Criteria Parameters

Line Search	Off	
DOF solution predictor	Prog Chosen	
Maximum number of iteration	100	
Cutback control	Cutback according to predicted number of iter.	
Equiv. Plastic Strain	0.15	
Explicit Creep ratio	0.1	
Implicit Creep ratio	0	
Incremental displacement	1,00,00,000	
Points per cycle	13	
Set Convergence Criteria		
Label	F	U
Ref. Value	Calculated	Calculated
Tolerance	0.001	0.01
Norm	L2	L2
Min. Ref.	Not applicable	Not applicable

Table 3.9 shows the command used for the advanced nonlinear settings. The program behaviour upon nonconvergence for this analysis is set such that the program will terminate but not exit. The rest of the commands are set to defaults.

Table 3.9: Advanced Nonlinear Control Settings Used

Program behaviour upon nonconvergence	Terminate but do not exit
Nodal DOF sol'n	0
Cumulative iter	0
Elapsed time	0
CPU time	0

3.1.10 Analysis Process

The FE analysis of the model is set up to examine three different behaviours: initial cracking of the beam, yielding of the steel reinforcement, and the strength limit state of the beam-column joint. The Newton-Raphson method of analysis is used to compute the nonlinear response.

The application of the loads up to failure is done incrementally as required by the Newton-Raphson procedure. After each load increment is applied, the restart option is used to go to the next step after convergence. A listing of the load steps, sub steps, and loads applied per restart file are shown in **Table 3.10**.

The time at the end of each load step corresponds to the loading applied. For the first load step the time at the end of the load step is 5000 referring to a load of, F, of 5000 N applied on the beam.

The two convergence criteria used for the analysis are Force and Displacement. These criteria are left at the default values up to the cracking load. However, when the joint begin cracking, convergence for the non-linear analysis is impossible with the default values. The displacement converges, but the force does not. Therefore, the convergence criterion for force is dropped and the reference value for displacement criteria is changed to 5. This value is then multiplied by the tolerance value of 0.05 to produce a criterion of 0.25 during the nonlinear solution for convergence. A small criterion must be used to capture correct response. This criterion is used for the remainder of the analysis.

Table 3.10: Load Increment for Analysis of Finite Element Model of Control Specimen

Beginning Time	Time at End of Loadtsep	Load Step	Sub Step	Load Increment (N)
0	5,000	1	1	5,000
5,000	6,000	2	10	1,000
6,000	7,000	3	10	1,000
7,000	8,000	4	10	1,000
8,000	9,000	5	10	1,000
9,000	10,000	6	10	1,000
10,000	15,000	7	20	5,000
15,000	20,000	8	20	5,000
20,000	25,000	9	10	5,000
25,000	30,000	10	10	5,000
30,000	35,000	11	10	5,000
35,000	40,000	12	10	5,000
40,000	45,000	13	10	5,000
45,000	50,000	14	10	5,000
50,000	55,000	15	10	5,000

Failure for the model is defined when the solution for a 1 N load increment still does not converge. The program then gives a message specifying that the model has a significantly large deflection, exceeding the displacement limitation of the ANSYS program.

ANSYS gives deflection and crack patterns at various load increments which are presented in Chapter 4. The results from the FEM study of the controlled specimen are compared with the results from the experimental study conducted by **Dar (2011)**. This ensures that the elements, material properties, real constants and convergence criteria are adequate to model the response of the member. This gives confidence in the use of ANSYS (**SAS, 2009**) and the model developed. This approach is then used to analyse a retrofitted beam-column joint.

3.2 RETROFITTED SPECIMEN

The control specimen is now retrofitted with externally bonded carbon-fiber reinforced polymer (CFRP) with a typical retrofitting scheme and analysed in ANSYS 12.1 software.

3.2.1 Assumptions

The assumptions made in the FEM modelling of the retrofitted specimen are summarized below:

- Concrete and steel are modelled as isotropic and homogeneous materials.
- Steel is assumed to be an elastic-perfectly plastic material and identical in tension and compression.
- The tensile behaviour of the FRP reinforcement is linear-elastic until failure.
- Initially plane sections remain plane after loading (that is, the strain in the concrete and the reinforcement is proportional to the distance from the neutral axis).
- The maximum compressive strain in the concrete is assumed to be 0.0035 mm/mm as suggested by **IS 456: 2000**.
- The tensile strength of the concrete is ignored.
- The FRP reinforcement is assumed to carry stress along its axis only.
- Perfect bond exits between different materials.

3.2.2 Failure Criteria for FRP

FRP composite materials are not homogeneous. Their properties are dependent on many factors, the most important of which are the type of fibre, quantity of fibre (as volume fraction) and the configuration of the reinforcement. They are generally completely elastic up to failure and exhibit neither a yield point nor a region of plasticity. They tend to have low strain to failure (less than 3%). If all the fibres are aligned in one direction then the composite is relatively stiff and strong in that direction, but in the transverse direction it has low modulus and low strength. Longitudinal tensile strength and elongation at break are generally the two parameters which govern the failure of the unidirectional FRP.

3.2.3 Element Types

The Solid185 element is used for the modelling Fiber Reinforced Polymer (FRP). This element is defined by eight nodes having three degrees of freedom at each node – translations in the nodal *x*, *y*, and *z* directions. The element is capable of plasticity, hyperelasticity, stress stiffening, creep, large deflection, and large strain capabilities.

SOLID185 is available in two forms:

- Homogeneous Structural Solid; and
- Layered Structural Solid.

Layered Structural Solid is used to model FRP. This element allows for up to 250 different material layers with different orientations and orthotropic material properties in each layer. The geometry, node locations, and the coordinate system are shown in **Fig. 3.13**.

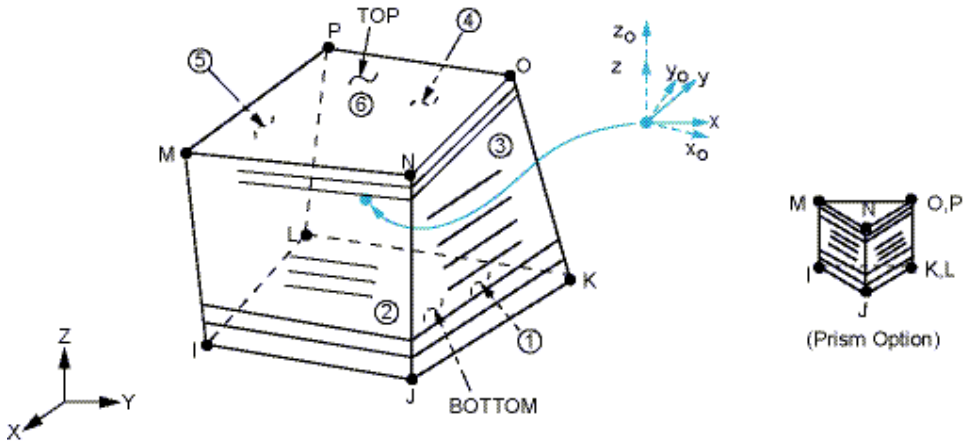

Fig. 3.13: Solid185 Element (Layered Structural Solid) **(SAS, 2009)**

Solid185 is a current-technology element and is preferred over the legacy element, Solid46, as suggested by ANSYS **(SAS, 2009)**.

The elements used for the retrofitted specimen are tabulated in **Table 3.11**.

Table 3.11: Element types for the Retrofitted Specimen

Material Type	ANSYS Element
Concrete	Solid65
Steel Reinforcement	Link180
Steel Plate	Solid185 (Homogeneous Structural Solid)
FRP	Solid185 (Layered Structural Solid)

3.2.4 Real Constants

No real constant set exists for the Solid185 element. Real constants for concrete and steel reinforcement in the retrofitted specimen are same as that for the control specimen (refer **Table 3.2**).

3.2.5 Material Properties

Parameters needed to define the material models for the retrofitted specimen are shown **Table 3.12**. Note that, there are multiple parts of the material model for each element. Concrete, steel reinforcement and steel plate properties are same as that for the Control Specimen (refer **Table 3.3**). Material properties for 230 gsm unidirectional Carbon Fiber sheets (MBrace CF 240) as specified by the chemical company BASF are taken in the present study.

Table 3.12: Material Models for the Retrofitted Specimen

Material Model Number	Element Type	Material Properties
1	Solid65	Refer **Table 3.3**
2	Link180	Refer **Table 3.3**
3	Link180	Refer **Table 3.3**
4	Solid185 (Homogeneous Structural Solid)	Refer **Table 3.3**

5	Solid185 (Layered Structural Solid)	Linear Isotropic	
		EX	240,000 MPa
		EY	19,000 MPa
		EZ	19,000 MPa
		PRXY	0.22
		PRXZ	0.22
		PRYZ	0.30
		GXY	12,500 MPa
		GXZ	12,500 MPa
		GYZ	7,500 MPa
		Section (SECID: 1, SECTYPE: Shell)	
		Layer No. 1	
		TK	0.117 mm
		THETA	0 degree
		Layer No. 2	
		TK	0.117 mm
		THETA	90 degree
		Section (SECID: 2, SECTYPE: Shell)	
		Layer No. 1	
		TK	0.117 mm
		THETA	0 degree
		Failure Criteria	
		Stress – XTEN	3,800 MPa
		Strain – XTEN	0.015

Material Model Number 4 refers to the Solid185 (Layered Structural Solid) element. Input data needed for the FRP composites in the finite element models are as follows:

- Number of layers.
- Thickness of each layer (TK).
- Orientation of the fiber direction for each layer (THETA).
- Elastic modulus of the FRP composite in three directions (EX, EY and EZ).
- Shear modulus of the FRP composite for three planes (GXY, GXZ and GYZ).
- Major Poisson's ratio for three planes (PRXY, PRXZ and PRYZ).

The failure criteria for the unidirectional carbon fiber sheets consists of longitudinal tensile strength (XTEN) as 3800 MPa and elongation at break (XTEN) as 1.5%.

Note that a local coordinate system for the FRP layered solid elements is defined where the *x* direction is the same as the fiber direction, while the *y* and *z* directions are perpendicular to the *x* direction (**Fig. 3.14**).

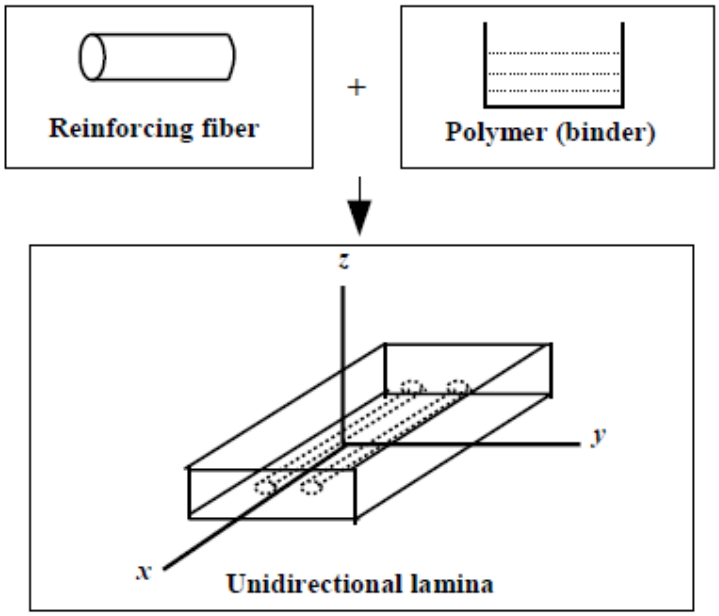

Fig. 3.14: Schematic of FRP composites

3.2.6 Modelling

A retrofitting scheme as shown in **Fig. 3.15** is adopted in the present study. It consists of applying CFRP sheets in three steps. In the first step, Layer 1 and 2 are applied. Second step consists of wrapping Layers 3, 4 and 5 on the three faces of the column. The final step involves wrapping Layer 6 on beam and Layer 7 on column.

The different FRP layers are modelled as volume in ANSYS. These dimensions are shown in **Table 3.13**. Note that volumes 1, 2 and 3 refer to the concrete column, beam and steel plate respectively and are already noted in **Table 3.4**. Thus **Table 3.13** starts with volume 4.

Vertical sheet of layer 1 is modelled as volume 4 and horizontal sheet is modelled as volume 5. Similarly, vertical sheet of layer 2 is modelled as volume 6 and horizontal sheet is modelled as volume 7. Layer 3 is modelled in three parts as volume 8, 9 and 10. Similarly, layers 4 and 5 are modelled as volumes 11, 12 & 13 and volumes 14, 15 & 16 respectively.

The front and back portions of layer 6 are modelled as volume 17 and 18 respectively. The top and bottom portions of layer 6 are covered in volumes 5 and 7 respectively and therefore not modelled separately. Similarly, layer 7 is covered in volumes 8, 10, 11, 13, 14 and 16 and therefore not modelled separately.

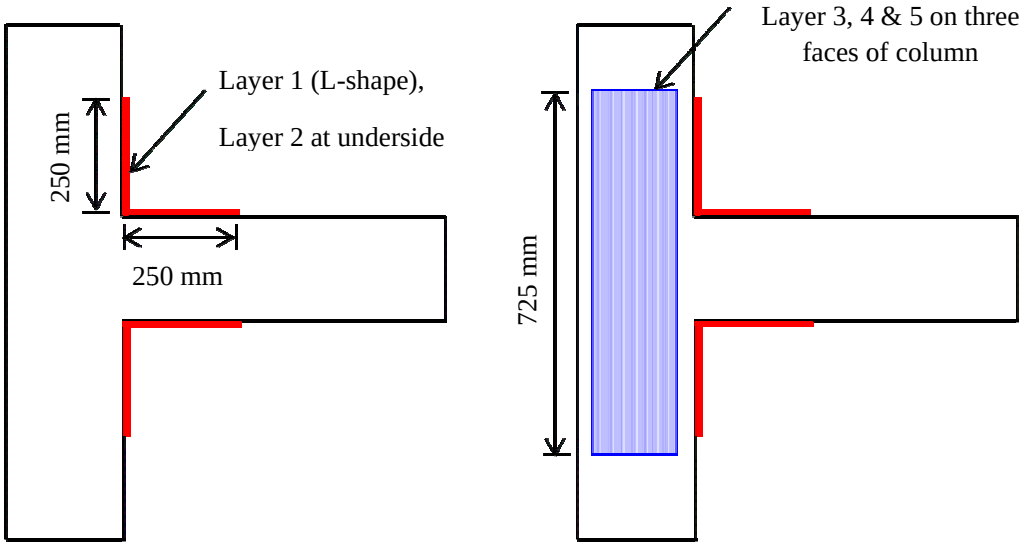

(a) Step 1 **(b) Step 2**

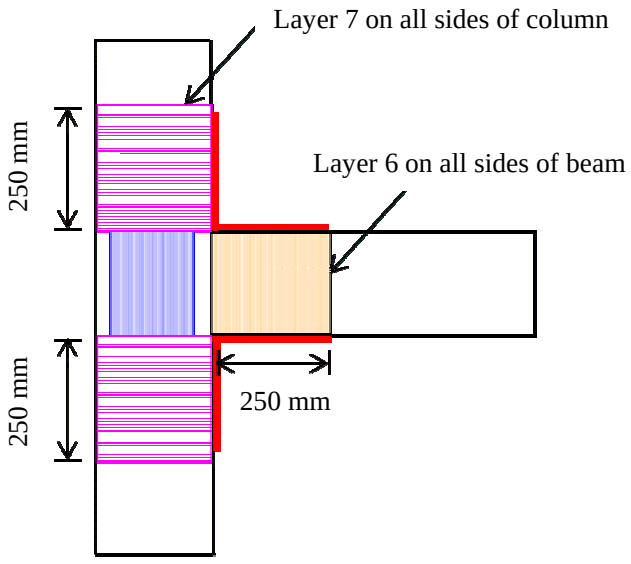

(c) Step 3

Fig. 3.15: Retrofitting Scheme adopted for the Retrofitted Specimen

Table 3.13: Dimensions for FRP in ANSYS

ANSYS	FRP					
Layer 1						
	Volume 4		Volume 5			
X1, X2 X-coordinates	225	250	250	475		
Y1, Y2 Y-coordinates	600	850	600	625		
Z1, Z2 Z-coordinates	-25	175	-25	175		
Layer 2						
	Volume 6		Volume 7			
X1, X2 X-coordinates	225	250	250	475		
Y1, Y2 Y-coordinates	125	375	350	375		
Z1, Z2 Z-coordinates	-25	175	-25	175		
Layer 3						
	Volume 8		Volume 9		Volume 10	
X1, X2 X-coordinates	0	225	0	225	0	225
Y1, Y2 Y-coordinates	125	375	375	600	600	850
Z1, Z2 Z-coordinates	150	175	150	175	150	175
Layer 4						
	Volume 11		Volume 12		Volume 13	
X1, X2 X-coordinates	0	-25	0	-25	0	-25
Y1, Y2 Y-coordinates	125	375	375	600	600	850
Z1, Z2 Z-coordinates	-25	175	-25	175	-25	175
Layer 5						
	Volume 14		Volume 15		Volume 16	
X1, X2 X-coordinates	0	225	0	225	0	225
Y1, Y2 Y-coordinates	125	375	375	600	600	850
Z1, Z2 Z-coordinates	0	-25	0	-25	0	-25
Layer 6						
	Volume 17		Volume 18			
X1, X2 X-coordinates	250	475	250	475		
Y1, Y2 Y-coordinates	375	600	375	600		
Z1, Z2 Z-coordinates	150	175	0	-25		

The combined volumes created in ANSYS are shown in **Fig. 3.16**.

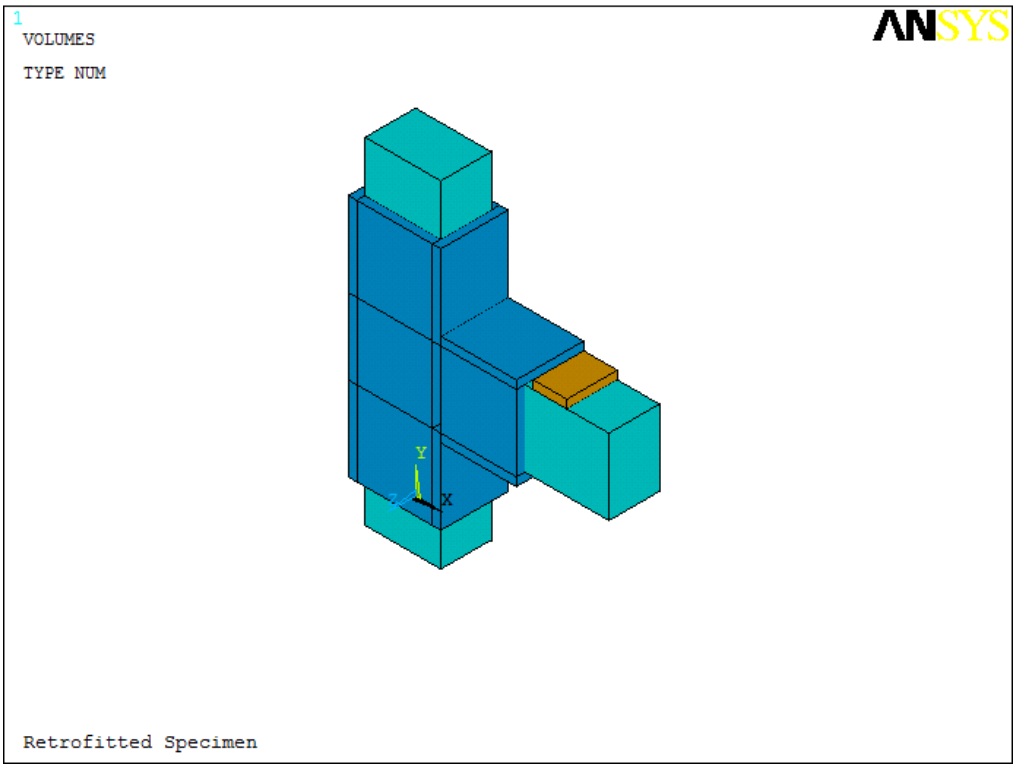

Fig. 3.16: Volumes created in ANSYS for the Retrofitted Specimen

As noted by **Kachlakev, et al. (2001)**, the various thicknesses of the FRP composites create discontinuities, which are not desirable for the finite element analysis. These may develop high stress concentrations at local areas on the models; consequently, when the model is run, the solution may have difficulties in convergence. Therefore, a consistent overall thickness of FRP composite is used in the models to avoid discontinuities. The equivalent overall stiffness of the FRP materials is maintained by making compensating changes in the elastic and shear moduli assigned to each FRP layer. For example, if the thickness of an FRP laminate was artificially doubled to maintain a constant overall thickness, the elastic and shear moduli in that material are reduced by 50% to compensate. Note that the relationship between elastic and shear moduli is linear. **Eq. 3.10** shows the relationship between elastic and shear moduli (**SAS, 2009**).

$$G_{xy} = \frac{E_x E_y}{E_x + E_y + 2\nu_{xy} E_x} \qquad (\mathbf{3.10})$$

where:

G_{xy}= Shear modulus in the *xy* plane;

E_x = Elastic modulus in the *x* direction;

E_y = Elastic modulus in the *y* direction;

ν_{xy} = Major Poisson's ratio.

3.2.7 Meshing

For the retrofitted specimen, meshing of concrete and reinforcement members is done in the same way as for the control specimen (see **Fig. 3.8** and **3.10**). FRP sheets are meshed as brick elements in such a way that the nodes of the FRP layered solid elements are connected to those of adjacent concrete solid elements in order to satisfy the perfect bond assumption. **Fig. 3.17** illustrates the element connectivity.

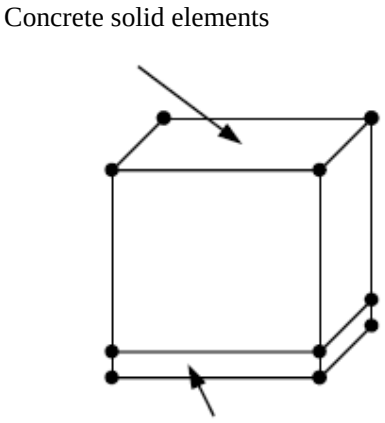

Fig. 3.17: Element connectivity: concrete solid and FRP layered solid elements

The overall mesh of the retrofitted specimen created in ANSYS is shown in **Fig. 3.18**.

To achieve the correct nodal ordering for the FRP layered element, the volumes are properly oriented before executing the meshing command. The command 'merge items' is used to merge separate entities that have the same location. The element type number, material number, real constant set number and section ID for the retrofitted specimen are set for each mesh as shown in **Table 3.14**.

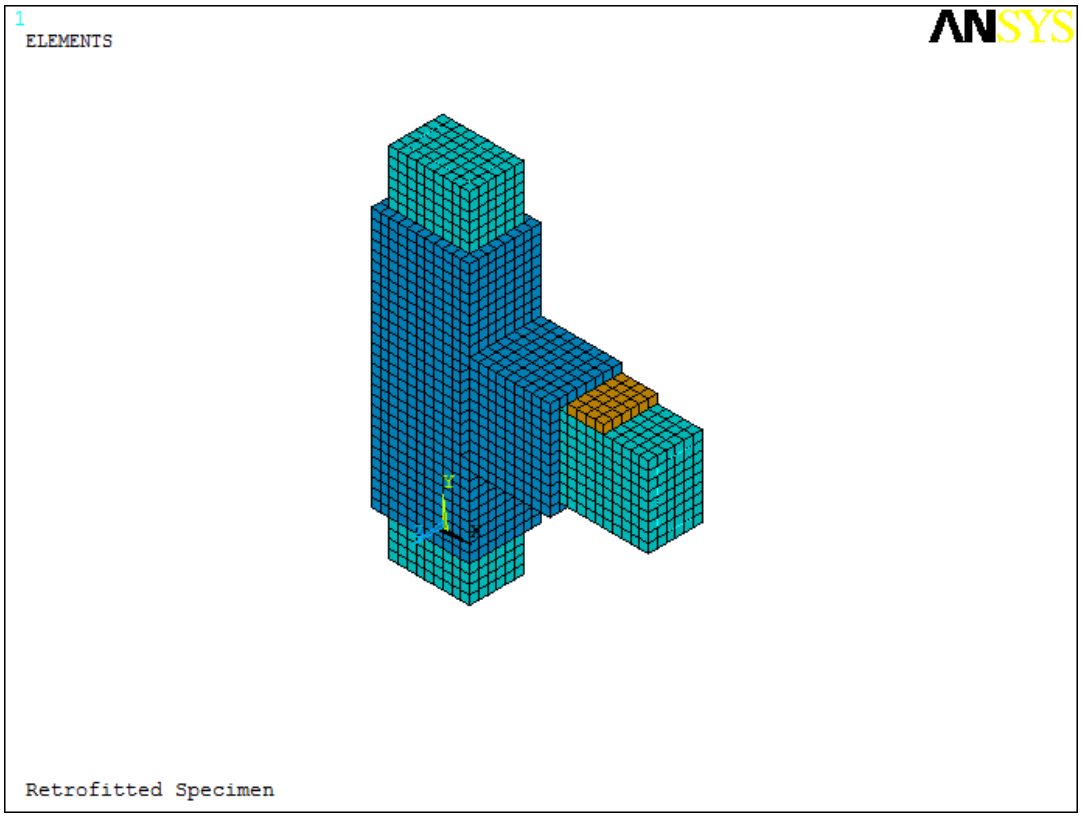

Fig. 3.18: Mesh created in ANSYS for the Retrofitted Specimen

Table 3.14: Mesh Attributes for the Retrofitted Specimen

Model Parts	Element Type	Material Number	Real Constant Set	SECID
Column	1	1	1	N/A
Beam	1	1	1	N/A
Rebar in Column	2	2	3	N/A
Top Rebar in Beam	2	2	2	N/A
Bottom Rebar in Beam	2	2	3	N/A
Stirrups	2	3	4	N/A
Steel Plate	3	4	N/A	N/A
Volume 4	4	5	N/A	1
Volume 5	4	5	N/A	1
Volume 6	4	5	N/A	1
Volume 7	4	5	N/A	1
Volume 8	4	5	N/A	1
Volume 9	4	5	N/A	2
Volume 10	4	5	N/A	1

Volume 11	4	5	N/A	1
Volume 12	4	5	N/A	2
Volume 13	4	5	N/A	1
Volume 14	4	5	N/A	1
Volume 15	4	5	N/A	2
Volume 16	4	5	N/A	1
Volume 17	4	5	N/A	2
Volume 18	4	5	N/A	2

3.2.8 Loads and Boundary Conditions

Displacement boundary conditions are applied to constrain the model as done in the modelling of control specimen. The translations at the nodes (UX, UY and UZ) are given constant values of 0. The support conditions at the bottom of the column are shown in **Fig. 3.19**. Similar support conditions are given at the top of the column.

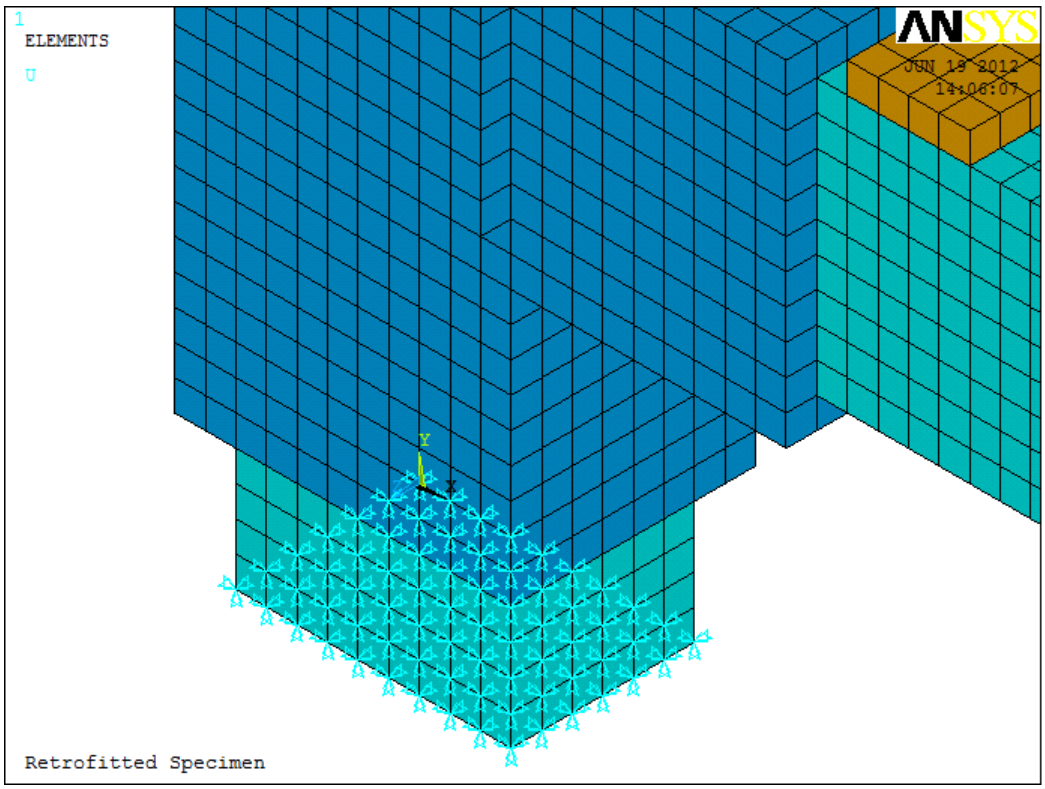

Fig. 3.19: Boundary Conditions for the Retrofitted Specimen

The force, F, is applied at a distance of 300 mm from the face of the column similar to the control specimen. **Fig. 3.20** illustrates the applied loading. The applied force is distributed among the nodes at that point.

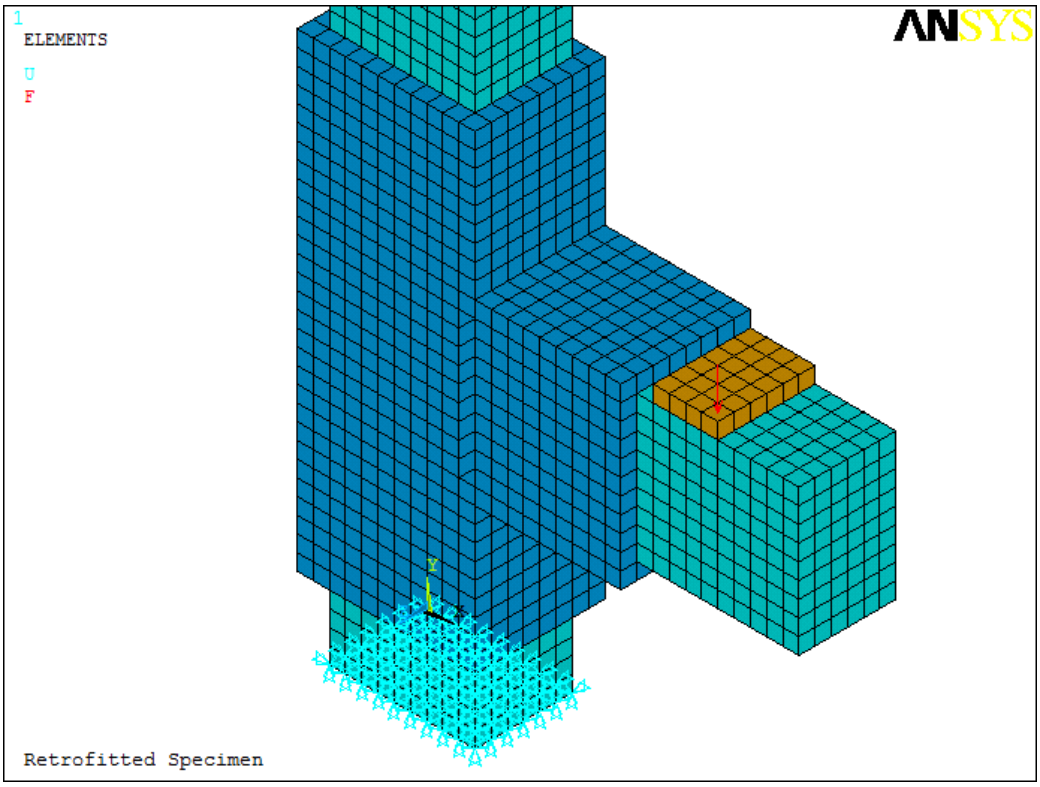

Fig. 3.20: Loading Conditions for the Retrofitted Specimen

3.2.9 Analysis Type

For the purpose of the retrofitted specimen, the Static analysis type is utilized. The Restart command is utilized to restart an analysis after the initial run or load step has been completed.

The Sol'n Controls commands utilized for the nonlinear static analysis are similar to the one used for the control specimen (**Table 3.6** to **3.9**).

3.2.10 Analysis Process

The application of the loads up to failure is done incrementally as required by the Newton-Raphson procedure. After each load increment is applied, the restart option is used to go to the next step after convergence. A listing of the load steps, sub steps, and loads applied per restart file are shown in **Table 3.15**.

The time at the end of each load step corresponds to the loading applied. For the first load step the time at the end of the load step is 5000 referring to a load of, F, of 5000 N applied on the beam.

The two convergence criteria used for the analysis are Force and Displacement. These criteria are left at the default values up to the cracking load. However, when the joint begin cracking, convergence for the non-linear analysis is impossible with the default values. The displacement converges, but the force does not. Therefore, the convergence criterion for force is dropped and the reference value for displacement criteria is changed to 5. This value is then multiplied by the tolerance value of 0.05 to produce a criterion of 0.25 during the nonlinear solution for convergence. A small criterion must be used to capture correct response. This criterion is used for the remainder of the analysis.

Table 3.15: Load Increment for Analysis of Finite Element Model of Retrofitted Specimen

Beginning Time	Time at End of Loadtsep	Load Step	Sub Step	Load Increment (N)
0	5,000	1	1	5,000
5,000	10,000	2	10	5,000
10,000	15,000	3	10	5,000
15,000	20,000	4	10	5,000
20,000	25,000	5	10	5,000
25,000	30,000	6	10	5,000
30,000	35,000	7	10	5,000
35,000	40,000	8	10	5,000
40,000	45,000	9	10	5,000
45,000	50,000	10	10	5,000
50,000	55,000	11	10	5,000
55,000	60,000	12	10	5,000
60,000	65,000	13	10	5,000
65,000	70,000	14	10	5,000
70,000	75,000	15	10	5,000
75,000	80,000	16	10	5,000

Failure for the model was defined when the solution for a 1 N load increment still does not converge. The program then gives a message specifying that the models have a significantly large deflection, exceeding the displacement limitation of the ANSYS program.

ANSYS gives deflection and crack patterns at various load increments which are presented in Chapter 4. The results from the FEM study of the retrofitted specimen are compared with the results of the controlled specimen.

In this chapter, the results from the FEM study of the controlled specimen are compared with the results from the experimental study conducted by **Dar (2011)**. Then, the results from the FEM study of the retrofitted specimen are compared with the results of the controlled specimen.

4.1 CONTROL SPECIMEN

The deflection values from the analysis of control specimen in ANSYS are noted at three junctions: beam free end, 150 mm from beam free end and 400 mm from beam free end. These are presented in **Table 4.1**, **4.2** and **4.3** respectively.

Table 4.1: Load-Deflection Results from ANSYS at beam free end for Control Specimen

Load (kN)	Deflection (mm)	Load (kN)	Deflection (mm)
5.0	0.0674	**25.0**	3.1441
6.0	0.0808	**30.0**	4.2905
7.0	0.0944	**35.0**	5.8500
8.0	0.1078	**40.0**	7.8651
9.0	0.7268	**45.0**	10.367
10.0	0.8633	**47.5**	11.811
15.0	1.4042	**52.0**	25.321
20.0	2.2959		

Table 4.2: Load-Deflection results from ANSYS at 150 mm from beam free end for Control Specimen

Load (kN)	Deflection (mm)	Load (kN)	Deflection (mm)
5.0	0.0486	**25.0**	2.2107
6.0	0.0584	**30.0**	3.0045
7.0	0.0682	**35.0**	4.0822
8.0	0.0779	**40.0**	5.4847

9.0	0.5173	**45.0**	7.1877
10.0	0.6163	**47.5**	8.7206
15.0	1.0038	**52.0**	22.125
20.0	1.6156		

Table 4.3: Load-Deflection results from ANSYS at 400 mm from beam free end for Control Specimen

Load (kN)	Deflection (mm)	Load (kN)	Deflection (mm)
5.0	0.0148	**25.0**	0.6736
6.0	0.0178	**30.0**	0.9119
7.0	0.0208	**35.0**	1.2332
8.0	0.0238	**40.0**	1.6526
9.0	0.1534	**45.0**	2.1606
10.0	0.1877	**47.5**	3.2670
15.0	0.3109	**52.0**	11.341
20.0	0.4917		

The deflected shape of the control specimen at 5000 N is shown in **Fig. 4.1**.

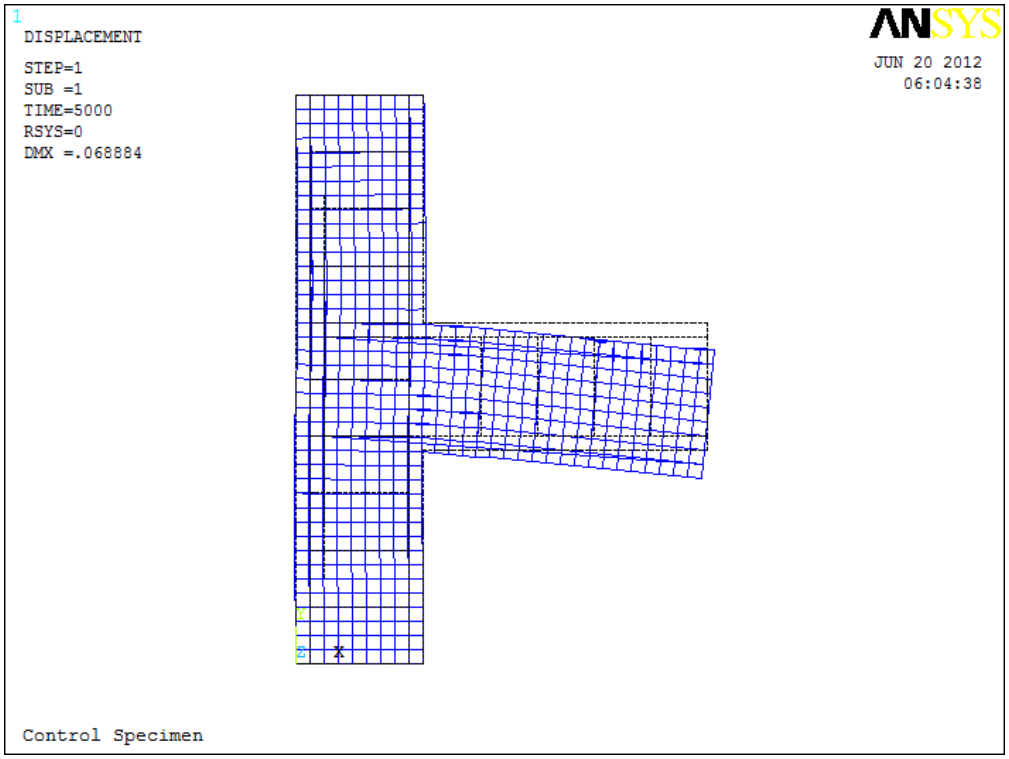

Fig. 4.1: Deflected shape of Control Specimen at 5000 N

The cracking patterns in the control specimen can be obtained in ANSYS using the Crack/Crushing plot option. Vector Mode plots must be turned on to view the cracking in the model. **Fig. 4.2** to **4.7** show the crack patterns at various load stages.

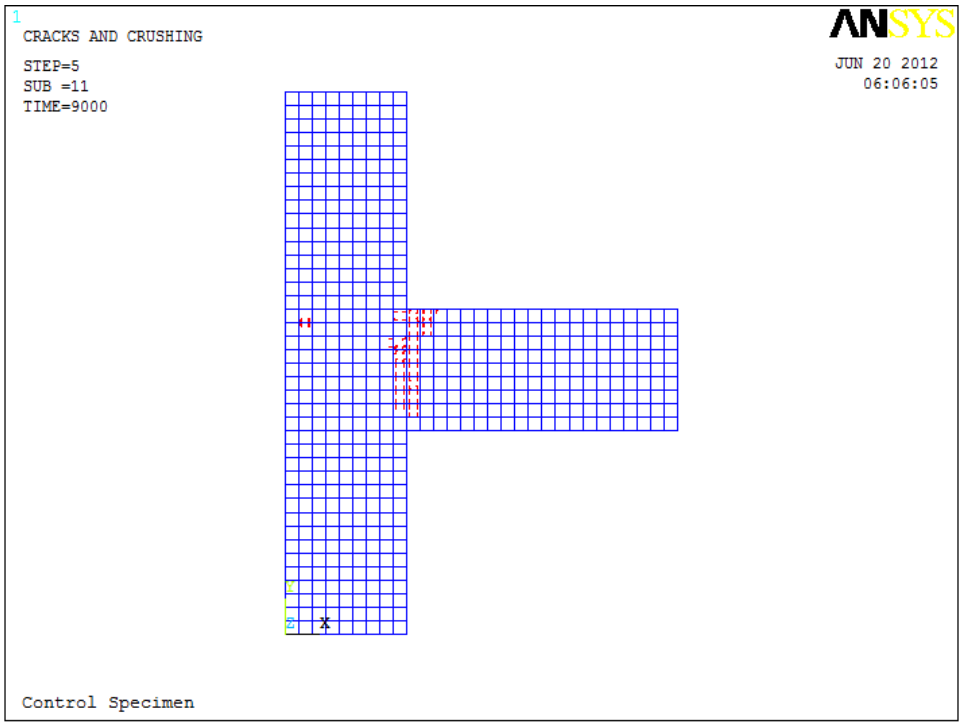

Fig. 4.2: 1st crack of the concrete model at 9000 N for control specimen

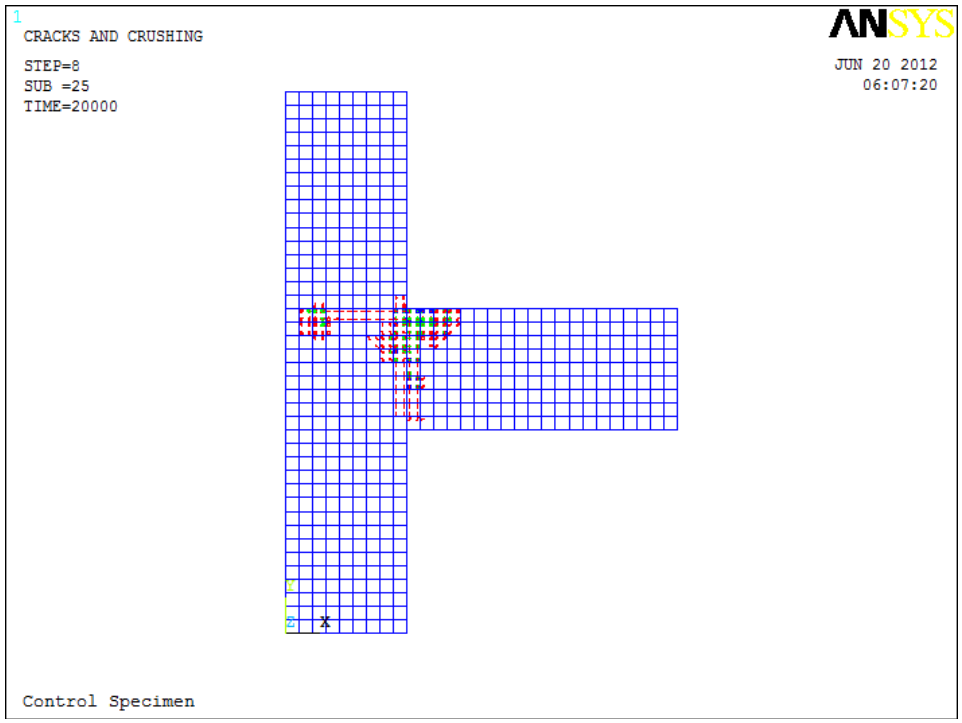

Fig. 4.3: Cracking of the concrete model at 20,000 N for control specimen

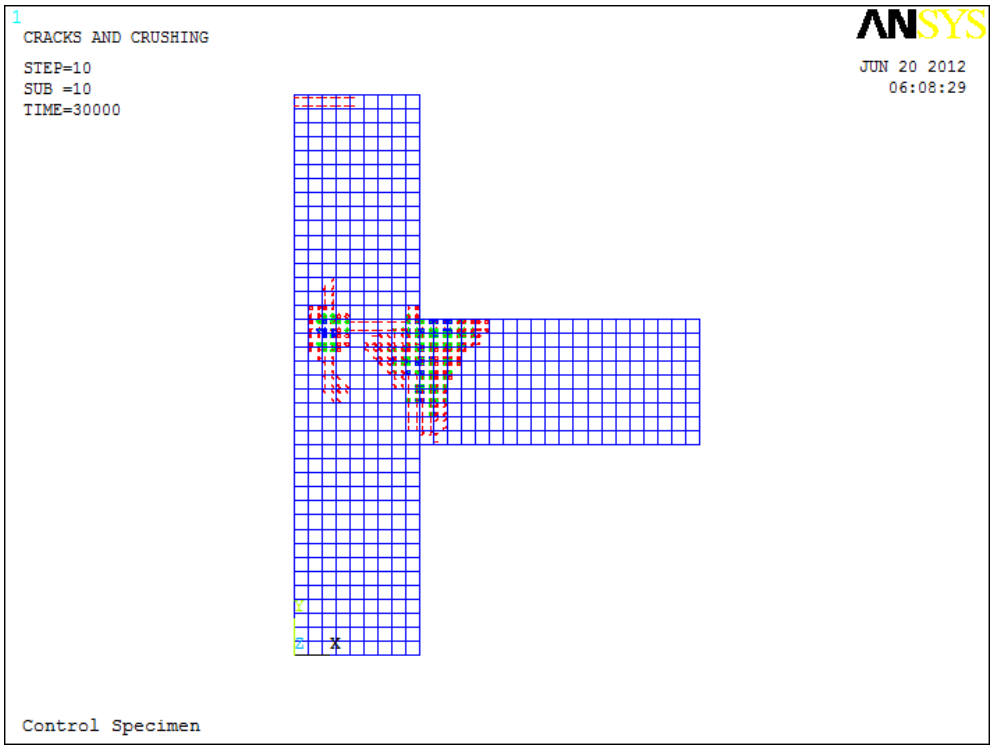

Fig. 4.4: Cracking of the concrete model at 30,000 N for control specimen

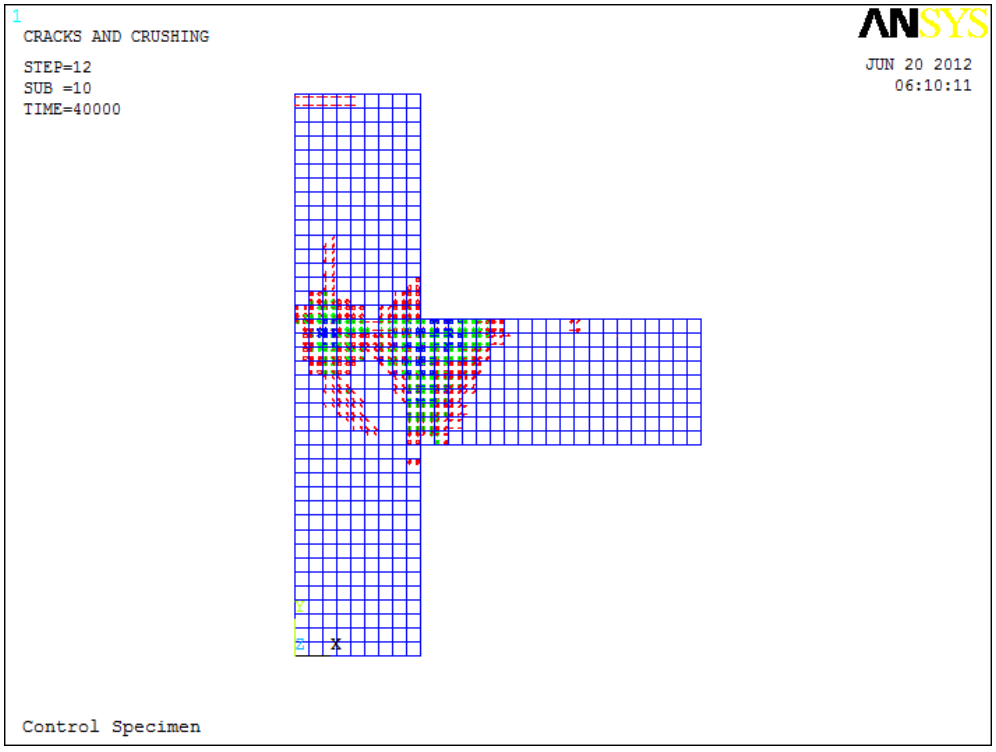

Fig. 4.5: Cracking of the concrete model at 40,000 N for control specimen

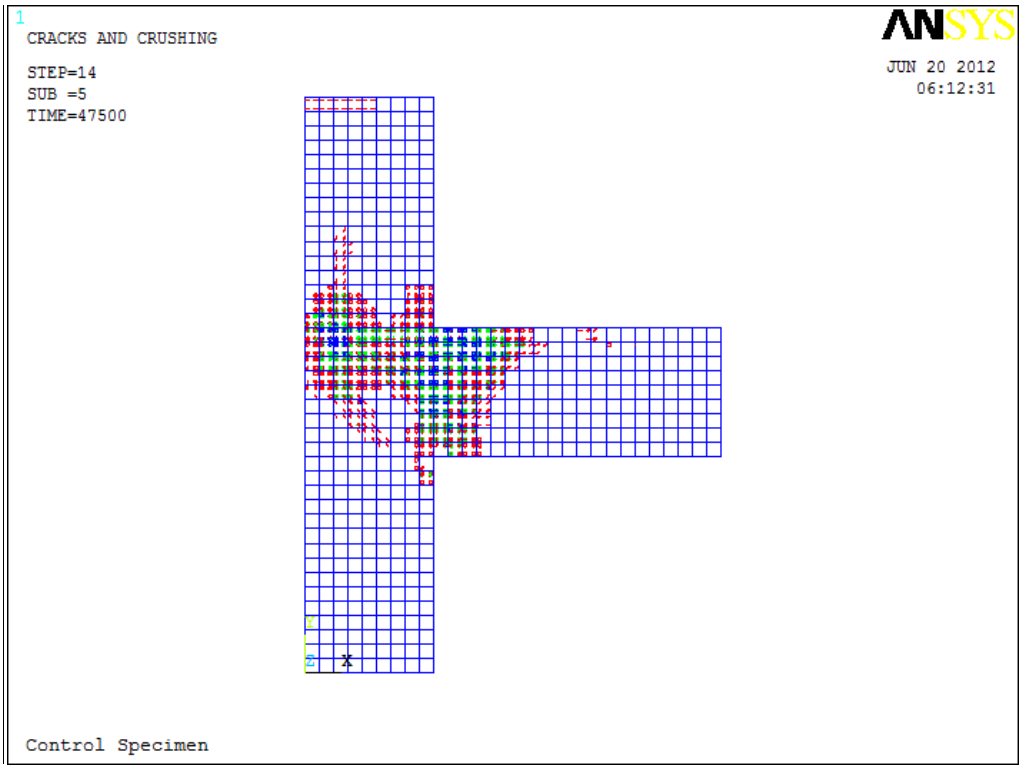

Fig. 4.6: Cracking of the concrete model at 47,500 N for control specimen

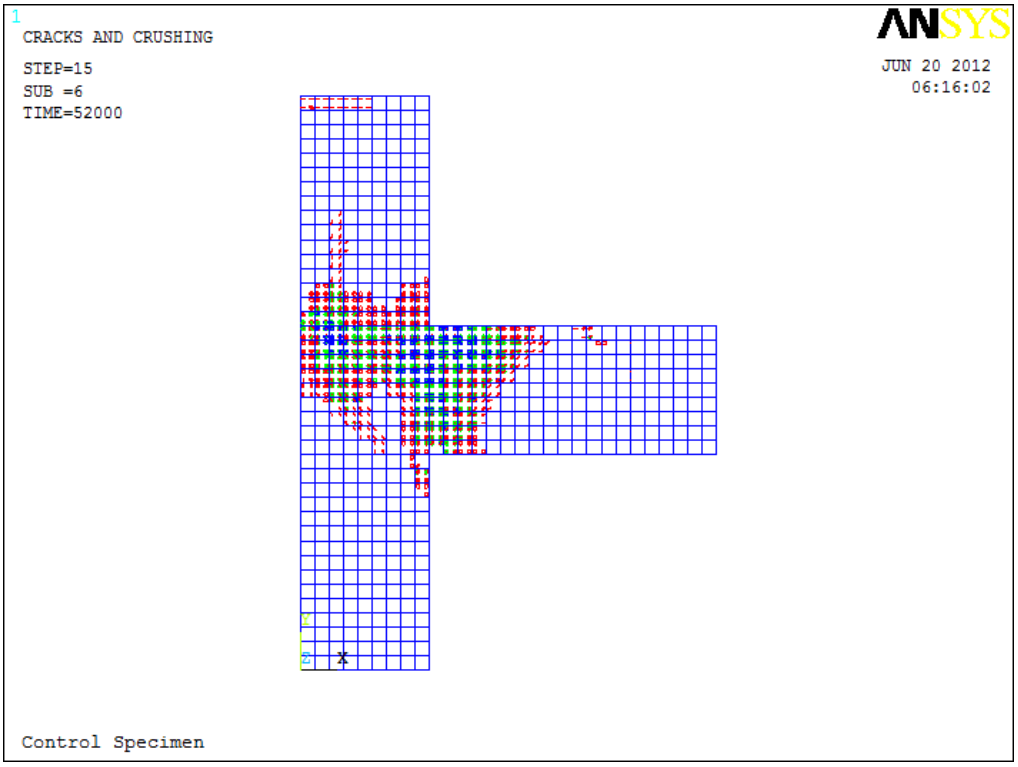

Fig. 4.7: Failure of the concrete model at 52,000 N for control specimen

The load-deflection results from ANSYS shown in **Table 4.1** to **4.3** are plotted in **Fig. 4.8**, **4.9** and **4.10**.

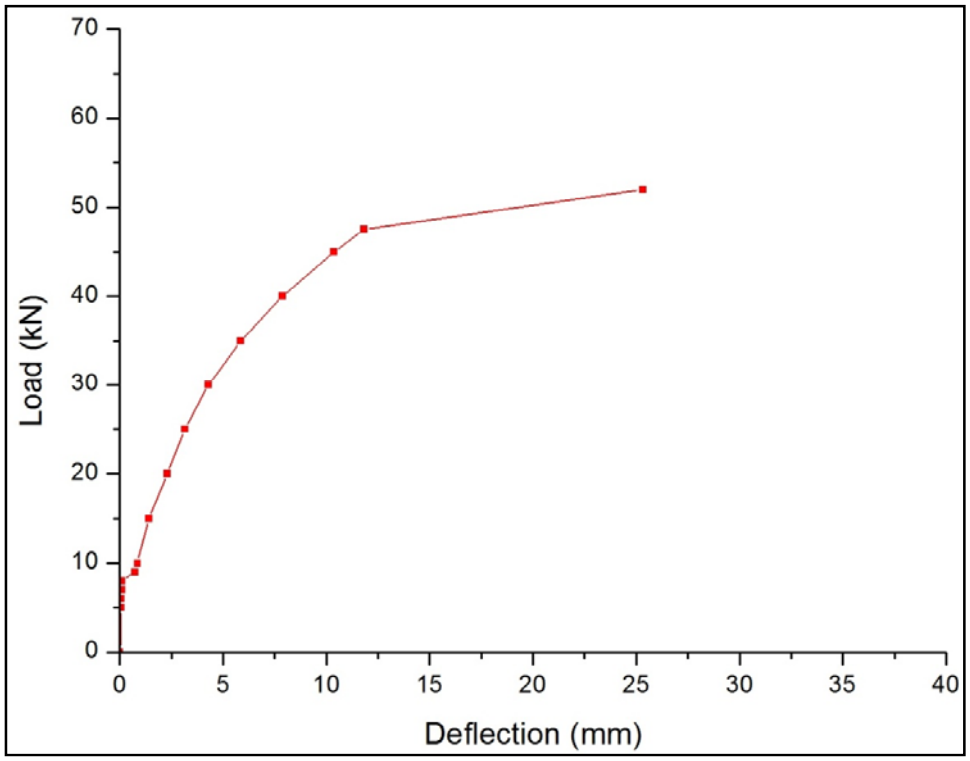

Fig. 4.8: Load-Deflection Results from ANSYS at beam free end for control specimen

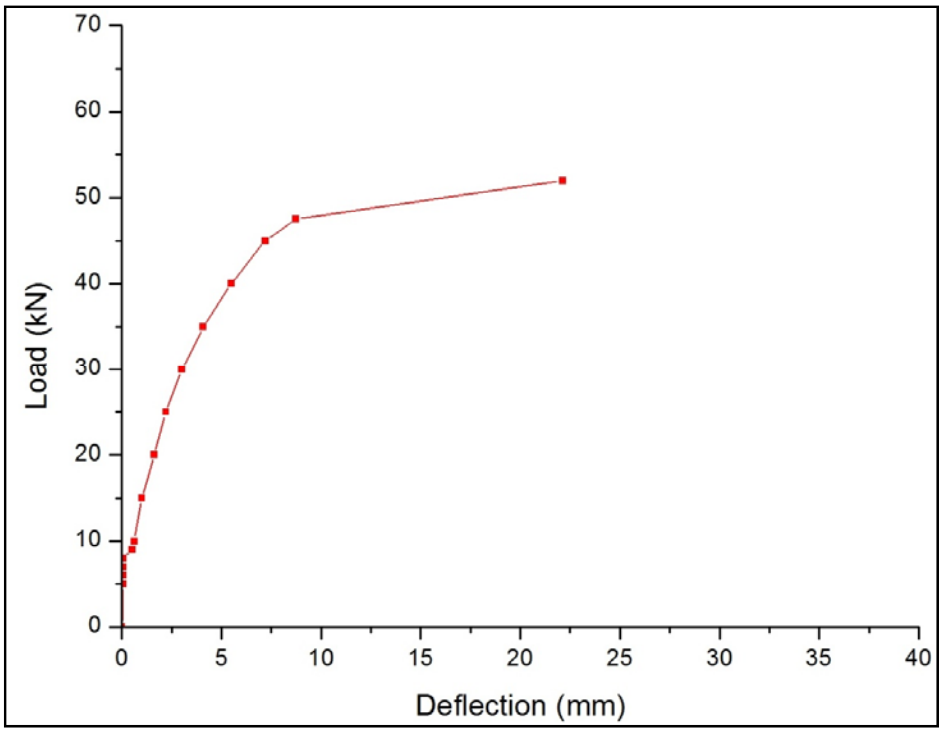

Fig. 4.9: Load-Deflection results from ANSYS at 150 mm from beam free end for control specimen

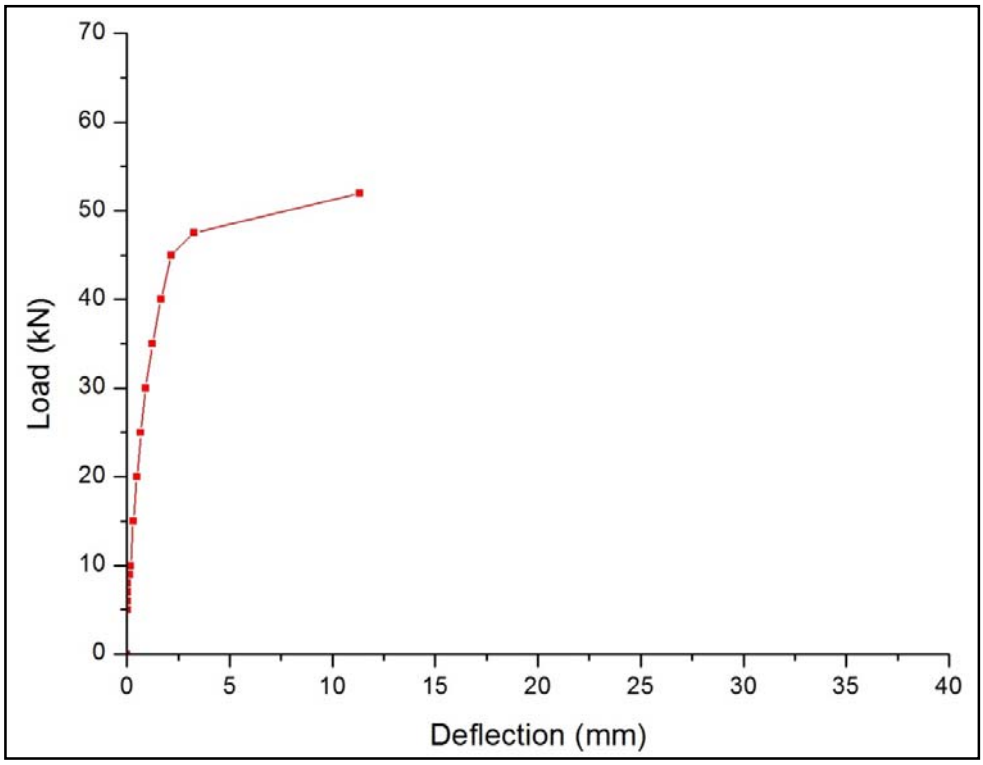

Fig. 4.10: Load-Deflection results from ANSYS at 400 mm from beam free end for control specimen

Fig. 4.8 to **4.10** shows that ANSYS is able to model the different components of a load-deflection curve i.e. the linear region, initial cracking, the nonlinear region, the yielding of steel, and failure.

Initially, the FE model remains in the linear region as represented by a straight line in **Fig. 4.8**. The first crack occurs at a load of around 9 kN as indicated by a change in slope of the linear region and is represented by point 'A' in **Fig. 4.8**. The crack pattern in **Fig. 4.2** also shows the presence of flexural cracks at this stage.

Once cracking occurs, deflections and stresses become more difficult to predict. After a load of 9 kN, the non-linear region starts and continues upto a load of 47.5 kN. This portion is represented from point 'A' to point 'B' in **Fig. 4.8**. In the non-linear region of the response, deflections increase and subsequent cracking occurs as more load is applied on the beam. Significant flexural and diagonal tension cracking occurs at the beam-column junction. Crack patterns at loads 20 kN, 30 kN and 40 kN are shown in **Fig. 4.3** to **4.5**.

After a load of 47.5 kN (point 'B' in **Fig. 4.8**), yielding of steel reinforcement occurs. At this point in the response, the displacements begin to increase at a higher rate as more load is applied. The cracked moment of inertia, yielding steel, and nonlinear concrete material,

now define the flexural rigidity of the member. The ability of the joint to distribute the load throughout the cross-section has diminished greatly and therefore greater deflections occur. Severe cracking of the joint is seen at this load in **Fig. 4.6**. At the ultimate load of 52.0 kN (point 'C' in **Fig. 4.8**), the joint can no longer support additional load as indicated by an insurmountable convergence failure. Failure of the joint is seen at this load in **Fig. 4.7**.

It is noted that due to the inability of ANSYS to model the strain softening effect of concrete, the load-deflection curves are only available till the ultimate load. Beyond this point, the program gives a message specifying that the model has a significantly large deflection, exceeding the displacement limitation of the ANSYS program. This indicates failure of the beam-column joint.

The load-deflection results from ANSYS shown in **Table 4.1** to **4.3** are now compared with the results from the experimental study conducted by **Dar (2011)** and plotted in **Fig. 4.11**, **4.12** and **4.13**.

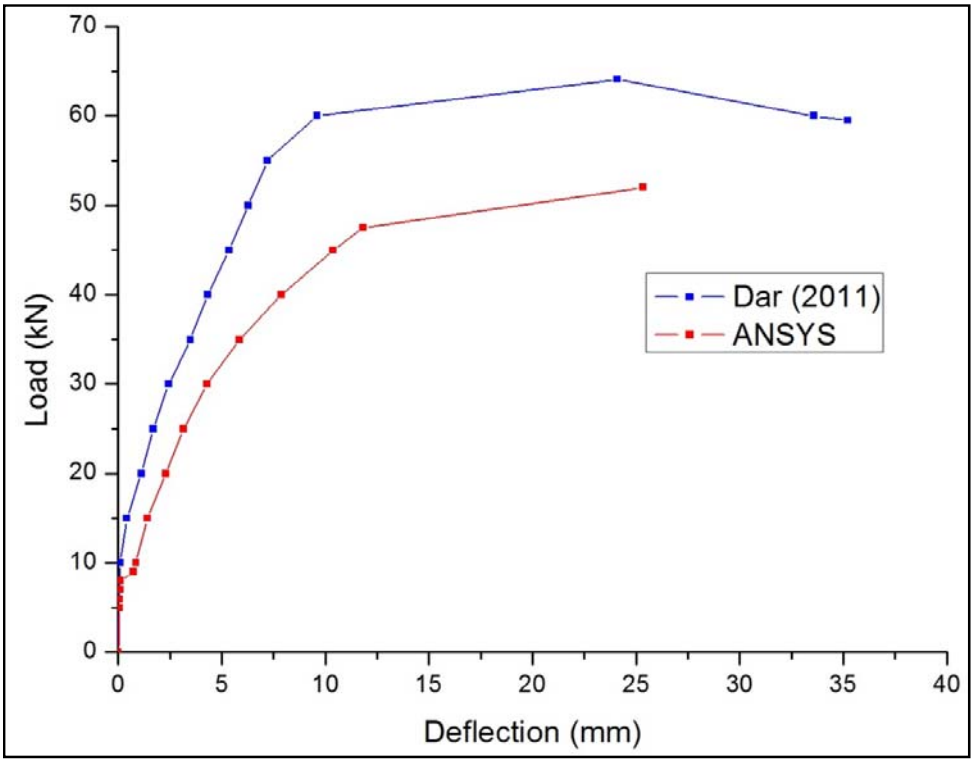

Fig. 4.11: Comparison of Load-deflection results at beam free end for control specimen with **Dar (2011)**

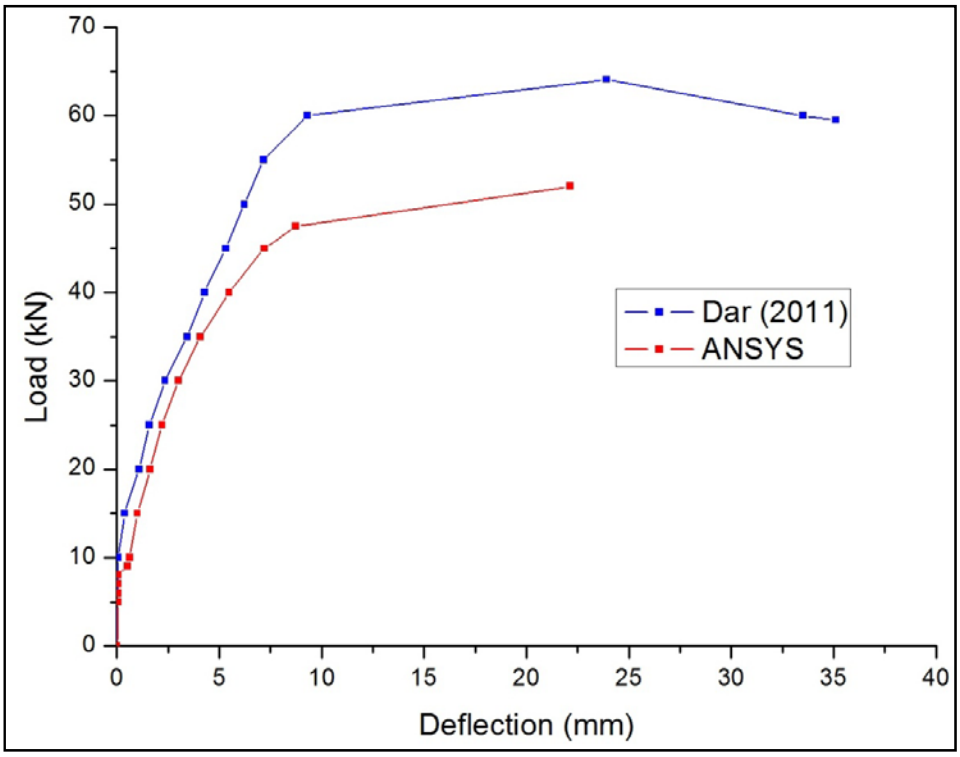

Fig. 4.12: Comparison of Load-deflection results at 150 mm from beam free end for control specimen with **Dar (2011)**

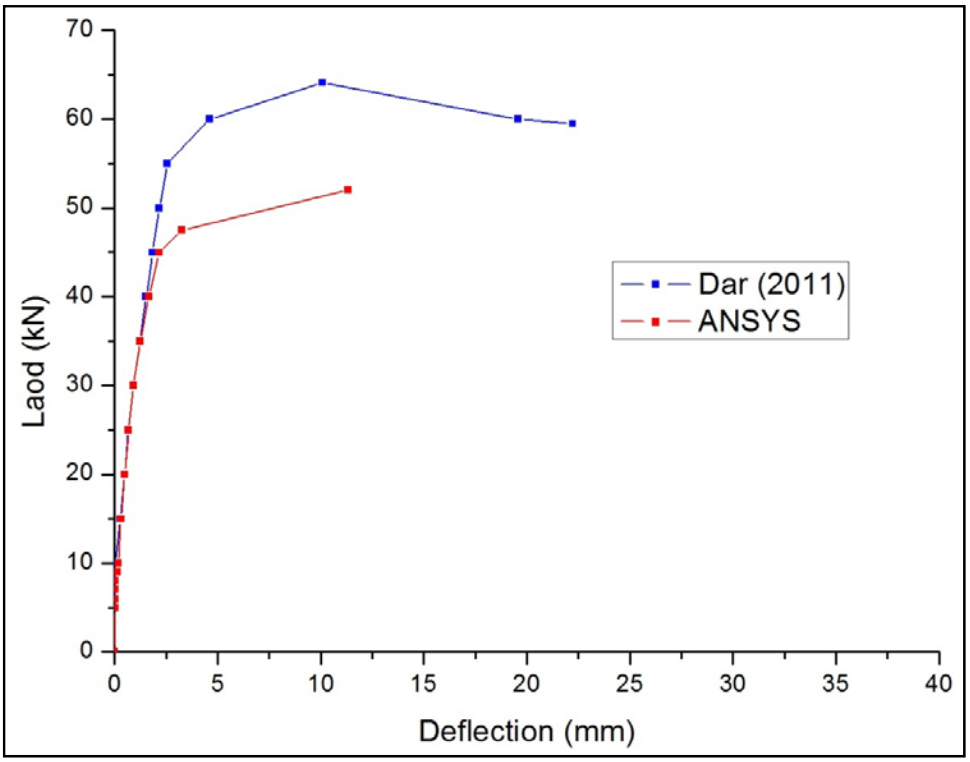

Fig. 4.13: Comparison of Load-deflection results at 400 mm from beam free end for control specimen with **Dar (2011)**

Comparison between the load-deflection results obtained from ANSYS and that from the experimental study conducted by **Dar (2011)** in **Fig. 4.11** to **4.13** shows that the ANSYS results are less stiff than the experimental results. The first crack load obtained in ANSYS at 9 kN is 10% lower to the first crack load of 10 kN obtained in the experimental study. The yield load obtained in ANSYS is 13.64% lower at 47.5 kN as compared to the value of 55 kN obtained from the experimental study. The ultimate load reached in ANSYS is 52.0 kN which is 18.88% lower than the ultimate load of 64.1 kN obtained in the experimental study.

At the yield load, the displacement obtained in ANSYS is 11.811 mm at beam free end as compared to 7.2 mm in the experimental study. The displacement at the ultimate load obtained in ANSYS is 25.321 mm at beam free end which is close to the value of 24.1 mm obtained in the experimental study.

This variation is attributed to the use of characteristic strength values for grade of concrete and steel in ANSYS which are lower than the actual material properties reported in the experimental study of concrete and steel.

4.2 RETROFITTED SPECIMEN

The deflection values from the analysis of retrofitted specimen in ANSYS are noted at three junctions: beam free end, 150 mm from beam free end and 400 mm from beam free end. These are presented in **Table 4.4**, **4.5** and **4.6** respectively.

Table 4.4: Load-Deflection Results from ANSYS at beam free end for retrofitted specimen

Load (kN)	Deflection (mm)	Load (kN)	Deflection (mm)
5.0	0.0656	**50.0**	4.3426
10.0	0.5478	**55.0**	5.0290
15.0	0.9364	**60.0**	5.7641
20.0	1.3260	**65.0**	6.5524
25.0	1.7928	**70.0**	7.4645
30.0	2.2163	**75.0**	8.3372
35.0	2.6421	**77.25**	8.9285
40.0	3.1748	**80.0**	16.2178
45.0	3.7256		

Table 4.5: Load-Deflection results from ANSYS at 150 mm from beam free end for retrofitted specimen

Load (kN)	Deflection (mm)	Load (kN)	Deflection (mm)
5.0	0.0474	**50.0**	2.8582
10.0	0.3912	**55.0**	3.3426
15.0	0.6699	**60.0**	3.9173
20.0	0.9472	**65.0**	4.5221
25.0	1.2766	**70.0**	5.2734
30.0	1.5121	**75.0**	5.8832
35.0	1.6786	**77.25**	6.3122
40.0	1.9635	**80.0**	13.5415
45.0	2.3367		

Table 4.6: Load-Deflection results from ANSYS at 400 mm from beam free end for retrofitted specimen

Load (kN)	Deflection (mm)	Load (kN)	Deflection (mm)
5.0	0.0145	**50.0**	0.8265
10.0	0.1180	**55.0**	0.9541
15.0	0.2056	**60.0**	1.1152
20.0	0.2892	**65.0**	1.3713
25.0	0.3911	**70.0**	1.4864
30.0	0.4642	**75.0**	1.6841
35.0	0.5364	**77.25**	1.7857
40.0	0.6186	**80.0**	7.6221
45.0	0.7362		

The load-deflection results of the retrofitted specimen are now compared with the results of the control specimen and presented in **Fig. 4.14** to **4.16**.

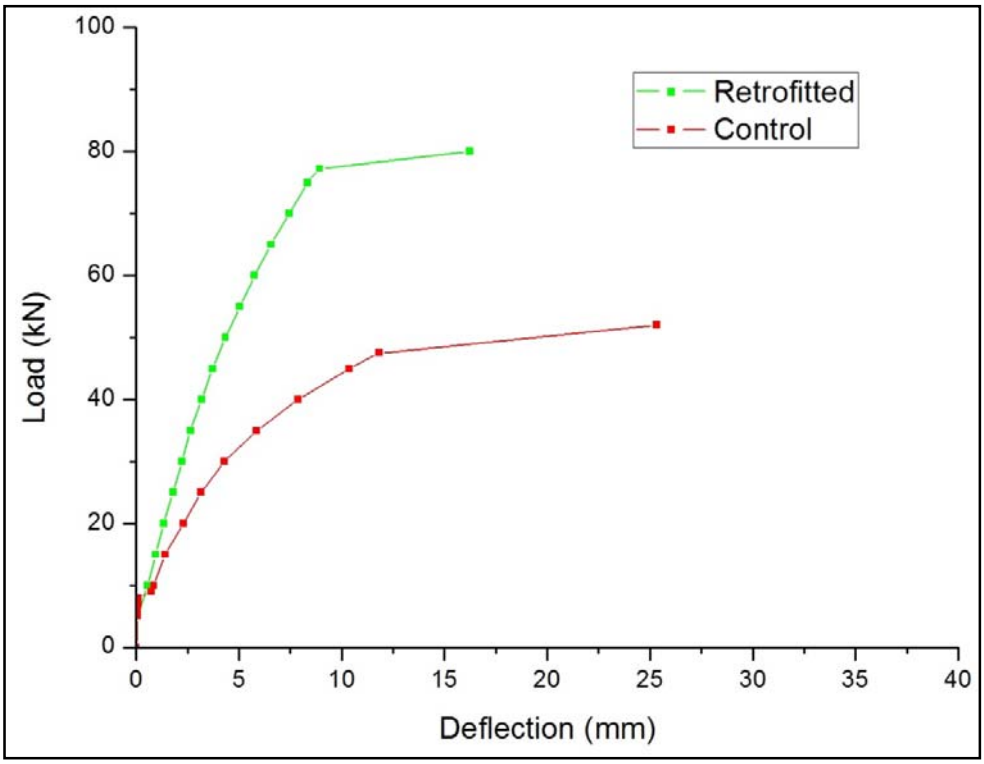

Fig. 4.14: Comparison of Load-deflection results of retrofitted and control specimen at beam free end

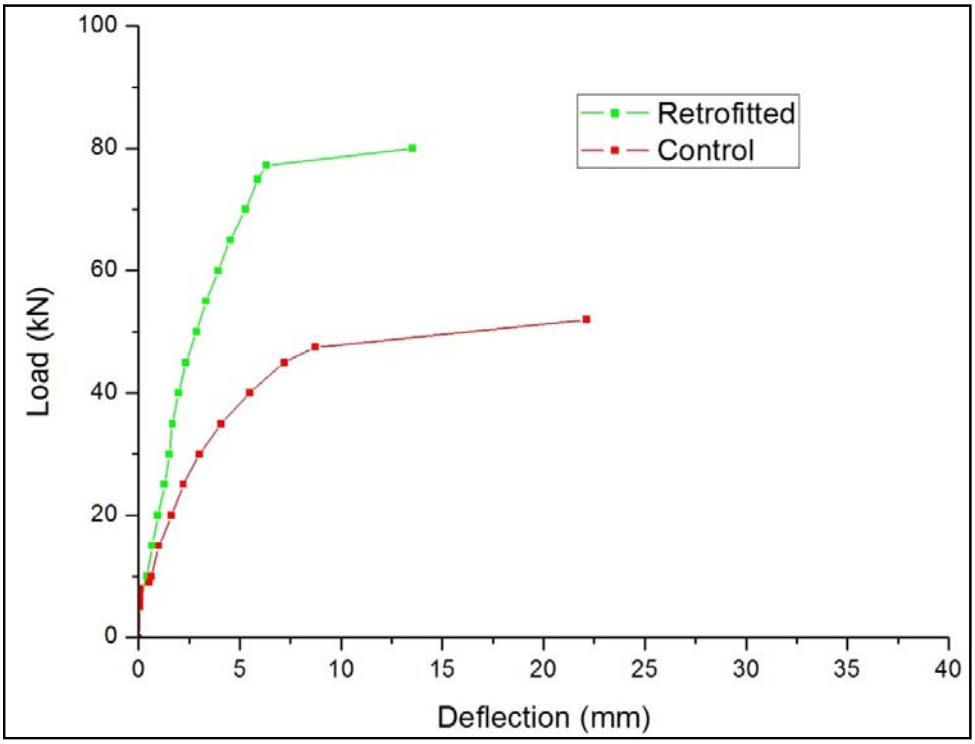

Fig. 4.15: Comparison of Load-deflection results of retrofitted and control specimen at 150 mm from beam free end

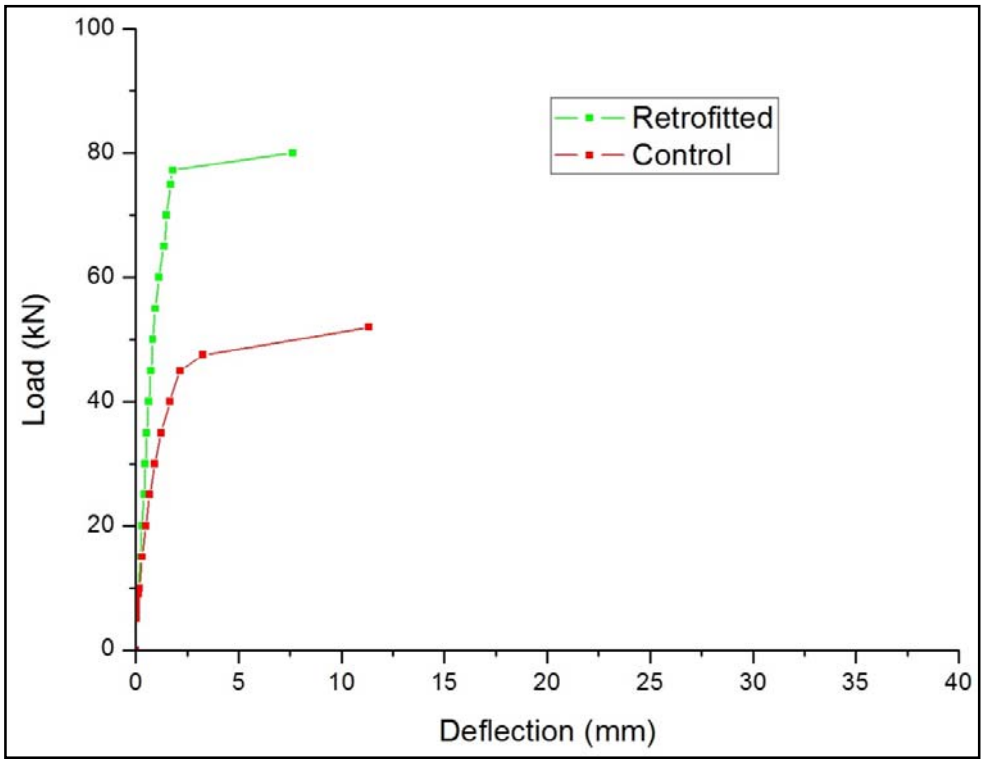

Fig. 4.16: Comparison of Load-deflection results of retrofitted and control specimen at 400 mm from beam free end

The deflected shape of the retrofitted specimen at 5000 N is shown in **Fig. 4.17**.

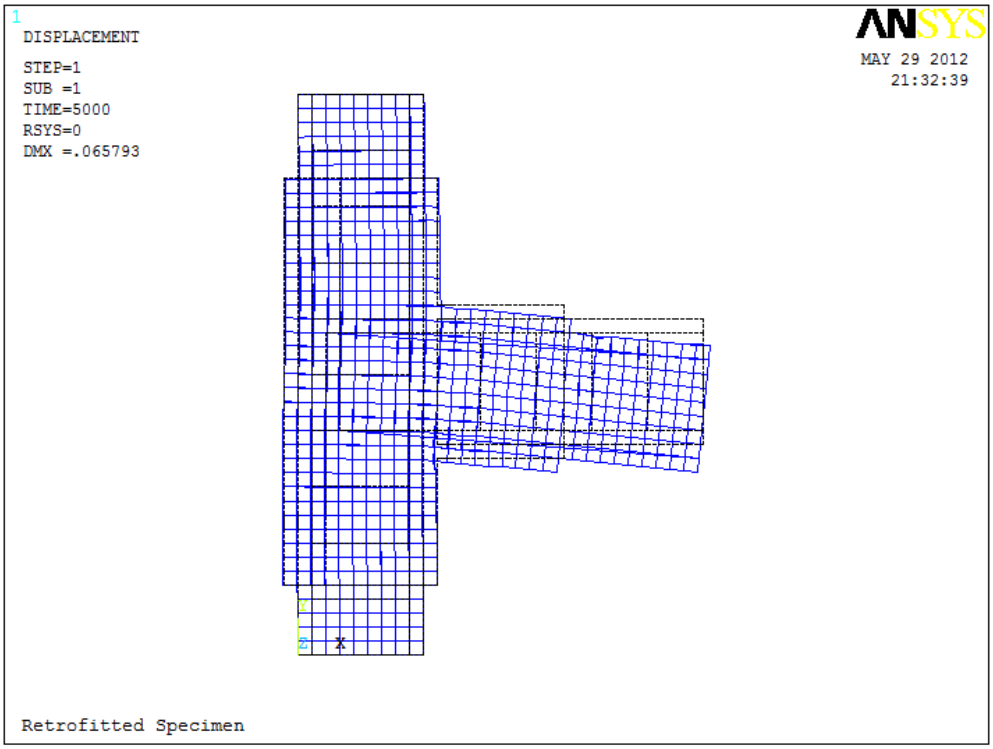

Fig. 4.17: Deflected shape of Retrofitted Specimen at 5000 N

Comparison between the load-deflection results obtained from ANSYS for control and retrofitted specimens shown in **Fig. 4.14** to **4.16** shows that the yield load and ultimate load has significantly increased for the retrofitted specimen. The yield load for the retrofitted specimen is observed at 77.25 kN which represents an increase of 62.63% from the yield load value of 47.5 kN for the control specimen. The ultimate load for the retrofitted specimen increases by 53.85% from 52.0 kN to 80.0 kN when compared with the control specimen.

The higher value of yield load and ultimate load for the retrofitted specimen is associated with lower deflections as compared to the control specimen. For example, at a load level of 40 kN, the deflection at beam free end is 7.8651 mm for the control specimen while it is only 3.1748 mm for the retrofitted specimen at the same location.

The deflection ductility ratio defined as the ratio of deflection at ultimate load and yield load is also compared for the two specimens. For the retrofitted specimen, ductility ratio is found out to be 1.82 at the beam free end which is less than the ductility ratio for the control specimen which is 2.14.

The values of energy absorption (given by the area under the load-deflection plots upto ultimate load) are also compared for the control and retrofitted specimens in **Fig. 4.18**. The value of energy absorption is found to be 984.02 kN-mm for the retrofitted specimen at beam free end as compared to the value of 1039.57 kN-mm for the control specimen.

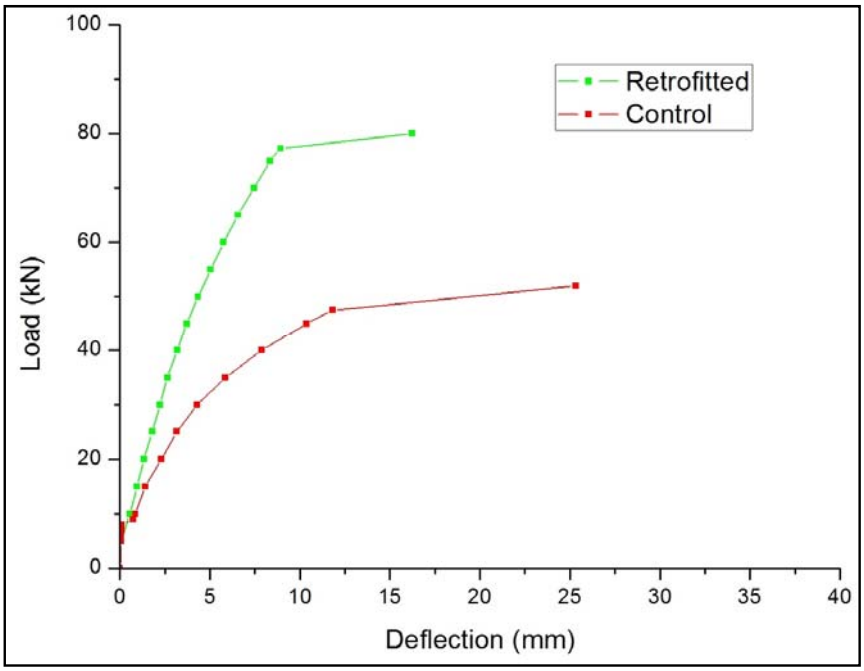

Fig. 4.18: Calculation of energy absorption for control and retrofitted specimens at beam free end

The cracking patterns in the retrofitted specimen are shown in **Fig. 4.19** to **4.23** at various load stages.

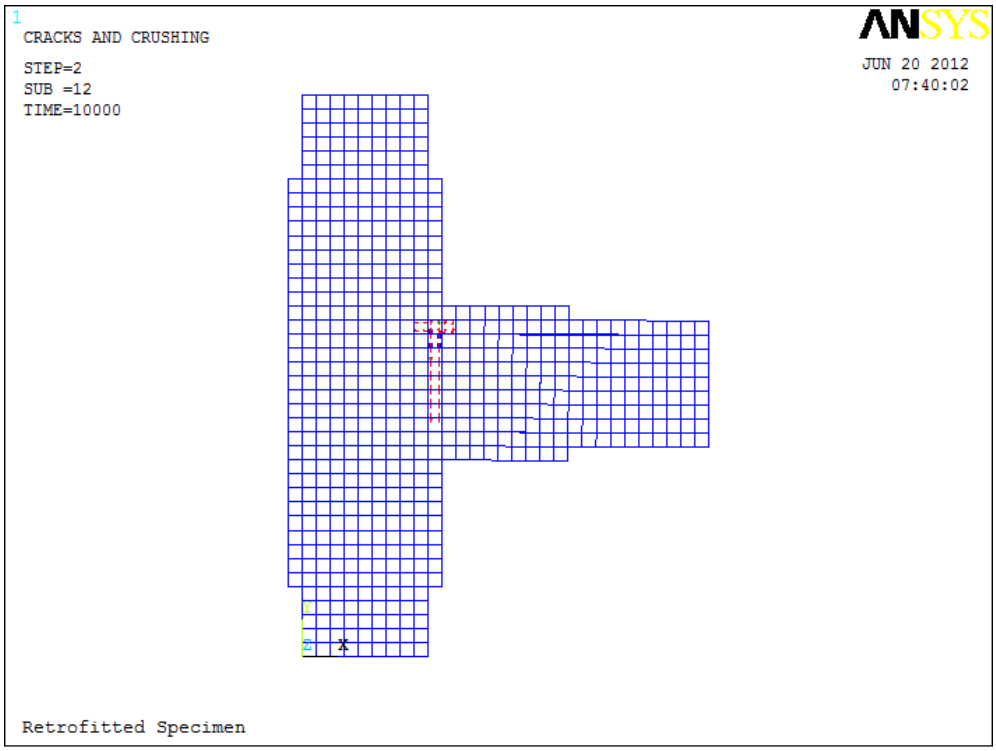

Fig. 4.19: 1st crack of the concrete model at 10,000 N for retrofitted specimen

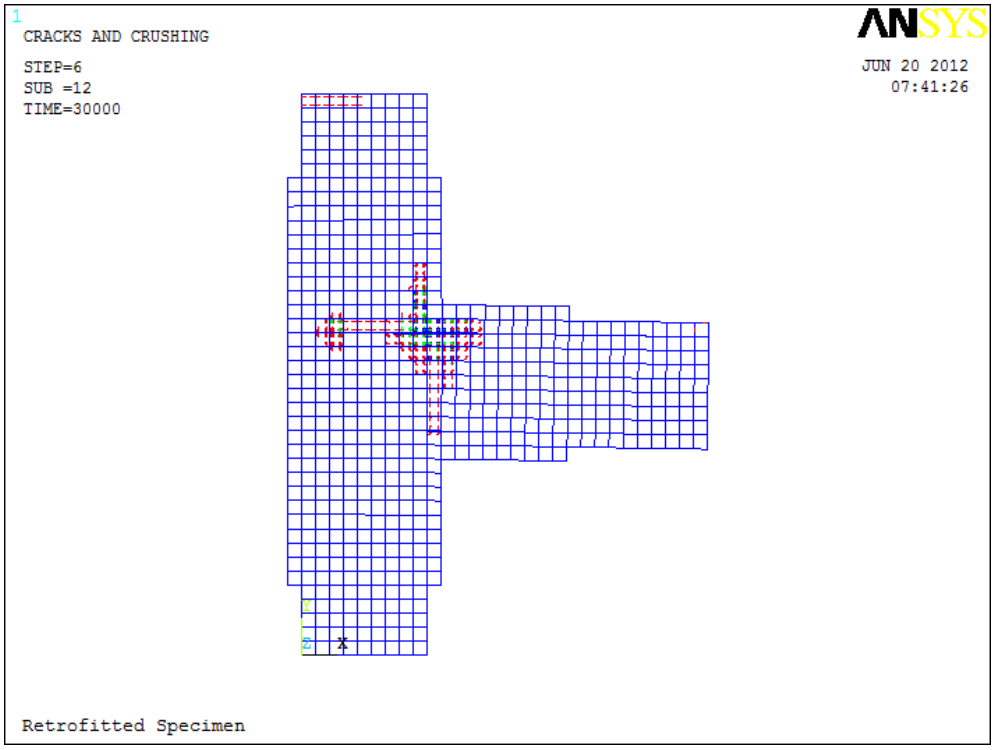

Fig. 4.20: Cracking of the concrete model at 30,000 N for retrofitted specimen

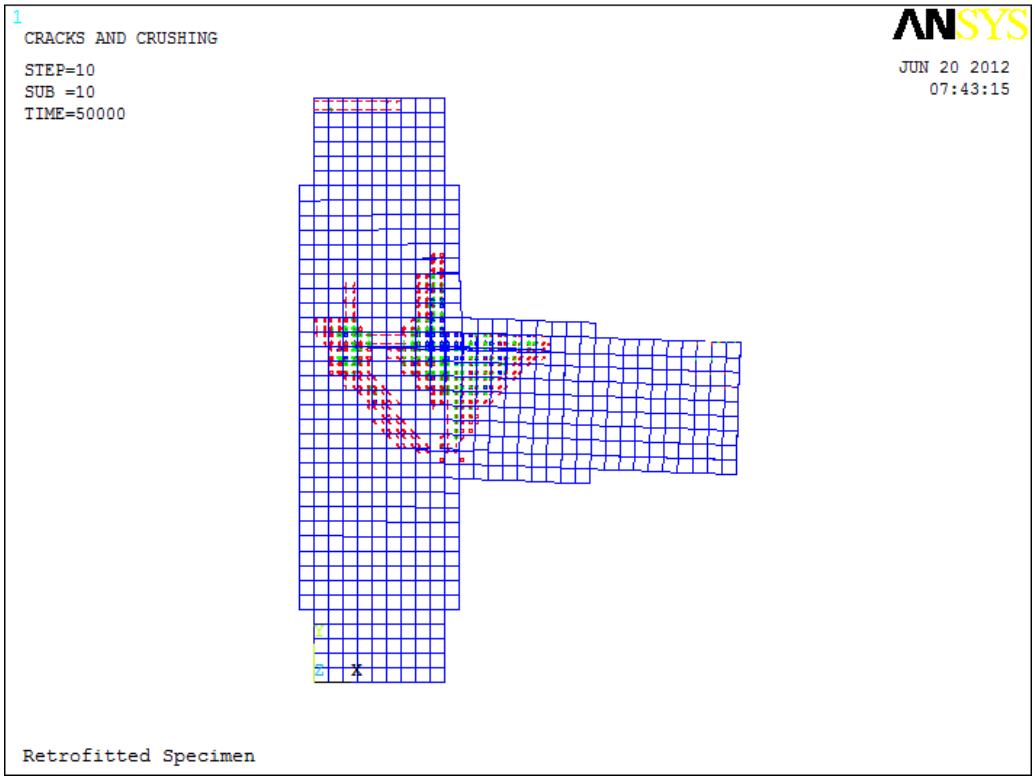

Fig. 4.21: Cracking of the concrete model at 50,000 N for retrofitted specimen

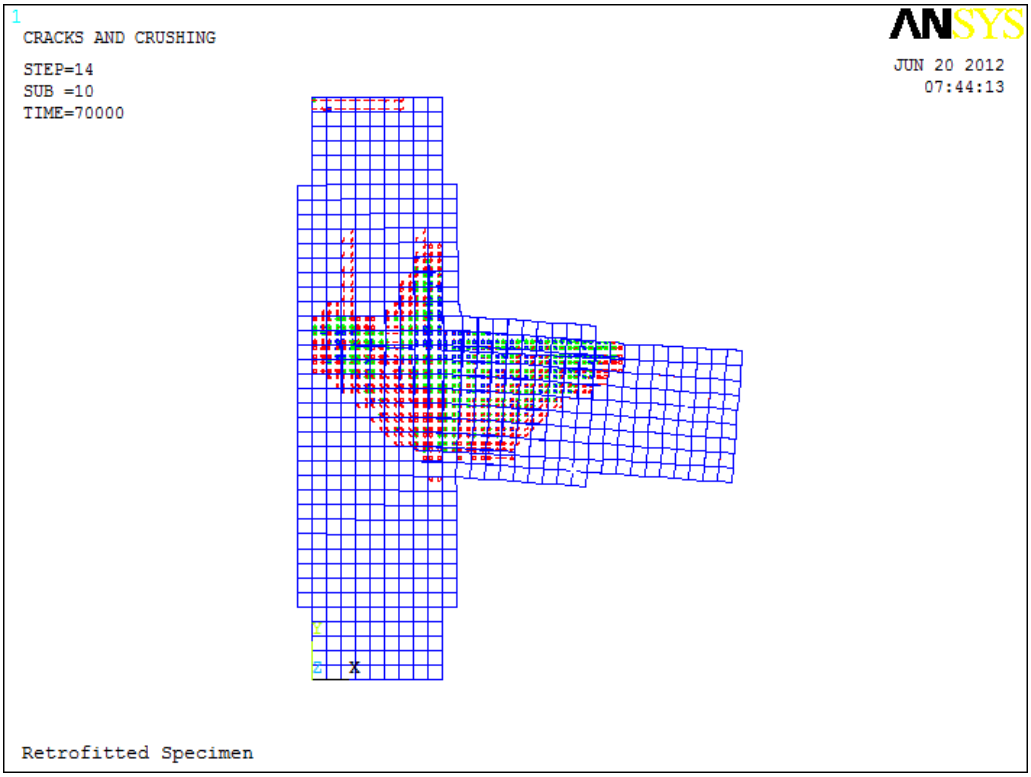

Fig. 4.22: Cracking of the concrete model at 70,000 N for retrofitted specimen

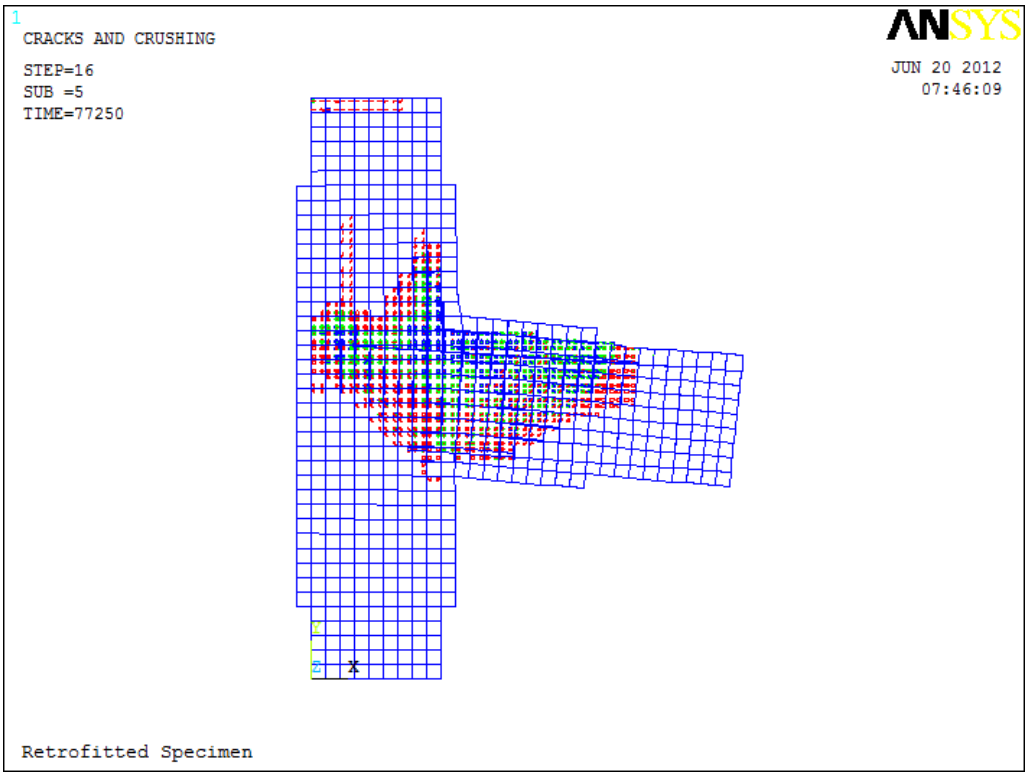

Fig. 4.23: Cracking of the concrete model at 77,250 N for retrofitted specimen

Conclusions from the present study are drawn in Chapter-5.

In the present study, finite element modelling of a reinforced concrete exterior beam-column joint retrofitted with externally bonded fiber reinforced polymer (FRP) is carried out with the help of commercially available software ANSYS 12.1.

5.1 CONCLUSIONS

The important conclusions drawn from the study are listed below:

1. ANSYS is able to model the different components of a load-deflection curve i.e. the linear region, initial cracking, the nonlinear region, the yielding of steel, and failure.
2. Comparison between the load-deflection results obtained from ANSYS and that from the experimental study shows that the ANSYS results are less stiff than the experimental results. The first crack load, yield load and ultimate load obtained in ANSYS are lower than the values obtained from the experimental study.
3. Comparison between the load-deflection results obtained from ANSYS for control and retrofitted specimens shows that the yield load and ultimate load has significantly increased for the retrofitted specimen.
4. The higher value of yield load and ultimate load for the retrofitted specimen is associated with lower deflections as compared to the control specimen.
5. The deflection ductility ratio for the retrofitted specimen is less than the ductility ratio for the control specimen.
6. The value of energy absorption for the retrofitted specimen is less than the energy absorption value for the control specimen.

5.2 FUTURE SCOPE OF WORK

In the present study, the use of FEM to evaluate beam-column joint is established. Further work can be directed towards comparative studies among different FEM softwares to know the preciseness and efficiency of each of them. Different retrofit materials like glass fiber reinforced polymer (GFRP), ferrocement etc. can be used and compared with

experimental results. Retrospective studies can be performed by collecting actual field data from sites where FRP retrofitting is done.

ACI 318-08, "Building Code Requirements for Structural Concrete and Commentary", American Concrete Institute, Farmington Hills, MI, 2008.

Akguzel, U., and Pampanin, S. (2012). Assessment and Design Procedure for the Seismic Retrofit of Reinforced Concrete Beam-Column Joints using FRP Composite Materials. *Journal of Composites for Construction*, ASCE, 16(1), 21-34.

Akguzel, U., and Pampanin, S. (2010). Effect of Axial Load Variation on the Retrofit of Exterior Reinforced Concrete Beam-Column Joints. *Proceedings of 2010 NZSEE Conference*, Christchurch, NZ, Paper No. 42.

Alsayed, S.H., Al-Salloum, Y.A., Almusallam, T.H., and Siddiqui, N.A. (2010). Seismic Response of FRP-Upgraded Exterior RC Beam-Column Joints. *Journal of Composites for Construction*, ASCE, 14(2), 195-208.

Antonopoulos, C.P., and Triantafillou, T.C. (2003). Experimental Investigation of FRP-Strengthened RC Beam-Column Joints. *Journal of Composites for Construction*, ASCE, 7(1), 39-49.

Antonopoulos, C.P., and Triantafillou, T.C. (2002). Analysis of FRP-Strengthened RC Beam-Column Joints. *Journal of Composites for Construction*, ASCE, 6(1), 41-51.

Bansal, P.P., Kumar, M., Kaushik, S.K. (2011). Effect of Initial Stress Levels on Strength Parameters of Reinforced Concrete Beams Retrofitted using Ferrocement Jackets. *Journal of Testing and Evaluation*, ASTM, 39(5), Paper ID: JTE102891.

Bansal, P.P., Kumar, M., Kaushik, S.K. (2010). Experimental Study on Retrofitting of Stressed RC Beams using GFRP Jackets. *Journal of Reinforced Plastics and Composites*, 29(2), 190-200.

Bansal, P.P., Kumar, M., Kaushik, S.K. (2008). Effect of Wire Mesh Orientation on Strength of Beams Retrofitted using Ferrocement Jackets. *International Journal of Engineering*, 2(1), 8-19.

Bousselham, A. (2010). State of Research on Seismic Retrofit of RC Beam-Column Joints with Externally Bonded FRP. *Journal of Composites for Construction*, ASCE, 14(1), 49-61.

Buckhouse, E.R. (1997). External Flexural Reinforcement of Existing Reinforced Concrete Beams Using Bolted Steel Channels, Master's Thesis, Marquette University, Milwaukee, Wisconsin.

Dar, M.A. (2011). Effect of Different Wrapping Techniques on Retrofitting of RCC Beam Column Joints using Ferrocement, Master's Thesis, Thapar University, Patiala, India.

El-Amoury, T., and Ghobarah, A. (2002). Seismic Rehabilitation of Beam-Column Joint using GFRP Sheets. *Engineering Structures: The Journal of Earthquake, Wind and Ocean Engineering*, 24(11), 1397-1407.

Engindeniz, M., Kahn, L.F., and Zureick, A.-H. (2005). Repair and Strengthening of Reinforced Concrete Beam-Column Joints: State of the Art. *ACI Structural Journal*, 102(2), 187-197.

EC8:1998. Earthquake Resistant Design of Structures – Part 1: General Rules and Rules for Buildings ENV 1998-1-1/2/3, CEN Technical Committee 250/SC8, Berlin, Germany.

Fanning, P. (2001). Nonlinear Models of Reinforced and Post-tensioned Concrete Beams. *Electronic Journal of Structural Engineering*, 2, 111-119.

FIB Bulletin No. 14, "Externally Bonded FRP Reinforcement for RC Structures", Fédération Internationale du Béton, Lausanne, Switzerland, 2001.

Gergely, J., Pantelides, C.P., and Reaveley, L.D. (2000). Shear Strengthening of RCT-Joints using CFRP Composites. *Journal of Composites for Construction*, ASCE, 4(2), 56-64.

Ghobarah, A., and El-Amoury, T. (2005). Seismic Rehabilitation of Deficient Exterior Concrete Frame Joints. *Journal of Composites for Construction*, ASCE, 9(5), 408-416.

Ghobarah, A., and Said, A. (2002). Shear Strengthening of Beam-Column Joints. *Engineering Structures: The Journal of Earthquake, Wind and Ocean Engineering*, 24(7), 881-888.

Ghobarah, A., and Said, A. (2001). Seismic Rehabilitation of Beam-Column Joints using FRP Laminates. *Journal of Earthquake Engineering*, 5(1), 113-129.

Haach, V.G., El Debs, A.L.H.de.C., El Debs, M.K. (2008). Evaluation of the Influence of the Column Axial Load on the Behavior of Monotonically Loaded RC Exterior Beam–Column Joints through Numerical Simulations. *Engineering Structures*, 30, 965-975.

Hakuto, S., Park, R., and Tanaka, H. (2000). Seismic Load Tests on Interior and Exterior Beam-Column Joints with Substandard Reinforcing Details. *ACI Structural Journal,* 97(1), 11-25.

Hegger, J., Sherif, A., and Roeser, W. (2004). Nonlinear Finite Element Analysis of Reinforced Concrete Beam-Column Connections. *ACI Structural Journal*, 101(5), 604-614.

Ibrahim, A.M., and Mahmood, M.S. (2009). Finite Element Modeling of Reinforced Concrete Beams Strengthened with FRP Laminates. *European Journal of Scientific Research*, 30(4), 526-541.

IS 13920-1993 Edition 1.2 (2002-03), "Indian Standard Code of Practice Ductile Detailing of Reinforced Concrete Structures Subjected to Seismic Forces", Bureau of Indian Standards, New Delhi, 2002.

IS 456: 2000 (Fourth Revision), "Indian Standard: Plain and Reinforced Concrete – Code of Practice", Bureau of Indian Standards, New Delhi, 2005.

Kachlakev, D., Miller, T.P., Yim, S., Chansawat, K., and Potisuk, T. (2001). Finite Element Modeling of Reinforced Concrete Structures Strengthened with FRP Laminates, Oregon Department of Transportation, Research Group, Salem, Oregon.

Lee, W.T., Chiou, Y.J., and Shih, M.H. (2010). Reinforced Concrete Beam–Column Joint Strengthened with Carbon Fiber Reinforced Polymer. *Composite Structures*, 92, 48-60.

Li, B., and Chua, H.Y.G. (2009). Seismic Performance of Strengthened Reinforced Concrete Beam-Column Joints Using FRP Composites. *Journal of Structural Engineering*, ASCE, 135(10), 1177-1190.

Liu, C. (2006). Seismic Behaviour of Beam-Column Joint Subassemblages Reinforced with Steel Fibers, Master's Thesis, University of Canterbury, Christchurch, New Zealand.

Ludovico, D. M., Manfredi, G., Mola E., Negro, P., and Prota, A. (2008). Seismic Behavior of a Full-scale RC Structure Retrofitted Using GFRP Laminates. *Journal of Composites for Construction*, ASCE, 134(5), 810-821.

Mahini, S.S., and Ronagh, H.R. (2010). Strength and Ductility of FRP Web-Bonded RC Beams for the Assessment of Retrofitted Beam–Column Joints. *Composite Structures,* 92, 1325-1332.

Mahini, S.S., Isfahani, A.D., and Ronagh, H.R. (2008). Numerical Modelling of CFRP-Retrofitted RC Exterior Beam Column Joints under Cyclic Loads. *Fourth International Conference on FRP Composites in Civil Engineering*, Zurich, Switzerland.

Mahini, S.S., and Ronagh, H.R. (2007). A New Method for Improving Ductility in Existing RC Ordinary Moment Resisting Frames Using FRPS. *Asian Journal of Civil Engineering (Building and Housing)*, 8(6), 581-595.

Mehta, A. (2011). Effect of Initial Stress Levels on Strength of Beams Retrofitted using Pre-stressed Fiber Composites, Master's Thesis, Thapar University, Patiala, India.

Mukherjee, A., and Joshi, M. (2005). FRPC Reinforced Concrete Beam-Column Joints under Cyclic Excitation. *Composite Structures*, 70(2), 185-199.

Murty, C.V.R., Rai, D.C., Bajpai, K.K., and Jain, S.K. (2003). Effectiveness of Reinforcement Details in Exterior Reinforced Concrete Beam-Column Joints for Earthquake Resistance. *ACI Structural Journal*, 100(2), 149-156.

NZS 3101:1995, "The Design of Concrete Structures", Standards New Zealand, Wellington, New Zealand, 1995.

Pampanin, S., Magenes, G., Carr, A. (2003). Modelling of Shear Hinge Mechanism in Poorly Detailed RC Beam-Column Joints. *Proceedings of the FIB 2003 Symposium*, Athens, Greece.

Pantazopoulou, S., and Bonacci, J. (1992). Consideration of Questions about Beam-Column Joints. *ACI Structural Journal,* 89(1), 27-36.

Park, P. and Paulay, T. (1994). Reinforced Concrete Structures, John Wiley & Sons Inc., New York.

Paulay, T. and Preistley, M.J.N. (1992). Seismic Design of Reinforced Concrete and Masonry Buildings, John Wiley Publications, New York.

Priestley, M.J.N. (1997). Displacement Based Seismic Assessment of Reinforced Concrete Buildings. *Journal of Earthquake Engineering*, 1(1), 157-192.

Prota, A., Nanni, A., Manfredi, G., and Cosenza, E. (2004). Selective Upgrade of Underdesigned Reinforced Concrete Beam-Column Joints Using Carbon Fiber-Reinforced Polymers. *ACI Structural Journal*, 101(5), 699-707.

Ravi, S.R., and Arulraj, G.P. (2010). Finite Element Modeling on behavior of Reinforced Concrete Beam Column Joints Retrofitted with Carbon Fiber Reinforced Polymer Sheets. *International Journal of Civil and Structural Engineering*, 1(3), 576-582.

SAS (2009). ANSYS 12.1 Finite Element Analysis System, SAS IP, Inc.

Sharma, A., Genesio, G., Reddy, G.R., Eligehausen, R., Pampanin, S., Vaze, K.K. (2010). Experimental Investigations on Seismic Retrofitting of Reinforced Concrete Beam-Column Joints. *Proceedings of the 14th Symposium on Earthquake Engineering*, Indian Institute of Technology, Roorkee, India, Paper No. A007.

Tavárez F.A. (2001). Simulation of Behavior of Composite Grid Reinforced Concrete Beams using Explicit Finite Element Methods, Master's Thesis, University of Wisconsin-Madison, Madison, Wisconsin.

Tsonos, A.G. (2007). Cyclic Load Behavior of Reinforced Concrete Beam-Column Subassemblages of Modern Structures. *ACI Structural Journal*, 104(4), 468-478.

Turner, M. J., Clough, R. W., Martin, H. C, and Topp, L. J. (1956). Stiffness and Deflection Analysis of Complex Structures. *Journal of the Aeronautical Sciences*, 23, 805-823.

Willam, K.J., and Warnke, E.P. (1975). Constitutive Model for Triaxial Behaviour of Concrete, *Proceedings of the International Association of Bridge and Structural Engineering*, Bergamo, Italy.

Wolanski, A.J.B.S. (2004). Flexural Behavior of Reinforced and Prestressed Concrete Beams Using Finite Element Analysis, Master's Thesis, Marquette University, Milwaukee, Wisconsin.